**Oleg Krol**

# MACHINE TOOL SPINDLE DYNAMICS FOR DESIGNERS

**Monograph**

**Prof. Marin Drinov Publishing House of Bulgarian Academy of Sciences**

**SOFIA 2020**

**Reviewers:**

**Permyakov Oleksandr**, Doctor of Sc., National Technical University "Kharkiv Polytechnic Institute", Ukraine.
**Nemtinov Vladimir**, Doctor of Sc., Tambov State Technical University, Russia.
**Tsankov Petko**, PhD, Technical University of Sofia, Bulgaria.
**Kovalevskyy Sergiy**, Doctor of Sc., Donbass State Engineering Academy, Ukraine.

**Oleg Krol**

**MACHINE TOOL SPINDLE DYNAMICS FOR DESIGNERS:** monograph / Krol O. – Sofia: Prof. Marin Drinov Publishing House of Bulgarian Academy of Sciences, 2020. – 143 p.: Table 10. Figure 62. Bibliogr. 87 names. English language.

The monograph considers the problems of assessing the dynamic quality of projected metal-cutting machines, their shaping spindle units. The procedures for solving problems of dynamics by the method of initial parameters and transfer matrix are presented. The features of the spindle assembly formalization as an elastic system "Spindle-Arbor-Tool", with modeling the spindle joint with the conical connection of the arbor by the matrix of the elastic-friction hinge are considered. The problem of elastic-deformative description of the spindle-arbor link of high-speed machines is presented as a quasi-static problem, taking into account the action of inertial centrifugal forces and gyroscopic moments at a steady state of motion. The software has been developed for assessing the frequency characteristics of metal-cutting machines elastic systems in the mathematical environment MATLAB.

A study of the stability of the spindle assembly using tools D-partitions based on the analysis of the number of roots of the characteristic equation. For leading designers and specialists in the field of machine tool system dynamics, researchers, teachers, graduate students and students.

ISBN 978-619-245-069-4
DOI 10.7546/MTSDD.2020



Prof. Marin Drinov Publishing House of Bulgarian Academy of Sciences

Acad. Georgi Bonchev Str., Bl. 6, 1113 Sofia, Bulgaria

**www.press.bas.bg**

# INTRODUCTION

Increasing requirements for the quality of drilling-milling-boring machines, their technological complexes in connection with a general increase in mechanical engineering precision, the manufacture of parts from difficult-to-machine materials, the rational use of high-performance cutting tools, forces us to look for ways to improve the main forming units that have a decisive effect on productivity and processing precision. The introduction of progressive machining modes, reducing to a minimum the time of idle running and auxiliary movements leads to a significant increase in the machines speed characteristics, in particular the spindle units of machine equipment. These main technological characteristics of metal-cutting equipment are limited, as a rule, by their vibrostability, for the assessment of which it is necessary to know the dynamic characteristics of multi-operational machines and its main elements.

Besides, an increase in the efficiency of processes implemented on modern technological complexes based on multi-operational equipment is associated with an increase in the dynamic stability of the main units of metal-cutting machines. Analysis of the balance of compliance and vibration modes of the shaping units of milling-drilling-boring machines showed that the most intense vibrations are characteristic of such forming units as "Spindle-Arbor - Tool" and "Table - Workpiece".

Interrupted cutting operations such as milling are characterized by a large range of force effects arising during machining, including the probabilistic component in the form of a set of dynamic harmonics.

It is difficult to overestimate the role of computational methods for choosing the optimal design options, both in terms of rigidity and vibrostability, which in many cases makes it possible to apply strict formal solutions instead of approximate solutions or complex experiments, and use them in the analysis of the dynamics of the functioning of metal-cutting equipment.

At the same time, the successful use of computers and software for the automation of production process control and engineering activities gives an effect only with comprehensive research and mathematical description of technological processes implemented on machine tools, and, consequently, the creation of mathematical models of these processes. There is a need for research work to create and improve algorithms for the implementation of these mathematical models using modern computing technology.

When studying the structures of shaping units according to the criterion of vibrostability, it becomes necessary to build 3D models in developed computer-aided design systems. It is efficient to carry out solid modeling in the integrated CAD KOMPAS-3D, developed by the ASCON group of companies. Since from KOMPAS-3D V.15 introduces a new design philosophy, relies on the commands "Layout geometry", "Collections" and "Copy geometry", the integrated use of which is aimed at optimizing the teamwork process. Thanks to a new round of development of KOMPAS-3D, the application “Shafts and mechanical transmissions”, which are most demanded in mechanical engineering, has reached a higher, in functional terms, level. In KOMPAS-3D, the MinD intelligent design technology has undergone fundamental changes in terms of convenience and quality of work. An irreplaceable "Select by properties" functionality has appeared in it, which allows you to find any objects by certain properties.

Along with geometric modeling, it is necessary to carry out a comprehensive engineering analysis of the designed object using CAE-analysis (Computer Aided Engineering) tools, as well as a complex of calculations based on strength and stiffness criteria.

We need programs that give an idea of the stress-strain state for the forming parts and machine units. Such a software package is represented by the well-known CAD/CAE system APM WinMachine, developed by the scientific and technical center STC APM.

Starting with the KOMPAS 3D V.13 version, the APM FEM module is integrated into its structure, they are an integral part of a unified design

and analysis environment using an associative geometric model, a unified library of materials and an interface common with KOMPAS-3D.

Based on these considerations, the correct choice of such design solutions that ensure the stable operation of metal-cutting machines in various ranges of cutting conditions becomes important.

The subject of this monograph is the processes and algorithms for assessing the dynamic quality of the functioning of metal-cutting machines, based on computer modeling and modern mathematical environments, such as MatLab.

The purpose of this kind of research is to improve the procedures for determining the frequency characteristics of spindle assemblies and to provide designers with algorithms for making optimal decisions on the criterion of vibrostability.

To achieve this goal, several objectives of this research have been put forward:

- development of methods and algorithms for determining the dynamic characteristics of the elastic system "Spindle-Arbor-Tool" (SAT) by the method of transfer matrices;
- creation of programs for the construction of frequency characteristics and Amplitude phase-frequency characteristics (APFC) of spindle nodes in the mathematical environment MatLab;
- development of methods and algorithms for the analysis of vibrostability by the D-partition method;
- formation of the toolkit for assessing the structures dynamic quality with a random nature of external influences using the finite Fourier transform;
- improvement of frequency characteristics estimates using the apparatus of spectral windows;
- implementation of procedures for assessing the dynamic quality of multifunctional lathes of turning and milling groups.

# ANALYSIS OF WORKS IN THE MACHINE DYNAMICS FIELD

In the fundamental work on the dynamics of machine tools [1], a system of indicators of the dynamic quality of machine tools (margin and degree of stability, operation speed and deviation of parameters of a dynamic system under external influences) is introduced. A general methodology for theoretical and experimental analysis and evaluation of machine tools [Кудинов] according to these indicators is given. A position on the closedness of the machine dynamic system, which is determined by the interaction of the elements of the elastic system "machine-tooling-part" with the working processes of cutting, friction and drives is introduced. At the same time, the author limits the variety of particular features of dynamic phenomena in machine tools to linearized systems. These limitations are justified by the possibility of analyzing a significant part of machine tool applications with the accuracy of the results sufficient for practice. The dynamic system of the machine according to V.A. Kudinov is formed by a combination of an elastic system (machine, arbor, tool, part) and work processes in their interaction.

The analysis of the dynamic system features for the machine made it possible to introduce a new concept of the "equivalent elastic system" (EES) of a metal-cutting machine. It is directly related to the division of zones where the working processes by the elements of the elastic system take place. This approach proved to be effective in solving the following tasks:

1. Tasks associated with the choice of a drive or its calculation, when the element "mechanical system", including the processes of cutting and friction with their connections, is considered as equivalent.

2. Tasks of the analysis of friction conditions in machine slideways or bearings of machine tool assemblies. Here the equivalent element combines the elastic system and the processes in the engines.

3. Problems of calculating cutting conditions, where the elastic system of the machine and the processes in the engine and friction are considered as an equivalent element.

The approach proposed by prof. V.A. Kudinov proved to be productive in various applications of the machine tool industry. So in work [2], the dynamics of auxiliary movement mechanisms, in particular, mechanisms of periodic rotation of nodes (Maltese, cam triebstock, gear-linkage and coulisse mechanisms) is considered. Besides, the dynamics of clamping and loading mechanisms, including those designed for an automatic tool change, are considered in detail.

In work [3], the research of the EES of special diamond boring machines is carried out and the frequency characteristics of boring bars for diamond boring heads are determined, and designs of a dynamic vibration damper are proposed to improve the dynamic quality. For these structures, a model has been built, based on which the APFC of the elastic system "spindle-cantilever" with a vibration damper is constructed. Based on the results obtained in [4], the dynamic characteristics of the thin boring process were determined, and the determination of the time constant of chip formation $T_p$ and specific cutting forces $K_p$ is carried out based on the constructed nomograms, which facilitates the calculation of the cutting process characteristics.

At the same time, the dynamic characteristic of the cutting process obtained in [1, 3], as a result of direct experiments, needs to be refined. For the case of flow chip formation, the refinement is associated with the representation of the process of chips deformation that moving along the cutter as along a beam on a compliance base [4]. Based on the found dependence of the contact length the chip and the tool, transfer functions that characterize the change in the contact length with a change in the cut

thickness are obtained. Comparing the results obtained with the available experimental data, one can note their qualitative agreement [4].

At the level of layout design, it is proposed to use not a generalized criterion as a criterion for comparing layouts, but an indicator of dynamic quality at limiting operations [5, 6]. Based on experiments on lathes, it was shown [5] that with stable cutting the level of oscillations in the cutting zone is most intense in the low-frequency region corresponding to the natural frequencies of oscillations of the carrier system (CS) of the machines. In this case, the dynamic characteristics of the CS, calculated under the selected design conditions, will characterize the quality of the layout from the standpoint of not only the stability of the process but also the influence of vibrations on the processing accuracy. A similar approach is used to compare the layouts of multipurpose machines of the milling-drilling-boring group [6, 7]. Comparison of the CS dynamic characteristics for various layouts, differing in the mutual arrangement of stationary and movable blocks, in particular, in the arrangement of tool storages and a spindle head on the rack is carried out. The indicator of dynamic compliance was used as a criterion for comparison. For different technological operations, the values of dynamic compliance are calculated at the first and second natural frequencies for different designs of the spindle head. On this basis, a rational design of the elements of the carrier systems was selected.

In the research of the dynamics of multi-purpose machine tools, the finite element method is widely used. Thus, in [8, 9], an integrated approach to the problem of multivariate analysis of the elastic systems (ES) dynamic characteristics of machine tools is presented. Based on their schematization with the help of super elements connected at the boundary nodal points of the finite element mesh. The balance of dynamic compliance of a multi-purpose machine with a cross table has been determined [8, 10]. To detail the influence of design parameters on its dynamic characteristics, the procedure of energy analysis of ES oscillations at certain vibration modes at frequencies of 41 Hz and 66 Hz

was used. The results of the analysis made it possible to give recommendations on changing the designs of the machine tool's ES elements to improve its dynamic characteristics.

The analysis of the dynamic quality of machine tools for high-speed machining (the operation speed parameter $n \cdot d = (2...3) \cdot 10^6$ mm/min, determined through the spindle rotational speed $n$ and the diameter of its front stage $d$) is associated with the monitoring of spindle assemblies according to the characteristics of displacements and vibrations [11–14]. To control and predict the nature and magnitude of vibrations during processing, special programs have been created that take into account the state of the spindle assembly and tool, the material of the workpiece, the rigidity of its fastening and other characteristics.

In [15, 16], a procedure for directed research of the design and technological parameters influence on the dynamics of the Spindle Node (SN) is considered using mathematical modeling based on the proposed model of the SN dynamics for the operation of surface grinding with the periphery of the abrasive wheel. When constructing the model, an analysis of the influence of external factors, such as cutting forces, was carried out, in the analytical dependences of which the main parameters of the cutting process were explicitly taken into account in the form of coefficients characterizing the parameters of the workpiece materials and the abrasive tool, as well as the grinding modes.

The peculiarity of this model is that, in addition to vertical and transverse vibrations, torsional vibrations of the spindle cross-sections are taken into account, which, in turn, affect the behaviour of the tool. The mathematical model is parametric and non-linear due to periodic changes and non-linearity of the stiffness and damping coefficients of the rolling bearings.

Simulation of the SN dynamics was carried out similarly, depending on the standard sizes and errors of the raceways of the rolling bearing units at fixed processing modes [15]. The author found that with an increase in the number of rolling elements of bearings from 10 for the 66408 series to

16 for the 46108 series at $n_s$ = 2000 rpm, the vibration displacements of the tool decrease in the vertical and transverse directions by about 10%.

The modeling procedure consisted of varying certain design and technological parameters and cutting conditions with the rest unchanged. The calculation results in the form of vibration displacement diagrams of the SN elements, depending on the change in the technological parameters of grinding, are presented in [15].

The calculation of the dynamic characteristics of the technological system is implemented in the form of the *Spindel Dynamic* 6.6020 software package [15, 16] using the C ++ programming language in the Visual Studio.NET environment.

The solution is based on the Runge-Kutta method with automatic step selection. The software package is aimed at solving problems:

1) calculation and forecasting of vibration characteristics of existing spindle nodes;

2) selection of cutting conditions and design of structural elements of the spindle node.

Scientists from MSTU "STANKIN" and "ENIMS" have developed the SpinDyna software package (version 2.3) [17], which make it possible to model the SN structures on elastic supports. The complex includes several modules: forming a geometric model, setting parameters of supports, etc. The program uses a modern interface using form panels; the SN model includes the following elements: span of a beam, joint, support, etc. So the “Support” element is intended for modeling bearings or their combinations, and the geometric dimensions of the bearings and their stiffness are set manually or selected from the database. When constructing models of spindle dynamics, the method of initial parameters in a matrix formulation [18] was used. It based on the formation of transfer matrices of individual sections between the initial and final nodes.

A feature of this author's product is the consideration of the spindle damping mechanisms in its supports and joints using a viscous and elastic

model based on the analysis of the imaginary part of the dynamic stiffness of the spindle node under research.

Along with the criterion of rigidity in high-speed spindle heads, the criterion of vibrostability and the phenomenon of loss of stability are decisive. This kind of problem for a rotating shaft transmitting torque is considered in [19]. The author estimates the moment of loss of stability of the deformed and rotating shaft depending on the axial force and torque.

The use of CAD SolidWorks Simulation made it possible to obtain the value of the critical load, to estimate the conditional time in which there is a sharp increase in the displacement of the shaft sections and to fix the corresponding interval of angular velocities. At the same time, the influence of the characteristics of the shaft supports on the behavior of the structure under research during loading is not considered.

Some works [20–22 ] are devoted to the research of the elastic system dynamics "Spindle-Arbor-Tool" (SAT). In researches of the vibrostability of milling machine spindles, elastic connections spindle-arbor and arbor-tool were often not taken into account when constructing dynamics models. At the same time, these connections form a significant proportion of errors inherent in the machines of this group.

The dynamic quality of the SAT system is influenced by the radial and rotational stiffness of the S-A, as well as the damping corresponding to these stiffnesses [20, 21]. Despite the insignificant mass of the arbor, the presence of backlash and dry friction forces leads to the appearance of nonlinear phenomena in the conical connection S-A and the need to take into account the forces of inelastic resistance and the phenomena of damping of oscillations in the general model of the dynamics of the system under consideration.

A similar approach is presented in [22], where the dynamic subsystem of the spindle group "Clamping fork" of automatic lathes is investigated. It is the presence of backlash in the connection of the fork with the clutch of the clamping mechanism through the bearings, as well as significant frictional forces when the fork is installed on the axes, which leads to

significant nonlinearity. The damping forces (in the case of proportionality of the latter to the displacement velocities) in the problem of the dynamics of the SAT system can be taken into account using the matrix of the concentrated damping force [22].

More and more works are considering the issues of the machine tools dynamics during cutting when oscillations caused by the simultaneous action of a significant number of disturbances can be considered as stationary random processes [23–25].

The advent of modern design systems (CAD) and engineering analysis (CAE) made it possible to more effectively solve the problems of dynamic quality and vibration resistance of metal-cutting machines. Such an integrated CAD system is APM WinMachine [23]. This system includes the APM Structure 3D module. It is a versatile system for researching and designing the rod, shell, solid, and mixed structures.

Based on this system, it is possible to calculate an arbitrary three-dimensional structure with arbitrary loading and fastening. As a result of the calculations performed by the system, the following information can be obtained:

- maps of stress and strain distribution in arbitrary spindle sections;
- the stability factor of the structure according to Euler;
- stress-strain state of the structure at large displacements (geometrically nonlinear problem);
- frequencies and forms of natural vibrations of the structure;
- change in the stress-strain state of a structure under the influence of loads arbitrarily changing in time.

The system implements the ability to automatically generate dynamic loading and perform stability analysis (according to Euler), which refers to structures that work in tension-compression. In this case, for each structure with a given loading scheme, the value of the load is determined at which the initial form of equilibrium becomes unstable. The calculation for the natural frequencies of the structure is carried out taking into account the distributed mass matrix and consists in solving the generalized eigenvalue

problem. When calculating for forced vibrations, it is considered that the structure is subject to the action of force factors that change over time according to a certain law.

For an approximate account of damping, the coefficients are selected in such a way that the decrements of the oscillations are constant at different natural frequencies. This provides the frequency-independent damping found in many machine tool designs.

To solve such a set of dynamics problems in a CAD environment, it is necessary to first build a solid 3D model of the spindle node, which can be researched using an appropriate CAE type system. To build a solid model, you can use the fast-progressing integrated CAD KOMPAS-3D. Starting with KOMPAS-3D v.13, the system has integrated the APM FEM program, developed by the scientific and technical center APM WinMachine [26, 27].

Thus, the availability of solid modeling toolkit and finite element method toolkit expands the area of research and significantly increases the labour productivity for the designer of modern metal-cutting equipment.

# 1. RESEARCH OF DYNAMIC SPINDLE-ARBOR-TOOL FOR MILLING MACHINE TOOL

## *1.1. Determination of dynamic characteristics by the method of transfer matrices*

The SAT elastic system (Figure 1.1) is considered as a beam on elastic supports with viscous damping [28-31]. The SAT system is divided into four sections, delimited by an abrupt change in the moments of the sections inertia, the concentrated mass of the gear wheel ($m_4$, $I_{4x}$) and the arbor ($m_0$, $I_{0x}$). The disturbing effect of the cutting process is force $P_0(\tau)$. When calculating the SAT dynamic characteristics, the initial parameters method in the matrix formulation is used [18, 28].

The differential equation of system oscillations is expressed through the amplitudes: displacements ($y_k$), the angle of rotation $\varphi_k \cdot L$, the bending moment $M_k L^2/EI$ and transverse force $Q_k L^3/EI$.

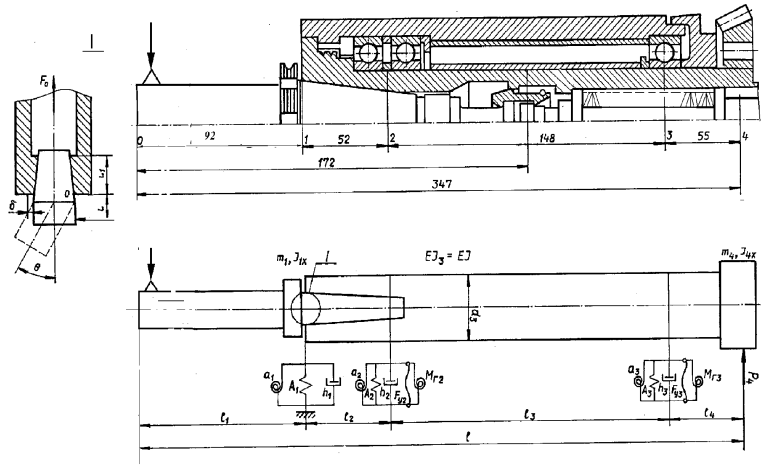


Figure 1.1. Elastic system spindle - arbor - tool

The transposed vectors of parameters at the SAT free ends (in the zero and fourth sections) without taking into account the external load have the form: $\mathbf{Y_0} = [y_0\ \varphi_0 L\ 0\ 0]^{\mathbf{T}}$; $\mathbf{Y_4} = [y_4\ \varphi_4 L\ 0\ 0]^{\mathbf{T}}$. The matrix equation without taking into account the external load takes the form:

$$\mathbf{Y_4} = \mathbf{P}\cdot\mathbf{Y_0} = \mathbf{M_4}\cdot\mathbf{A_3}\ \mathbf{R_3}\cdot\mathbf{R_2}\cdot\mathbf{T_1}\cdot\mathbf{G_0}\cdot\mathbf{Y_0}, \qquad (1.1)$$

where $\mathbf{M_4}$ – concentrated mass matrix, which takes into account the action of the concentrated force $P_4$ and the inertial forces moment of the gear; $\mathbf{A_3}$, $\mathbf{G_0}$ – transitional stiffness matrices of rods of length $L_3$ and $L_0$ [1]; $\mathbf{R_3}$, $\mathbf{R_2}$ – matrices of upper and lower supports, elastic concerning transverse $\varepsilon_i$ and angular $\sigma_i$ displacements, taking into account the centrifugal forces $z_i$, gyroscopic moments $g_i$ and damping in the support $f_i$ [18]; $\mathbf{T_1}$ – matrix of elastic-friction joint modeling the conical connection of the spindle and the shank of the arbor (Figure 1), elastic concerning the transverse $Q_1$ and angular $F_1$ displacements in the presence of a concentrated mass of the arbor $M_1$ $(I_{1x}\ \mu_1)$:

$$\mathbf{T_1} = \mathbf{M_1}\cdot\mathbf{Q_1}\cdot\mathbf{\Phi_1} = [1\ 0\ 0\ 0;\ 0\ 1\ 0\ 0;\ 0\ (\sigma_1 - \delta_1)\ 1\ 0;\ (\nu_1 - \varepsilon_1)\ 0\ 0\ 1]^{\mathbf{T}},$$

where $\nu_1 = \mu_1 w^2 L^3/EI$; $\delta_i = I_{1x} w^2 L/EI$ – amplitude values of the concentrated force and the inertial forces moment; $\varepsilon_i$, $\delta_i$ – coefficients characterizing the rigidity of the conical connection [3]. For this variant of calculations, the matrix of the hinge $\mathbf{T_1}$:

$$\mathbf{T_1} = [1\ 0\ 0\ 0;\ 0\ 1\ 0\ 0;\ 0\ (3.27 - 4.3\cdot 10^{-8} w^2)\ 1\ 0;\ (1.05\cdot 10^{-5} w^2 - 2071)\ 0\ 0\ 1]^{\mathbf{T}}.$$

Taking into account the external load in sections "0" and "4", equation (1.1) takes the form:

$$\mathbf{Y_4} = \mathrm{P}\ (\mathbf{Y_0} - \mathbf{S_0}) - \mathbf{S_4};$$

$$\mathbf{S_0} = [0\ 0\ 0\ (P_0L^3/EI)]^T = [0\ 0\ 0\ 0.32];\ \mathbf{S_4} = [0\ 0\ 0\ 0.2]. \quad (1.2)$$

The definition of a transfer matrix is reduced to the multiplication of six matrices of size 4×4. So at the SAT node ends, two of the four parameters in the matrices – columns $\mathbf{Y_0}$ and $\mathbf{Y_4}$ are equal to zero, which makes it possible to reduce the complexity of calculations by keeping only a part of the elements in the matrix **P** (the rest are marked with a sign ∗ ). To determine the pattern of the SAT node displacement, we detail expression (1.2):

$$\mathbf{Y_4} = \begin{bmatrix} * & * & * & * \\ * & * & * & * \\ g_{31} & g_{32} & * & g_{34} \\ g_{41} & g_{42} & * & g_{44} \end{bmatrix} \times \begin{bmatrix} y_0 \\ \varphi_0 L \\ 0 \\ -P_0L^3/EI \end{bmatrix} - \begin{bmatrix} 0 \\ 0 \\ 0 \\ P_4L^3/EI \end{bmatrix} \quad (1.3)$$

From the matrix equation (1.3) we select two linear equations concerning the sought parameters $y_0$ and $\varphi_0 L$:

$$\begin{aligned} & g_{31}y_0 + g_{32}\varphi_0 L - g_{34}\frac{P_0L^3}{EI} = 0;\ g_{41}y_0 + \\ & + g_{42}\varphi_0 L - g_{44}\frac{P_0L^3}{EI} - \frac{P_4L^3}{EI} = 0, \end{aligned} \quad (1.4)$$

where the complex coefficients $g_{ij}$ are functions of frequency, as well as inertial, dissipative and stiffness SAT parameters. Directly from (1.4), we obtain an expression for estimating the transverse displacements and angles of rotation in the $0_{th}$ section:

$$y_0 = \frac{\frac{P_0 L^3}{EI}\left(g_{34}g_{42} - g_{44}g_{32}\right) - g_{32}\frac{P_4 L^3}{EI}}{g_{31}g_{42} - g_{41}g_{32}};$$
$$\varphi_0 L = \frac{\frac{P_0 L^3}{EI}\left(g_{31}g_{41} - g_{44}g_{31}\right) - g_{31}\frac{P_4 L^3}{EI}}{g_{32}g_{41} - g_{42}g_{31}}. \qquad (1.5)$$

As an example, we give the expression $g_{41} = f(w)$:

$$g_{41} = 65041 + 0.01w^2 + 1.5\cdot10^{-10} w^4 - 1.4\cdot10^{-20} w^6 + \\ + j\,(5.7\,w - 2.1\,10^{-7} w^3 - 5.7\,10^{-16} w^5). \qquad (1.6)$$

From the found values of the initial parameters, we determine the elements of the matrices **P** using the equations:

$$\mathbf{Y_1 = T_1 G_0 Y_0\,;\ Y_2 = R_2 Y_1;\ Y_3 = A_3 R_3 Y_2\,;\ Y_4 = M_4 Y_3} \qquad (1.7)$$

For an SAT elastic system, it is enough to determine the first few, and most often the first one, natural frequency to know the resonant spindle rotation speed and the frequency at which self-oscillations occur. To compose the frequency equation, it is necessary to keep in the transfer matrix **P** of the system (1.1) the elements at the intersection of those rows whose numbers coincide with the numbers of zero rows of the matrix $\mathbf{Y_4}$ and those columns whose numbers coincide with the numbers of nonzero rows of the matrix $\mathbf{Y_0}$. Opening the determinant $g_{31}g_{42} - g_{41}g_{32} = 0$ from the elements retained in the matrix **P**, we find the natural frequency:

$$1{,}8\cdot10^{-43} w^{12} - 1{,}7\cdot10^{-31} w^{10} - 2{,}7\cdot10^{-22} w^8 - 0{,}6\cdot10^{-13} w^6 + 1{,}7\cdot10^{-5} w^4 - 3250\, w^2 + 0{,}2\cdot 10^{11} + j\cdot(2{,}3\cdot10^{-36} w^{11} - 2{,}4\cdot10^{-26} w^9 - 1{,}4\cdot10^{-17} w^7 - 6\cdot10^{-9} w^5 - 0{,}2\, w^3 - 5{,}9\cdot10^6 w) = 0.$$

From the frequency equation we determine the real values of the angular frequency: $w_1 = 2800$, $s^{-1}$; $w_2 = 104930$, $s^{-1}$; $w_3 = 956860$, $s^{-1}$, which corresponds to natural frequencies $f_1 = 445.86$ Hz; $f_2 = 16709$ Hz; $f_3 = 152366$ Hz.

To assess the displacements in the considered SAT sections, it is necessary to plot the amplitude diagrams of the initial parameters at the first natural frequency. The parameters $y_0$ and $\varphi_0 L$ in the zero section at frequency $f_1$ take the form:

$$\mathbf{Y_0} = [(2{,}1\cdot10^{-3}\text{-}2{,}5\cdot10^{-5}\,\text{j})\ (-1{,}9\cdot10^{-3}\text{-}2{,}5\cdot10^{-5}\text{j})\ 0\ 0]^{\mathbf{T}} =$$
$$= [2{,}1\cdot10^{-3}\ -1{,}9\cdot10^{-3}\ 0\ 0]^{\mathbf{T}}.$$

The complex data modules result in actual vibration amplitudes.

Using equations (1.7), we construct an elastic line of transverse displacements *y(z)* and amplitude diagrams of other initial parameters (Table 1.1, Figure 1.2). From equation (1.3) we obtain an expression for the frequency transfer function $W_0$ in terms of the action from the cutting process (at $\mathbf{S_4} = 0$):

$$W_0 = \frac{L^3}{EI}\left(\frac{k_{1R}k_{2R} + k_{1I}k_{2I}}{k_{2R}^2 + k_{2I}^2} - j\ \frac{k_{1R}k_{2I} - k_{1I}k_{2R}}{k_{2R}^2 + k_{2I}^2}\right),$$

where $k_{1R}, k_{2R}, k_{1I}, k_{2I}$ – real and imaginary terms of the transfer function, which are functions of frequency. For example, the term $k_{2R}$:

$$k_{2R} = g_{31R}g_{42R} - g_{31I}g_{42I} - g_{41R}g_{32R} + g_{41I}g_{32I},$$

where $g_{ijR(I)}$ – the real and imaginary parts of the term $k_{2R}$ obtained as a result of using the apparatus of transfer matrices and presented similarly to expression (1.6).

Table 1.1

**Values of initial parameters in various sections**

| Node number | 0 | 1 | 2 | 3 | 4 |
|---|---|---|---|---|---|
| $Z_i$ | 0 | 92 | 144 | 292 | 347 |
| $Y_i$ | $2.1 \cdot 10^{-3}$ | $1.59 \cdot 10^{-3}$ | $-1.7 \cdot 10^{-3}$ | $-2.8 \cdot 10^{-3}$ | $-5.25 \cdot 10^{-3}$ |
| $\varphi_i L$ | $-1.9 \cdot 10^{-3}$ | $-1.9 \cdot 10^{-3}$ | $-5.7 \cdot 10^{-2}$ | -0.14 | -0.18 |
| $M_i L^2 / EI$ | 0 | -0.08 | -0.16 | -0.51 | -0.64 |
| $Q_i L^3 / EI$ | 0 | -0.32 | -1.09 | -0.81 | -0.72 |

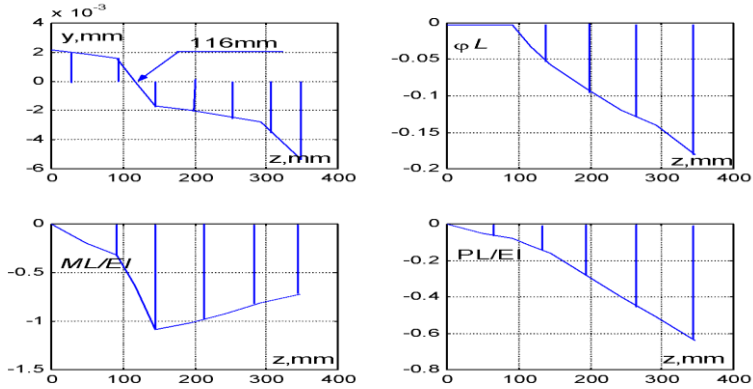


Figure 1.2. Elastic calculation lines of the spindle assembly

Figure 1.3 shows the Amplitude-Phase-Frequency Characteristic (APFC) of the spindle node, also called the Nyquist Plot (NP). In this case, it does not take into account the compliance of the Spindle–Arbor, which marked with a dashed line, in which the Arbor – Tool node is modeled by the matrix of a weightless section of the rod with the concentrated mass of the arbor.

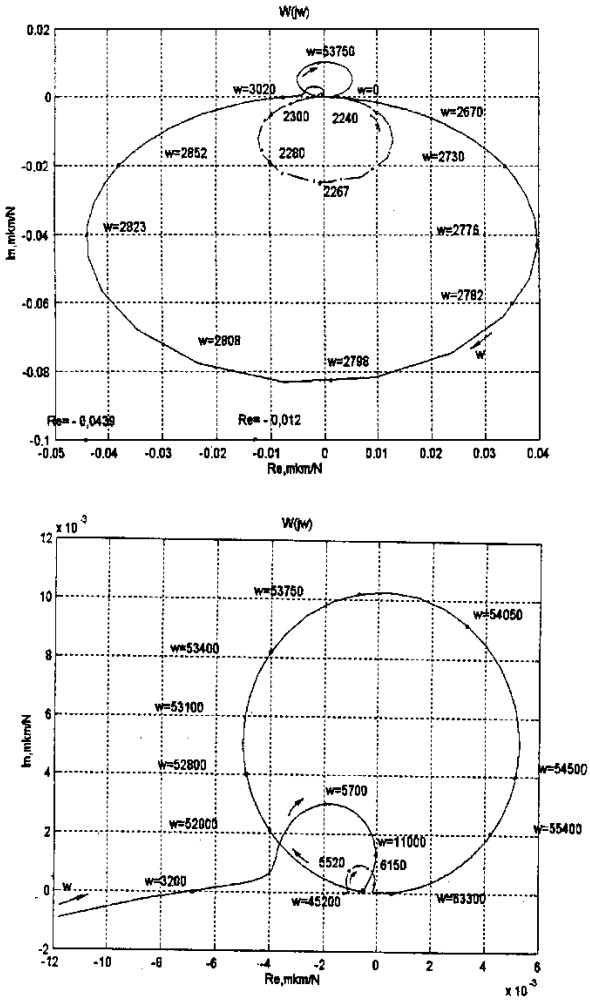


Figure 1.3. APFC of the spindle node:

- - - - - without taking into account the compliance of the conical connection: spindle – arbor;

——— taking into account the compliance of the conical connection: the spindle – arbor

Taking into account the compliance of the S–A joint (Figure 1.4) using the $\mathbf{T_1}$ hinge matrix leads to an increase in the vibration amplitude (from 0.025 to 0.083 μm/N) at increased frequencies. The modulus min$Re$ also decreases to -0.0439 μm/N.

The dynamic quality of the SAT system is influenced by the radial and rotational stiffness of the S–A, as well as the damping corresponding to these stiffnesses [20, 21]. Despite the insignificant mass of the arbor, the presence of backlash and dry friction forces leads to the appearance of nonlinear phenomena in the conical connection S–A and the need to take into account the forces of inelastic resistance and the phenomena of damping of oscillations in the general model of the system dynamics under consideration. A similar approach is presented in [22], where the dynamic subsystem of the spindle group "Clamping fork" of automatic lathes is investigated.

The damping forces (proportional to the displacement velocities) in the problem of the dynamics of the SAT system can be taken into account using the matrix of the concentrated damping force $\mathbf{D_1}$:

$$\mathbf{D_1} = [1\ 0\ 0\ 0;\ 0\ 1\ 0\ 0;\ 0\ 0\ 1\ 0;\ -f_1\ 0\ 0\ 1]^{\mathrm{T}},$$

where $f_1 = j\xi_1 L_1 w L^3/EI$ is defined similarly to $f_3 \in R_3$.

Then the hinge matrix $\mathrm{T}_1^*$ is represented as the product:

$$\mathbf{T}_1^* = \mathbf{T_1}\cdot\mathbf{D_1} = [1\ 0\ 0\ 0;\ 0\ 1\ 0\ 0;\ 0\ (\sigma - \delta_{\mathrm{i}})\ 1\ 0;\ (\nu_1 - \varepsilon_{\mathrm{i}} - f_1)\ 0\ 0\ 1]^{\mathrm{T}}.$$

The transfer matrix **P** and frequency characteristics change similarly. In Figure 1.5 and 1.6 show APFC, APC and other characteristics of the SAT system taking into account oscillation damping. Analysis of the APFC hodograph makes it possible to estimate the magnitude of the decrease in the amplitude (from 0.083, μm/N to $0.9\cdot10^{-3}$, μm/N) and the increase in the stability margin from (1-0.0439) to ($1-8.96\cdot10^{-4}$).

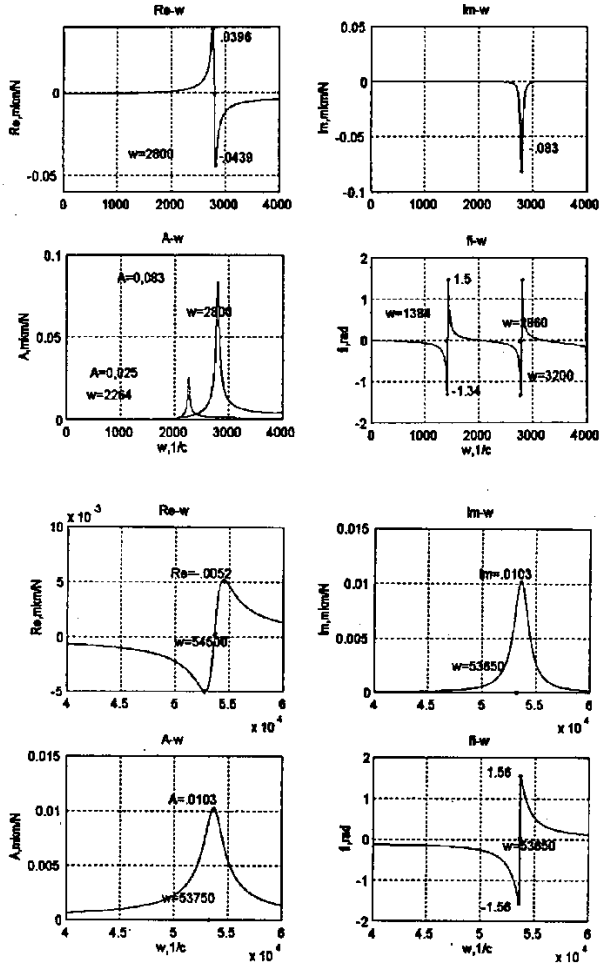


Figure 1.4. Frequency characteristics of the spindle node

With a wide variety of sizes and designs of tooling and cutting tools used on milling machines, the number of modifications of the spindle-support (S-Sp) assembly is limited. Therefore, it is advisable to look for a

solution in the form of two independent components: unchanged for a given standard size of the S-Sp node; customizable for A-T node.

This division makes it expedient to construct static and dynamic forms of the SAT node [3, 32, 33]. Using the beam formalization, similarly to [32], the static form $\Delta = f(L_k)$ was found, which connects the compliance of the SAT ($\Delta$) node and the length of the A-T console ($L_k$):

$$\Delta = 2{,}17 \cdot 10^{-5} + 2{,}35 \cdot 10^{-7} L_k + 3{,}9 \cdot 10^{-9} L_k^2 + 2{,}54 \cdot 10^{-11} L_k^3 . \quad (1.8)$$

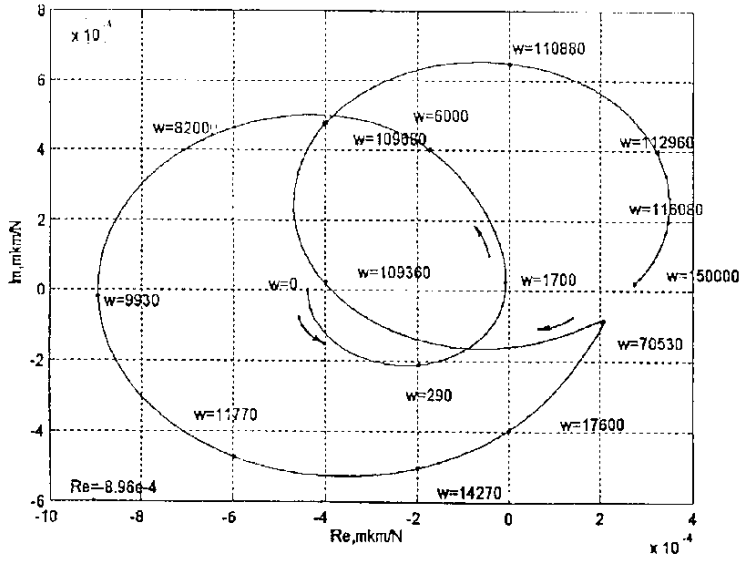


Figure 1.5. APFC of the spindle node (taking into account oscillation damping in the hinge)

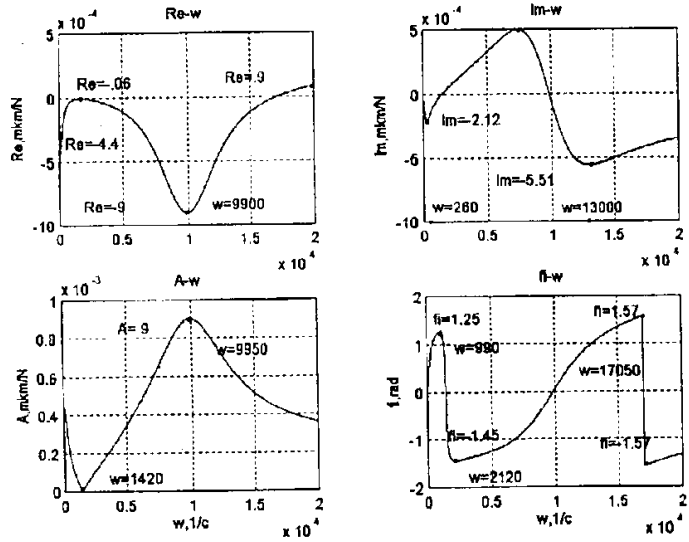


Figure 1.6. Frequency characteristics of the spindle node (including damping)

For some fixed version of the A–T design (arbor and boring cutter with an overhang $L_k$ = 32 mm), the compliance reduced to the cutting position is $3.4 \cdot 10^{-5}$mm/N. The mass $m_i$ reduced to the cutting position, the damping coefficient $h_i$ and the stiffness of the elastic link $c_i$ for SAT ($i$ = 1) and the Table-Workpiece ($i$ = 2) are determined by the following expressions:

$$c_1 = 1/\Delta = 2.9 \cdot 10^4, \text{ N/mm}; \; c_2 = 6{,}54 \cdot 10^3; \; h_1 = \frac{\lambda c_1}{2\pi^2 f_1} = 0.89, \text{ N·s/мм};$$

$$h_2 = 0.2\text{N·s/mm}; \; m_1 = \frac{c_1}{4\pi^2 f_1^2} = 0.0037\text{N·s}^2\text{/mm}; \; m_2 = 8.3 \cdot 10^{-4};$$

$$\mathrm{T}_p = \alpha \mathrm{a} \varsigma / \mathrm{V} = 0.0029\mathrm{s}^{-1},$$

where $\lambda$ – decrement of oscillation; $\alpha$ – coefficient of proportionality; $a$ – nominal thickness of the cut layer, mm; $\varsigma$ – chip shrinkage coefficient; V – cutting speed, m/min; $T_p$ – time constant of chip formation, $s^{-1}$.

### *1.2. Dynamics of an elastic system "Spindle-Arbor-Tool" considering inertial components*

High-precision spindle units of metal-cutting machine tools are difficult objects for modeling due to the static uncertainty and nonlinearity of the mechanical system, the difficulties of a complex mathematical description of existing phenomena. The general conceptual model of the "Spindle–Arbor–Tool" link includes relatively independent elastic-deformation and dynamic models [34-37].

The basis of the complex SAT mathematical model is the elastic-deformation model, without which it is impossible to solve any problem of calculating or modeling the spindle node. The methods of initial parameters [28, 38] and finite elements [28] are most widely used in these calculations. When using these methods, the SAT elastic link is considered as a rod system with distributed parameters, mounted in elastic supports.

The problem of elastic-deformation description for the SAT link of high-speed machines is a quasi-static problem, which involves the inclusion of not only physical but also inertial forces in the equilibrium equations, for example, centrifugal forces and gyroscopic moments acting on the bearing balls during rotation. In this case, however, a steady-state mode of motion is considered when the angular velocities of all elements are constant.

As the results of experiments [35] show, with an increase in the rotation frequency as a result of the action of centrifugal forces and gyroscopic moments on the balls, the elastic-deformation properties of ball bearings change. This is reflected in a decrease in stiffness with constant or even increasing axial load. The latter is since the ball bearing begins to

work as a three-link mechanism (outer ring–balls–inner ring) on the intermediate link of which (balls) centrifugal forces ($F_c$) and gyroscopic moments ($M_g$) act.

Considering the inertial forces $F_c$ and $M_g$ are associated with the criterion of the critical frequency $f_c$ [39]:

$$f_c = 4{,}46 \cdot 10^3 \frac{(F_p / z)^{2/3}}{\left(1 \pm \frac{d_b}{d_{av}} \cos\alpha\right) \sqrt{d_b^3 d_{av}} \sqrt[6]{K_g} \sin^{7/6}\alpha \sqrt[4]{r_1 + r_2 - d_b}}, \quad (1.9)$$

where $F_p$ – preload force, N;

$z$ – number of rolling elements in the bearing;

$d_b$ – ball diameter, mm;

$d_{av}$ – average bearing diameter, mm;

$r_1$, $r_2$ – radii of curvature of the raceways of the outer and inner rings, mm;

$$K_g = \sqrt{d_b} \cdot (C_n + C_b)^{-1.5},$$

where the coefficients $C_n$ and $C_b$ are determined either analytically or in a tabular way [39].

The applicability of quasi-static models, taking into account $F_c$ and $M_g$, is permissible in the case when the rotation frequency of the bearing ring exceeds the value of $f_c$ calculated by the formula (1.9). In this formula, the "+" sign corresponds to the rotating outer ring and the "-" sign to the rotating inner ring. It should be noted that with a rotating inner ring $f_c$ is greater than with a rotating outer ring.

Let us consider the procedure for calculating the dynamic characteristics of the rapidly rotating spindles of the SF68VF4 machine and its modifications [12-14]. The design and calculation diagram is shown in Figure 1.7, and the initial data in Table 1.2.

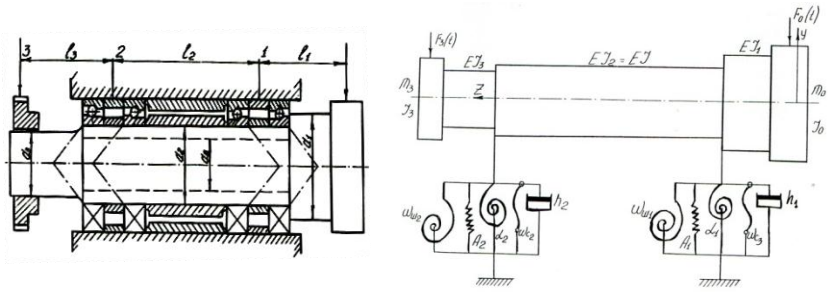

а б

Figure 1.7. Spindle node schemes: a – constructive; b – calculated

Table 1.2

**Initial data**

| $l$ | $l_1$ | $l_2$ | $l_3$ | $d_1$ | $d_2$ | $d_3$ | $d_i$ | $E$, MPa |
|---|---|---|---|---|---|---|---|---|
| 467 | 70 | 312 | 85 | 75 | 65 | 60 | 35 | $2{,}2 \cdot 10^5$ |

The use of the method of initial parameters assumes the division of the spindle into $N$ sections, delimited by an abrupt change in the diameters (moments of sections inertia $I_k$) of the concentrated mass (characterized by the value of $m_k$ and the moment of inertia $I_k$), support, external concentrated load ($F_k$), etc.

The spindle shown in Figure 1.7 is divided into three sections. At its ends, there are concentrated masses $m_0$ (boring bar) and $m_3$ (gear wheel). The front end of the spindle (in the zero section) is affected by disturbances from the cutting process – the force $F_0(t)$, and the rear end (in section 3) – by disturbances from the drive of the main motion $F_3(t)$.

Denoting in the $k$th section the amplitudes of the transverse displacement of the rod, the angle of rotation, the bending moment and the transverse force, respectively, through $y_k$, $\varphi_k$, $M_k$ and $Q_k$, we express the solution of the free vibrations differential equation of the rod (1.10)

$$y^{IV} - \frac{\lambda_k^4}{l_4} y = 0; \frac{\lambda_k^4}{l_4} = \frac{m_k \omega^2}{EI_k} \tag{1.10}$$

through the initial parameters:

$$\left\{ y(0); \varphi(0)\mathrm{l}; \frac{M(0)\mathrm{l}^2}{EI}; \frac{Q_0 l^3}{EI} \right\}. \tag{1.11}$$

Here $\omega$ – circular frequency of natural vibrations.

The general integral of equation (1.10) contains four arbitrary constants, which are expressed in terms of the initial parameters (1.11). The solution to equation (1.10) takes the form [40]:

$$Y(x) = Y(0)A_k(x) + \varphi_0 l B_k(x) + \frac{M(0)l^2}{EI} C_k(x) + \frac{Q(0)l^3}{EI} D_k(x), \tag{1.12}$$

where the functions $A_k$, $B_k$, $C_k$, and $D_k$ are calculated by the formulas

$$\begin{aligned} A_k &= \frac{1}{2}(ch\lambda_k + \cos\lambda_k); B_\mathrm{k} = \frac{1}{2\lambda_k}(sh\lambda_k + \sin\lambda_k); \\ C_k &= \frac{1}{2\lambda_k^2}(ch\lambda_k - \cos\lambda_k); D_\mathrm{k} = \frac{1}{2\lambda_k^3}(sh\lambda_k - \sin\lambda_k), \end{aligned} \tag{1.13}$$

where *ch*, *sh* – hyperbolic cosine and sine, respectively.

In matrix form, the parameter vectors at the free ends of the spindle without taking into account the external load have the form:

$$\mathbf{Y_0} = \begin{vmatrix} y_0 \\ \varphi_0 l \\ \dfrac{M_0 l^2}{EI} \\ \dfrac{Q_0 l^3}{EI} \end{vmatrix} = \begin{vmatrix} y_0 \\ \varphi_0 l \\ 0 \\ 0 \end{vmatrix}; \mathbf{Y_3} = \begin{vmatrix} y_3 \\ \varphi_3 l \\ \dfrac{M_3 l^3}{EI} \\ \dfrac{Q_3 l^3}{EI} \end{vmatrix} = \begin{vmatrix} y_3 \\ \varphi_3 l \\ 0 \\ 0 \end{vmatrix}. \qquad (1.14)$$

The relationship between the initial parameters and their values in a certain section *n*, given through the *n*-th boundary of the section is represented using a chain of matrices; starting from the zero section, they reach the left end of the spindle.

In the zero section, the concentrated force and inertial forces moment of the technological equipment (boring arbor) act, the amplitude values of which are respectively equal: $m_0\omega^2 I_0$ and $I_0\varphi\omega^2$.

Let us introduce the concentrated mass matrix $\mathbf{G_0}$:

$$\mathbf{G_0} = \begin{vmatrix} 1 & 0 & 0 & 0 \\ 0 & 1 & 0 & 0 \\ 0 & -\delta_0 & 1 & 0 \\ \nu_0 & 0 & 0 & 1 \end{vmatrix} = \begin{vmatrix} 1 & 0 & 0 & 0 \\ 0 & 1 & 0 & 0 \\ 0 & -1.57\cdot 10^{-4} & 1 & 0 \\ 0.0071 & 0 & 0 & 1 \end{vmatrix}, \qquad (1.15)$$

where $\delta_0 = I_0\omega^2 l / EI = m_0 R_0^2 \omega^2 l / EI$; $\nu_0 = m_0\omega^2 l^3 / EI$.

Here $m_0$ – concentrated mass of the arbor;

$R_0$ – the radius of inertia of the arbor.

Using the matrix $\mathbf{G_0}$, we transform the parameters $\mathbf{Y_0}$ when passing through the zero section.

The first section of the spindle has a distributed mass $\tilde{m}_1$ and a stiffness $EI_1$. The relationship between the parameters at its ends is determined by the transfer matrix of the $\mathbf{U_1}$ section:

$$\mathbf{U_1} = \begin{vmatrix} A_1 & \beta_1 B_1 & \frac{\beta_1^2 C_1}{\alpha_1} & \frac{\beta_1^3 D_1}{\alpha_1} \\ \frac{\lambda_1^4 D_1}{\beta_1} & A_1 & \frac{\beta_1 B_1}{\alpha_1} & \frac{\beta_1^2 C_1}{\alpha_1} \\ \frac{\alpha_1 \lambda_1^4 D_1}{\beta_1^2} & \frac{\alpha_1 \lambda_1^4 D_1}{\beta_1} & A_1 & \beta_1 B_1 \\ \frac{\alpha_1 \lambda_1^4 D_1}{\beta_1^3} & \frac{\alpha_1 \lambda_1^4 D_1}{\beta_1^2} & \frac{\lambda_1^4 D_1}{\beta_1} & A_1 \end{vmatrix} \quad (1.16)$$

For the case of considering an elastic spindle system with damping (in the presence of inelastic resistance), taking into account dissipative forces, the value $\alpha_1$ and $\lambda_1$ become complex. Value $\alpha_1$ and $\lambda_1$ should be introduced into the transfer matrix $\mathbf{U_1}$, expressed by the formulas:

$$\alpha_1 = \frac{EI_1}{EI}(1 + i\gamma); \quad (1.17)$$

$$\lambda_1^4 = \frac{(m_1\omega^2 - i\gamma\omega)l_1^4}{EI_1}, \quad (1.18)$$

where $\gamma$ – coefficient of inelastic resistance.

It has been experimentally established that for an angular contact ball bearing the coefficient $\gamma = 0.2...0.35$.

Coefficient $\beta$ depends on the ratio of the lengths of the sections: $\beta = l_1/l$.

Constants $A_1$, $B_1$, $C_1$, and $D_1$ are calculated by formulas (1.13) taking into account the values of $\lambda_1$ (1.19):

$$\begin{aligned} &\lambda_1^4 = 1.25 \cdot 10^{-4} - 0.03i;\ \lambda_1 = 0.38 - 0.16i;\ A_1 = 1 - 0.0012i; \\ &B_1 = 1 - 0.002i;\ C_1 = 0.5 - 4 \cdot 10^{-5} i;\ D_1 = 0.17 - 5.7 \cdot 10^{-6} i. \end{aligned} \quad (1.19)$$

After substitution of the initial data (Table 1.1), we obtain the transfer matrix of the first section $\mathbf{U_1}$ in the form:

$$\mathbf{U_1} = \begin{vmatrix} 1-0.0012i & 0.15-3\cdot10^{-4}i & 0.003-0.0009i & 0.00015-4.54\cdot10^{-5}i \\ 3.27\cdot10^{-5}-7.8\cdot10^{-3}i & 1-0.0012i & 0.04-0.012i & 0.003-0.0009i \\ 0.7-2.31i & 0.036-0.0012i & 1-0.0012i & 0.15-3\cdot10^{-4}i \\ 0.2-0.7i & 0.7-2.31i & 3.27\cdot10^{-5}-7.8\cdot10^{-3}i & 1-0.0012i \end{vmatrix} \quad (1.20)$$

In support 1, the shearing force changes abruptly by the value of the support reaction, for which, in the problem under consideration, not only the elastic and dissipative components of the reaction are taken into account, but also the centrifugal force $F_c$ and the gyroscopic moment $M_g$.

The validity of such an inclusion is associated with the fulfilment of the inequality $f \geq f_k$ for the considered finishing methods of boring, which are characterized by high speeds. According to the considered version of the spindle node, the supports are duplexed from bearings 2-446112 at the front and 2-446111 at the rear and are characterized by the following design data (Table 1.3).

Table 1.3

**Bearing characteristics**

| Type | $z$ | $d_b$, mm | $d_{av}$, mm | $r_1$, mm | $r_2$, mm | $D_1$, мм | $D_2$, мм | $C_n$ | $C_b$ | $F_p$, N |
|---|---|---|---|---|---|---|---|---|---|---|
| 2-446111 | 18 | 10.3 | 72.5 | 7.0 | 7.0 | 62.0 | 82.0 | $3.2\cdot10^{-4}$ | $3.3\cdot10^{-4}$ | 340 |
| 2-446112 | 18 | 11.1 | 77.5 | 7.5 | 7.5 | 68.0 | 88.0 | $3.2\cdot10^{-4}$ | $3.3\cdot10^{-4}$ | 340 |

The calculations performed by the method [12–14] showed that at the rotation frequency of the inner ring $f \geq 1100$ rpm, it is necessary to take into account the factors $F_c$ and $M_g$ (1.9).

The step force when passing through the support is taken into account by multiplying the parameter vector $\mathbf{Y_1}$ by the support matrix $\mathbf{R_1}$.

$$\mathbf{R_1} = \begin{vmatrix} 1 & 0 & 0 & 0 \\ 0 & 1 & 0 & 0 \\ 0 & -\beta_{c_1} & 1 & 0 \\ (-\varepsilon_1 - f_1 + \beta_{gb_1}) & 0 & 0 & 1 \end{vmatrix} = \begin{vmatrix} 1 & 0 & 0 & 0 \\ 0 & 1 & 0 & 0 \\ 0 & -0.0013 & 1 & 0 \\ (-1.1 \cdot 10^4 - 36.5i) & 0 & 0 & 1 \end{vmatrix} \quad (1.21)$$

where $\varepsilon_1 = c_1 l^3/EI_1$ – coefficient reflecting the elastic properties of the support and depending on the value of the stiffness coefficient $c_1$;

$f_1 = ih_1\omega l^3/EI$ – coefficient reflecting the properties of energy dissipation in the support and depending on the damping coefficient $h_1$;

$\beta_{c1} = F_{c1} l^3/EI$ – coefficient reflecting the action of centrifugal forces $Fc$;

$\beta_{g1} = M_{g1}\, l^2/EI$ – coefficient of reflecting the action of the gyroscopic effect, expressed through the gyroscopic moment $M_g$.

The value of these inertial loads can be calculated using the formulas [39]:

$$F_c = \frac{1}{2} m_b d_{av} \omega_t^2; \quad (1.22)$$

$$M_g = \pm I_b \omega_b\, \omega_t \sin\alpha, \quad (1.23)$$

where $m_b$, $I_b$ – mass and moment of inertia of the ball;

$\omega_b$, $\omega_t$ – relative and drift angular speed of the ball [12–14].

When the inner ring is rotating, the gyroscopic moment is directed so that it tends to move the rings apart (the "-" sign in formula (1.23)).

The drift rotational motion of the ball $\omega_t$ is characterized by the rotation of the movable coordinate system centred in the center of the ball around the *X*-axis of the stationary system, which coincides with the axis of rotation of the rings. The relative motion is characterized by the rotation of the ball in the moving coordinate system and is determined by the vector of the relative angular velocity $\omega_b$.

Using the hypothesis of the driving ring [39] (a ring concerning which there is no spinning of the ball), we write the expression for $\omega_t$ and $\omega_b$ with a driving outer ring:

$$\omega_t = \frac{\omega}{2}(1 - \frac{d_b}{d_{av}}\cos\alpha); \tag{1.24}$$

$$\omega_b = \omega \frac{(1 - \frac{d_b}{d_{cav}}\cos\alpha)\sqrt{1 + 2\frac{d_b}{d_{av}}\cos\alpha + (\frac{d_b}{d_{av}})^2}}{2\frac{d_b}{d_{av}}(\cos\alpha + \frac{d_b}{d_{av}})}. \tag{1.25}$$

After substitution of the initial data (Table 1.2 and Table 1.3), we obtain the numerical value of the matrix $\mathbf{R_1}$ (1.21).

The second section of the spindle has a distributed mass $\tilde{m}$ and stiffness $EI_2 = EI$. The relationship between the parameters at its ends is determined by the transfer matrix $\mathbf{U_2}$:

$$\mathbf{U}_2 = \begin{vmatrix} 0.95-1.6i & 0.66-0.21i & 0.19-0.08i & 0.046-0.03i \\ -0.47-9.9i & 0.95-1.6i & 0.55-0.37i & 0.19-0.08i \\ 8.74-44.97i & 2.52-10.09i & 0.95-1.6i & 0.66-0.21i \\ -2.96-141.5i & 8.74-44.97i & -0.47-9.9i & 0.95-1.6i \end{vmatrix} \tag{1.26}$$

In support 2, the shear force changes abruptly, which is taken into account by multiplying the parameter vector by the support matrix $\mathbf{R_2}$:

$$\mathbf{R}_2 = \begin{vmatrix} 1 & 0 & 0 & 0 \\ 0 & 1 & 0 & 0 \\ 0 & -\beta_{g2} & 1 & 0 \\ (-\varepsilon_2 - f_2 + \beta_{c1}) & 0 & 0 & 1 \end{vmatrix} = \begin{vmatrix} 1 & 0 & 0 & 0 \\ 0 & 1 & 0 & 0 \\ 0 & -9.25\cdot10^{-4} & 1 & 0 \\ (-24880-36.5i) & 0 & 0 & 1 \end{vmatrix}, \tag{1.27}$$

Similarly to matrix $\mathbf{R_1}$, matrix $\mathbf{R_2}$ takes into account the elastic and dissipative components of the reaction $\varepsilon_2$ and $f_2$, as well as the centrifugal force $F_c$ and the gyroscopic moment $M_g$ (1.27).

Similarly, the transition to the third section is carried out with the following value of the components:

$$\lambda_3^4 = \frac{(\tilde{m}_3 \omega^2 - i j \omega)\lambda_3^4}{E I_3} = 7.12 - 0{,}45i; \lambda_3 = 1.63 - 0.03i;$$

$$\alpha_3 = 0.48 + 0.14i; \quad \beta_3 = 0.18; \quad A_3 = 1.29 - 0.02i;$$
$$B_3 = 1.05 - 0.004i; \quad C_3 = 0.51 - 0.0007i; \quad D_3 = 0{,}17 - 0.0001i.$$

The transition matrix of the third section takes the form:

$$\mathbf{U_3} = \begin{vmatrix} 1 - 0.037i & 0.18 - 0.0014i & 0.028 - 0.009i & 0.0017 - 0005i \\ -0.009 - 0.84i & 1 - 0.037i & 0.31 - 0.1i & 0.028 - 0.009i \\ 2.18 - 7.28i & 0.13 - 0.45i & 1 - 0.037i & 0.18 - 0.0014i \\ 23.82 - 81.06i & 2.8 - 7.28i & -0.009 - 0.84i & 1 - 0.037i \end{vmatrix} \quad (1.28)$$

Finally, similarly to the previous one, the matrix of the concentrated mass $\mathbf{G_3}$ is introduced, which reflects the influence of the inertial forces of the gear wheel on the deformation pattern:

$$\delta_3 = j_3 \omega^2 l / EI = 0.0021;$$
$$V_3 = m_3 \omega^2 l^3 / EI = 0.14.$$

Matrix $\mathbf{G_3}$ is presented as

$$\mathbf{G}_3 = \begin{vmatrix} 1 & 0 & 0 & 0 \\ 0 & 1 & 0 & 0 \\ 0 & -\delta_3 & 1 & 0 \\ V_3 & 0 & 0 & 1 \end{vmatrix} = \begin{vmatrix} 1 & 0 & 0 & 0 \\ 0 & 1 & 0 & 0 \\ 0 & -0.0021 & 1 & 0 \\ 0.14 & 0 & 0 & 1 \end{vmatrix}. \qquad (1.29)$$

The parameters in the third section $\mathbf{Y_3}$, taking into account the external load, depending on the initial parameters $\mathbf{Y_0}$ under the following relationship:

$$\mathbf{Y_3 = P\ (Y_0 - S_0) - S_3}, \qquad (1.30)$$

where **P** is the transition matrix, which is the product:

$$\mathbf{\Pi = G_3 \cdot U_3 \cdot R_2 \cdot U_2 \cdot R_1 \cdot U_1 \cdot G_0}; \qquad (1.31)$$

$\mathbf{S_0}$ and $\mathbf{S_3}$ are columns matrix of external load:

$$\mathbf{S_0} = \begin{vmatrix} 0 \\ 0 \\ 0 \\ \frac{F_0 l_3}{EI} \end{vmatrix}; \qquad \mathbf{S_3} = \begin{vmatrix} 0 \\ 0 \\ 0 \\ \frac{F_3 l^3}{EI} \end{vmatrix}. \qquad (1.32)$$

The definition of the transfer matrix **P** is reduced to multiplying 7 matrices of size 4×4. Usually, at the ends of the spindle, two from the four parameters in the column matrices $\mathbf{Y_0}$ and $\mathbf{Y_3}$ are equal to zero, which makes it possible to significantly rationalize the computational work by storing only a part of the elements in the transfer matrix. Expression (1.30) in the expanded form is presented below

$$\begin{vmatrix} Y_3 \\ \varphi_3 l \\ 0 \\ 0 \end{vmatrix} = \begin{vmatrix} * & * & * & * \\ * & * & * & * \\ a_{31} & a_{32} & * & a_{34} \\ a_{41} & a_{42} & * & a_{44} \end{vmatrix} \cdot \begin{vmatrix} Y_0 \\ \varphi_0 l \\ 0 \\ -\dfrac{F_0 l^3}{EI} \end{vmatrix} - \begin{vmatrix} 0 \\ 0 \\ 0 \\ \dfrac{F_3 l^3}{EI} \end{vmatrix} \qquad (1.33)$$

In the matrix **P** of 16 elements, only six are preserved, which makes it possible to distinguish two linear equations for the sought variables $Y_0$ and $\varphi_0 l$:

$$Y_0 = \frac{\dfrac{F_0 l^3}{EI}(a_{34}a_{42} - a_{44}a_{32}) - a_{32}\dfrac{F_3 l^3}{EI}}{a_{31}a_{42} - a_{41}g_{32}};$$

$$\varphi_0 l = \frac{\dfrac{F_0 l^3}{EI}(a_{34}a_{41} - a_{44}a_{31}) - a_{31}\dfrac{F_3 l^3}{EI}}{a_{32}a_{41} - a_{42}a_{31}},$$

where the complex coefficients $a_{ij}$ are functions of the frequency $\omega$, as well as the inertial, dissipative, stiffness and geometric parameters of the SAT link. For operations with complex coefficients and matrices, the MATLAB software environment was used. The functions *real (z)*, *imag (z)*, *abs (z)*, and *angle (z)* return *real* (*R* (z)), imaginary (*Im* (z)), modulus ($\sqrt{R_e^2(z) + I_m^2(z)}$), and complex *z* argument ($arctg\dfrac{I_m(z)}{R_e(z)}$).

Using the initial data (see Table 1.2 and Table 1.3), we obtain a vector of initial parameters:

$$\mathbf{Y_0} = \begin{vmatrix} -0.0098 - 6.3 \cdot 10^{-4} i \\ 0.0026 - 3.3 \cdot 10^{-4} i \\ 0 \\ 0 \end{vmatrix}.$$

The modulus of the vector of initial parameters $|Y_0|$ found using MATLAB leads to real amplitudes of oscillations corresponding to harmonic disturbances.

$$|Y_0| = \begin{vmatrix} -0.0098 \\ 0.0026 \\ 0 \\ 0 \end{vmatrix}.$$

In the zero section, the vector $\mathbf{Y_0}$ is transformed using the matrix $\mathbf{G_0}$:

$$\mathbf{G_0 Y}_0 = \begin{vmatrix} -0.0098 - 0{,}0006i \\ 0.0026 - 0.0003i \\ -4.1 \cdot 10^{-7} + 5.18 \cdot 10^{-8} i \\ -6.95 \cdot 10^{-5} - 4.47 \cdot 10^{-6} i \end{vmatrix}.$$

Complex elements of matrices $\mathbf{Y_i}$ are determined in a similar way using the following equations:

$$\mathbf{Y_1 = U_1 G_0 Y_0 - S_0}; \qquad \mathbf{Y_2 = U_2 R_1 Y_1}; \qquad \mathbf{Y_3 = G_3 U_3 R_2 Y_2 - S_3}.$$

Table 1.4 summarizes the actual values of the parameters $Y_i$ and $\varphi_i l$.

Table 1.4

**Displacement parameters**

| Node number | 0 | 1 | 2 | 3 |
|---|---|---|---|---|
| $X$, mm | 0 | 70 | 382 | 467 |
| $Y_i$, mm | -0.0098 | -0.0087 | 0.0011 | -0.0049 |
| $\varphi_i l$ | 0.0026 | -0.0026 | -0.0056 | -0.0062 |

In Figure 1.8 shows the graphs of changes in the parameters $Y_i$ and $\varphi_i l$.

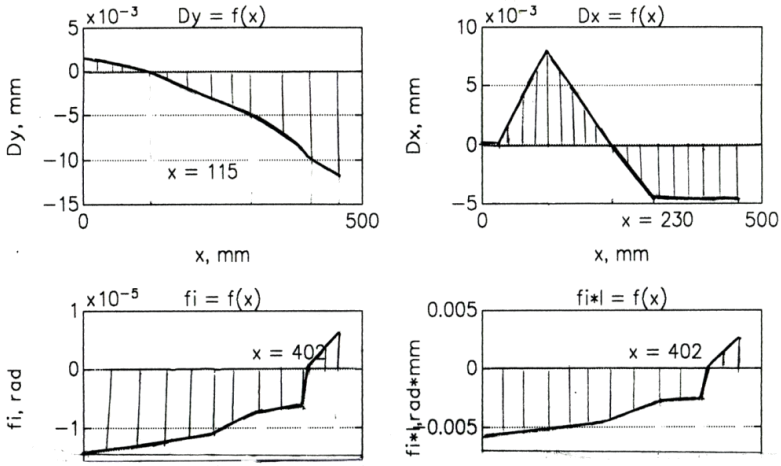


Figure 1.8. Calculation lines of spindle deflection

### *1.3. The dynamics of the cutting process*

One of the technological operations carried out on machines of the SF68PF3(F4) type is boring holes in parts of various nomenclature. Adjustment for boring operation using the above-considered version of the spindle assembly (the cantilever of which is considered a boring bar), shown in Figure 1.9.

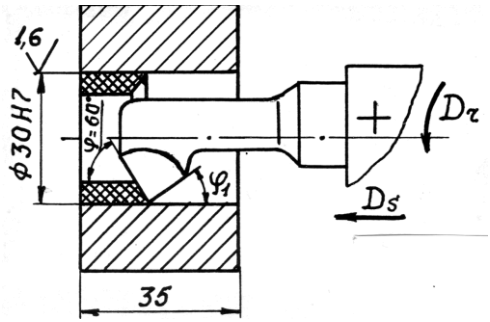


Figure 1.9. Fragment of adjustment for boring operation

Table 1.5 presents the initial data characterizing the cutting pattern when boring.

Table 1.5

**Initial data**

| Processed Material | Cutting tool | Cutting mode elements | | | | |
|---|---|---|---|---|---|---|
| | | *d*, mm | $f_r$, mm/rev | $f_m$, mm/min | *V*, m/min | *n*, min$^{-1}$ |
| Steel 45 GOST 1050-74 | Cutter 2142-0353 T15K6 GOST 9795-84 | 0,4 | 0,1 | 80 | 75 | 800 |

The transfer function of the cutting process is described by the well-known expression [Kudinov]:

$$W_p = \frac{k_p}{T_p^2\omega^2 + 1} - i\frac{k_p T_p \omega}{T_p^2\omega^2 + 1},\ k_p = 1,4\sigma_b \xi b;\quad T_p = \alpha\frac{\xi a}{V},$$

where $k_p$ – cutting coefficient, N/mm;

$T_p$ – time constant of chip formation, s;

$\xi$ – coefficient of shrinkage of the chips;

$a$, $b$ – thickness and width of chips, mm;

$\alpha$ – coefficient of proportionality, usually for stationary processing methods, $\alpha = 4.5$;

$\sigma_b$ – temporary resistance of the processed material, MPa.

In Figure 1.10 shows the frequency characteristics of the cutting process, and Figure 1.11 frequency hodograph of the cutting process, as the inertial link of the first order, obtained using the MATLAB software environment.

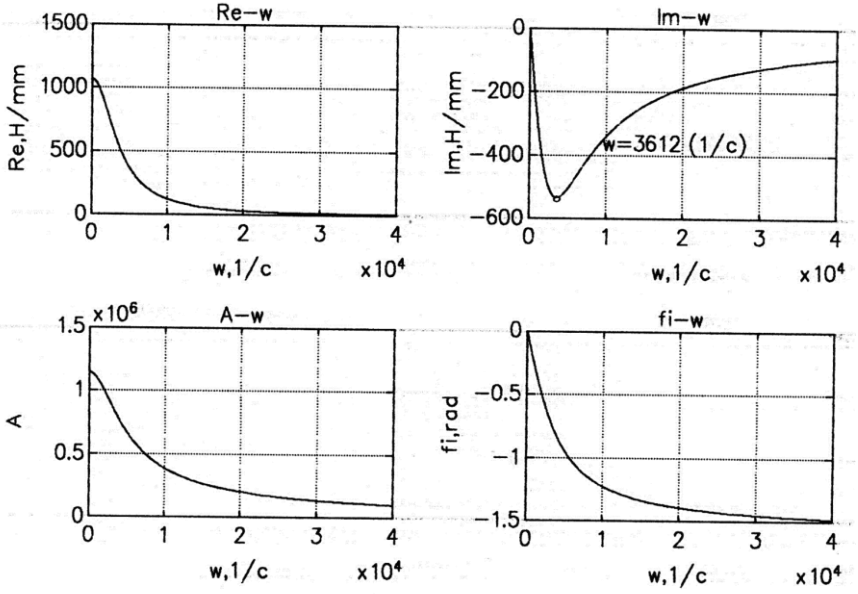


Figure 1.10. Frequency characteristics of the cutting process

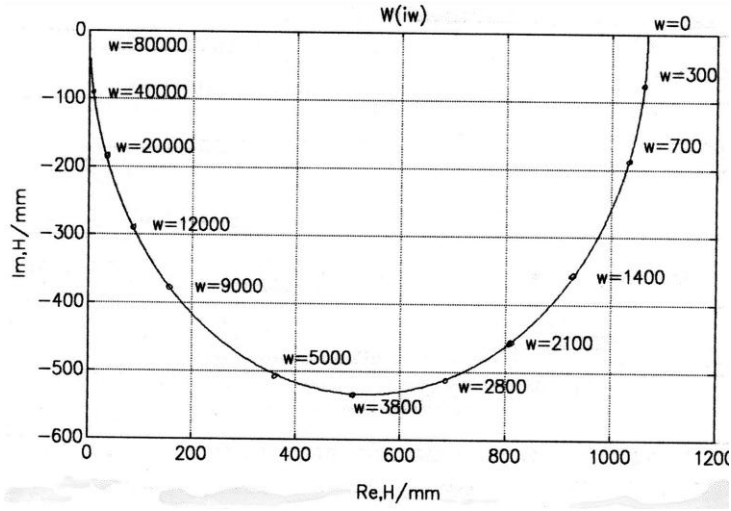


Figure 1.11. APFC of the cutting process

### *1.4. Dynamics of closed-loop subsystems*

Vibration stability of the closed-loop elastic system Spindle-Arbor-Tool-Cutting Process (SATCP) can be estimated by the open-loop system SATCP. In Figure 1.12 shows the APFC hodographs of the elastic link $W_{el}$ of the cutting process ($W_p$), open $W_{os}$ and closed $W_{cs}$ systems, and in Figure 1.13 hodograph APFC of the closed elastic system SATCP on an enlarged scale.

Similarly, taking into account the experimentally determined balance of elastic links compliance for the machine tool, the parameters of the dynamics model of the "Table-Workpiece" link were calculated:

$m_2 = 8.65$ (Ns$^2$/mm); $h_2 = 38.51$ (Ns/mm); $c_2 = 0.93\ 10^5$ (N/mm).

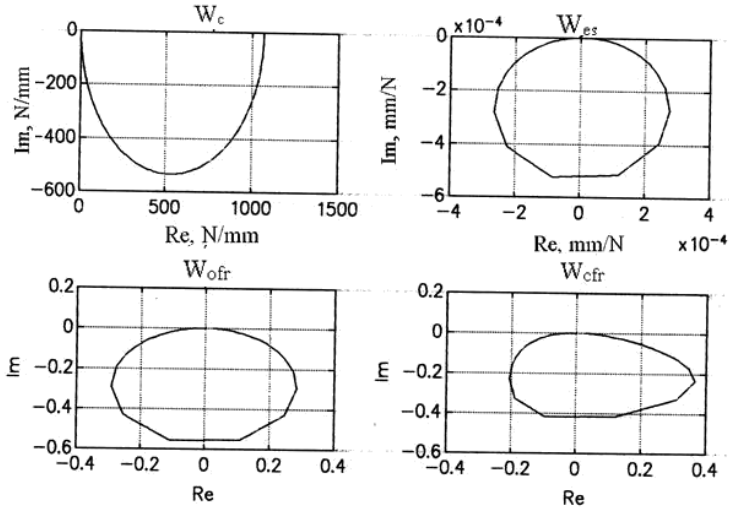


Figure 1.12. APFC of a dynamic system "Spindle-Arbor-Tool-Cutting Process"

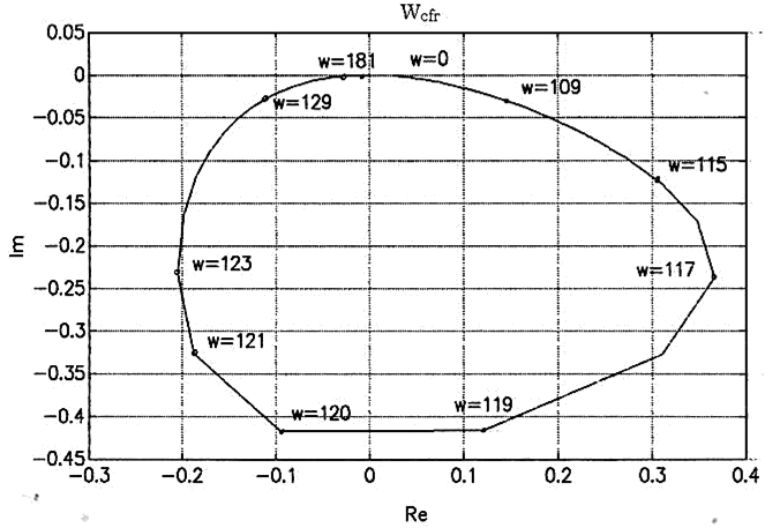


Figure 1.13. APFC of a closed-loop system "Spindle-Arbor-Tool-Cutting Process"

Based on expression (1.6), a dependence to determine the transfer function in a complex-frequency form (calculations in Appendix 2) was obtained. With the help of the MATLAB software environment, the software for analyzing the dynamics of the functioning of a technological system (TS) based on the SF68VF4 machine was developed. Figure 1.14 and Figure 1.15 show the frequency characteristics of the elastic system, which includes links: “Spindle-Arbor-Tool” + “Cutting Process” + “Table-Workpiece” ("SAT + CP + TW") and its amplitude phase-frequency characteristic.

Analysis of the frequency hodographs of the elastic links of the investigated TS shows that all of them are vibrostability, and with the addition of additional elastic links to the contour, the critical circular frequency of vibrations tends to decrease $j_n$ = 119.56 $s^{-1}$ for the "Spindle-Cantilever" link to $j_n$ = 106 $s^{-1}$ for the "SAT + CP + TW" system.

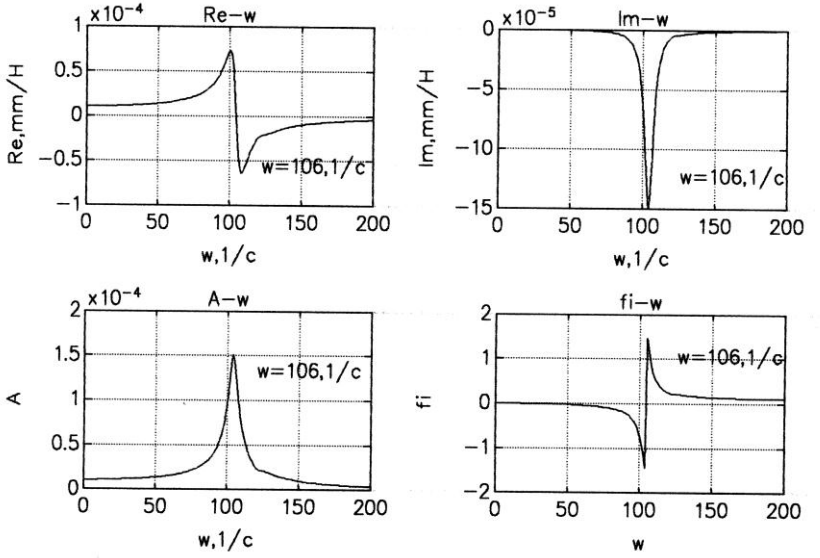


Figure 1.14. Frequency characteristics of the elastic system "Spindle-Arbor-Tool" –"Cutting Process" – "Table-Workpiece"

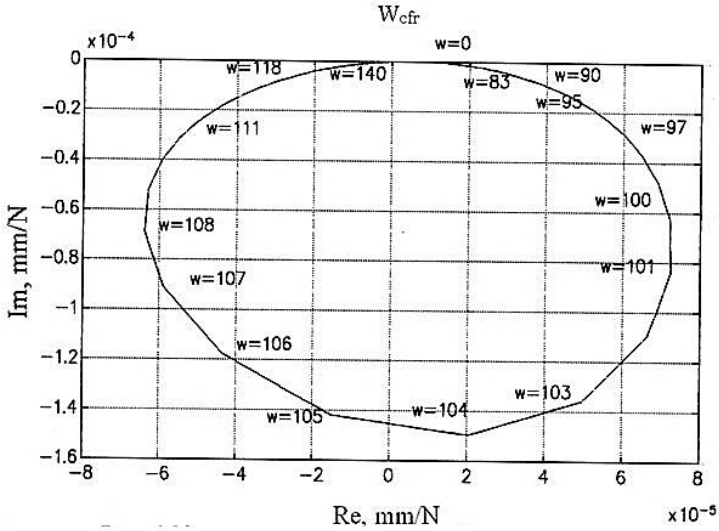


Figure 1.15. APFC of the closed-loop system "Spindle-Arbor-Tool" – "Cutting process" – "Table-Workpiece"

### *1.5. Sustainability of work processes machines based on single and two-parameter D-partitions*

To research the stability of the technological system, D-partitions method was used [30, 41, 42], based on the analysis of the number of roots of the characteristic equation lying in the right half-plane of the system parameter space.

The characteristic polynomial of the transfer function denominator, which determines stability, can be written as:

$$K_p\,[A(p) + B(p)] + A(p)\,B(p)\,[T_p\,p + 1] = 0 \qquad (1.34)$$

To determine the numerical values of the one-parameter D-partition parameters on the $K_p$ plane, we use a transformation of the form:

$$Kp = -\frac{A(p)\cdot B(p)\left(T_p p+1\right)}{A(p)+B(p)}. \qquad (1.35)$$

After passing to the Fourier transform $p = i\,\omega$ and separating the real and imaginary parts of expression (1.35), an algorithm is built and a program is written in the MATLAB environment.

To solve the problem, let us construct (i.e. determine the values of $K_p$ at which the given system is stable) the boundary of the D-partition in the plane of the complex parameter Kp; in this case, only the partition of the real axis will be of interest, i.e. actual values of $K_p$.

From (1.35) it follows that the boundary of the D-partition corresponds to the equation:

$$K_p = \frac{L_1h_2L_3T_p\omega^2 - h_1L_2L_3T_p\omega^2 + L_1L_2L_3 - h_1h_2L_3\omega^2 + L_1L_2L_4T_p\omega - h_1h_2T_pL_4\omega + L_1h_2L_4\omega + h_1L_2L_4\omega}{L_3^2 + L_4^2} - \qquad (1.36)$$
$$- i\frac{L_1L_2L_3T_p\omega + h_1h_2TL_3\omega^3 + L_1h_2L_3\omega + h_1L_2L_3\omega + L_1h_2L_4T_p\omega^2 + h_1L_2L_4T\omega^2 - L_1L_2L_4 + h_1h_2L_4\omega^2}{L_3^2 + L_4^2}$$

where $L_1 = c_1 - m_1\,\omega^2$; $\quad L_1 = c_2 - m_2\,\omega^2$;

$$L_3 = (c_1 + c_2) - (m_1 + m_2)\,\omega^2; \quad L_4 = (h_1 + h_2)\,\omega.$$

Here $m_1$, $h_1$, $c_1$ and $m_2$, $h_2$, $c_2$ are the parameters of the dynamic models of the elastic links "Spindle-Cantilever" and "Table-Workpiece", respectively.

The boundaries of the D-partition according to (1.36) are shown in Figure 1.16.

Two variants of adjustments were experimentally researched with a cantilever length of $1_k$ = 500 mm (the limiting capabilities of the SF68PF4 machine for programmed movement along the Z-axis) and $1_k$ = 300 mm. With an increase in the cantilever length, the cutting rigidity decreases from $K_p$ = 4466 N/mm (at $f$ = 181.4 Hz) to $K_p$ = 2008 N/mm and $f$ = 181.75

Hz. A contender for the stability region is the region *S*, to which the shading of the D-partition is directed. It can be shown that this area is not only a contender but also the area of sustainability itself. Indeed point (0,0), i.e. $K_p = 0$, lying in the region *S*, belongs to the stability region *D*(0), because at $K_p = 0$ the characteristic equation (3.26) turns into the equation

$$7.47\ 10^9 \cdot p^5 + 3\ 10^5 \cdot p^4 + 0.02 \cdot p^3 + 33.38 \cdot p^2 + 8624 \cdot p + 8.64 \cdot 10^6 = 0,$$

all five roots ($p_1 = -3.59$; $p_{2,3} = -0.13 + 0.77i$; $p_{4,5} = -0.074 \pm 0.72i$), which lie in the left half-plane of the roots. Thus, the system is stable if the actual values of $K_p$ change within the limits determined by the segment $\omega = 0$ ... $\omega = 1142$ ($s^{-1}$).

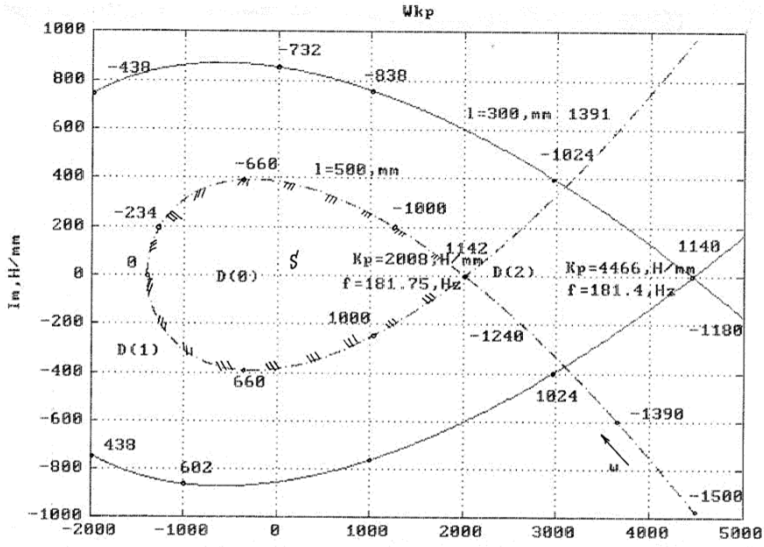


Figure 1.16. Parametric D-partition in the plane of the parameter $K_p$

The limiting value of rigidity $K_p^{lim}$= 2008 N/mm will correspond to the optimal value of the depth of cut:

$$d = \frac{K_p^{lim}}{1.4 \cdot \xi \sigma_B sin60^0} = 1.003\ mm.$$

The influence of two parameters $K_p(d)$ and $T_p(f)$ on the stability of the system can be effectively solved if these parameters enter linearly into the characteristic equation:

$$K_p M(p) + T_p Q(p) + R(p) = 0$$

where $M(p) = A(p) + B(p)$; $Q(p) = p \cdot A(p) \cdot B(p)$;

$$R(p) = A(p) \cdot B(p).$$

The boundary of the D-partition in the plane $K_p$ and $T_p$ is determined by the equations:

$$K_p M_1(\omega) + T_p Q_1(\omega) + R_1(\omega) = 0; \quad (1.37)$$

$$K_p M_2(\omega) + T_p Q_2(\omega) + R_2(\omega) = 0; \quad (1.38)$$

$$M(i\omega) = M_1(\omega) + iM_2(\omega);$$

$$Q(i\omega) = Q_1(\omega) + iQ_2(\omega);$$

$$R(i\omega) = R_1(\omega) + iR_2(\omega).$$

Solving the system of equations (1.37, 1.38) to $K_p$ and $T_p$, we obtain

$$K_p = \Delta_1 / \Delta; \quad T_p = \Delta_2 / \Delta, \quad (1.39)$$

where

$$\Delta = \begin{vmatrix} M_1(\omega) & Q_1(\omega) \\ M_2(\omega) & Q_2(\omega) \end{vmatrix} \quad (1.40)$$

$$\Delta_1 = \begin{vmatrix} -R_1(\omega) & Q_1(\omega) \\ -R_2(\omega) & Q_2(\omega) \end{vmatrix} \quad (1.41)$$

$$\Delta_2 = \begin{vmatrix} M_1(\omega) & -R_1(\omega) \\ M_2(\omega) & -R_2(\omega) \end{vmatrix} \qquad (1.42)$$

When A ≠ 0 for each value of ω according to the equations (1.39 ... 1.42) it is possible to determine the values of $K_p$ and $T_p$ and, thus, in the plane $K_p$ and $T_p$, to construct the boundary of the D-partition.

For the case of constructing a two-parameter D-partition in the problem of analyzing the stability of the SF68PF4 machine and finding the optimal cutting conditions $\{d_0, f_0\}$ during boring, the above values take the values:

$$M(i\omega) = (L_3 - L_1\omega^2) + iL_2\omega;$$

$$Q(i\omega) = (L_5\omega^4 - L_7\omega^2) + i(L_4\omega^5 - L_6\omega^3 + L_8\omega);$$

$$R(i\omega) = (L_4\omega^4 - L_6\omega^2 + L_8) + i(L_7\omega - L_5\omega^3),$$

where $L_1 = m_1 + m_2$; $L_2 = h_1 + h_2$; $L_3 = C_1 + C_2$;

$$L_4 = m_1 m_2;\ L_5 = m_1 h_2 + h_1 m_2;$$

$$L_6 = m_1 C_2 + h_2 h_1 + C_1 m_2;\ L_7 = h_1 C_2 + C_1 h_2;\ L_8 = C_1 C_2$$

Then the values of the main determinant Δ are equal to:

$$\Delta = L_9\omega^7 + L_{10}\omega^5 + L_{11}\omega^3 + L_{12}\omega$$

where $L_9 = -L_1 L_4$; $L_{10} = L_3 L_4 + L_1 L_6 - L_2 L_5$;
$L_{11} = L_2 L_7 - L_3 L_6 - L_1 L_8$; $L_{12} = L_3 L_8$.

The values of the partial determinants $\Delta_1$ and $\Delta_2$ are equal:

$$\Delta_1 = L_{14}\omega^7 + L_{15}\omega^5 + L_{16}\omega^3 - L_8\omega,$$

where $L_{14} = 2L_4L_6 - L_5^2$; $L_{15} = 2L_5L_7 - 2L_4L_8 - L_6^2$;

$L_{16} = 2L_8L_6 - L_7^2$.

$$\Delta_2 = L_{17}\omega^5 + L_{18}\omega^3 + L_{19}\omega,$$

where $L_{17} = L_4L_2 - L_1L_5$; $L_{18} = L_1L_7 + L_3L_5 - L_6L_2$;

$L_{19} = L_8L_2 - L_3L_7$.

Using equations (1.39 ... 1.42) we find expressions for $K_p$ and $T_p$:

$$K_p = \frac{L_{14}\omega^7 + L_{15}\omega^5 + L_{16}\omega^3 - L_8\omega}{L_9\omega^7 + L_{10}\omega^5 + L_{11}\omega^3 + L_{12}\omega}; \qquad (1.43)$$

$$T_p = \frac{L_{17}\omega^5 + L_{18}\omega^3 + L_{19}\omega}{L_9\omega^7 + L_{10}\omega^5 + L_{11}\omega^3 + L_{12}\omega}. \qquad (1.44)$$

The boundary of a two-parameter D-partition is determined by equations (1.43) and (1.44). To facilitate construction, Figure 1.17, *a*; *b* show the curves $K_p(\omega)$ and $T_p(\omega)$ with a critical frequency $w = 753$ ($s^{-1}$).

Using these curves, the boundary of the D-partition was built (Figure 1.18). It is shaded (hatched) according to the following rules: on the left, when walking in the direction of increasing $\omega$, if the main determinant is $\Delta > 0$, and on the right, if $\Delta < 0$.

Since the boundary of the D-partition for positive and negative values of $\omega$ coincides (the quantities, $K_p$ and $T_p$ are even functions of $\omega$, it is hatched twice from the same side. The singular lines [31] corresponding to the values: $\omega = 0$ and $\omega = \infty$ hatched singly so that near the point of the

conjugation of a straight line and a curve, the shaded and unshaded sides of the straight line and the curve were directed towards each other.

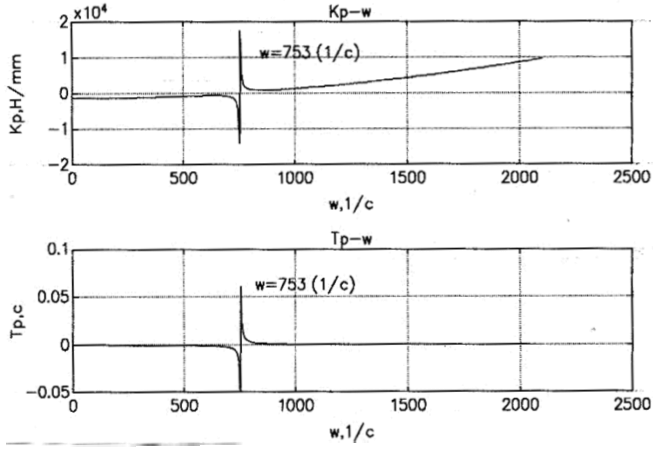


Figure 1.17. Cutting coefficient graphs $K_p$ and characteristics the time constant of chip formation $T_p$

The special straight line is obtained by equating to zero the coefficient of the characteristic equation at the leading term.

The stability region is formed by the positive part of the singular line and the D-decomposition curve.

The extremum points of the D-partition border: $K_p$ = 865, N/mm; $T_p$ = 0.0013, s can be associated with a pair of optimal cutting modes $f_0$ and $d_0$, according to the criterion of technological system stability based on the SF68VF4 machine. These values are determined by the formulas for the cutting process dynamics:

$$f_o = \frac{0.0013 \cdot 75 \cdot 10^3}{4 \cdot 60 \cdot 2.2 \cdot \sin 60} = 0{,}21 \; mm/rev;$$

$$d_o = \frac{865}{1.4 \cdot 2.2 \cdot 750 \cdot \sin 60} = 0.43 \; mm.$$

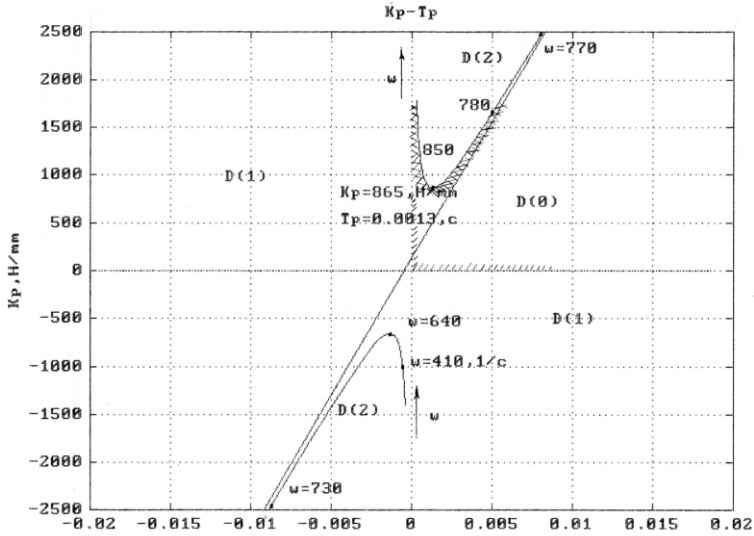


Figure 1.18. Two-parameter D-partition in the plane "$K_p$ – $T_p$"

### *1.6. System stability "Spindle-Arbor-Tool" by "D - partitions method"*

The tasks of assessing the stability of the SAT unit are included in the task of analyzing the technological system (TS) of a milling machine, the main power contour of which is the shaping units SAT and the Table–Workpiece with a closure on the side of the cutting process by force $P_0$. The transfer function $W_{cs}(p)$ for such a closed-loop system is [1]:

$$W_{\text{cs}}(p) = \frac{A(p) \cdot (T_p p + 1)}{K_p (A(p) + B(p)) + (T_p p + 1) \cdot A(p) \cdot B(p)}, \qquad (1.45)$$

where $A(p) = m_1 p^2 + h_1 p + c_1$; $B(p) = m_2 p^2 + h_2 p + c_2$; $K_p \approx 1{,}4 \cdot \varsigma \sigma_B b$.

Here $K_p$ – specific cutting force, N/mm; $\sigma_B$ – tensile strength of the processed material, MPa; $b$ – width of the cut layer, mm.

To assess the stability of a technological system based on a milling machine, taking into account the SAT system, we use the "D-partitions" method [41, 42], which consists in analyzing the number of roots of the characteristic equation (1.45) lying in the right half-plane of the studied parameters space. The characteristic polynomial of the transfer function denominator (1.45), which determines the stability, allows us to find the values of the parameters D-partition into $K_p$ planes:

$$K_p = -\frac{A(p) \cdot B(p) \cdot (T_p p + 1)}{A(p) + B(p)}. \qquad (1.46)$$

The program is developed in MATLAB environment. As a result of the numerical analysis, the stability regions were researched and the $D$ curves were constructed – the partitions in the parameter $K_p$ plane (Figure 1.19), where the shaded area denotes the region of the candidate for stability $s$. Since the point is (0,0), i.e. $K_p = 0$ belongs to the stability region $D(0)$, then this region is the stability region itself; in this case, only the division of the real axis – real values $K_p$ will be of interest. From expression (1.46) it follows that the boundary $D$-partition corresponds to the equation:

$$1.36 \cdot 10^{-6} p^5 + 6.5 \cdot 10^{-4} p^4 + 1.79 p^3 + (0.057 K_p + 715.8) p^2 +$$
$$+ (3.86 \times \times K_p + 591205) p + (35540 K_p + 1.9 \cdot 10^8) = 0.$$

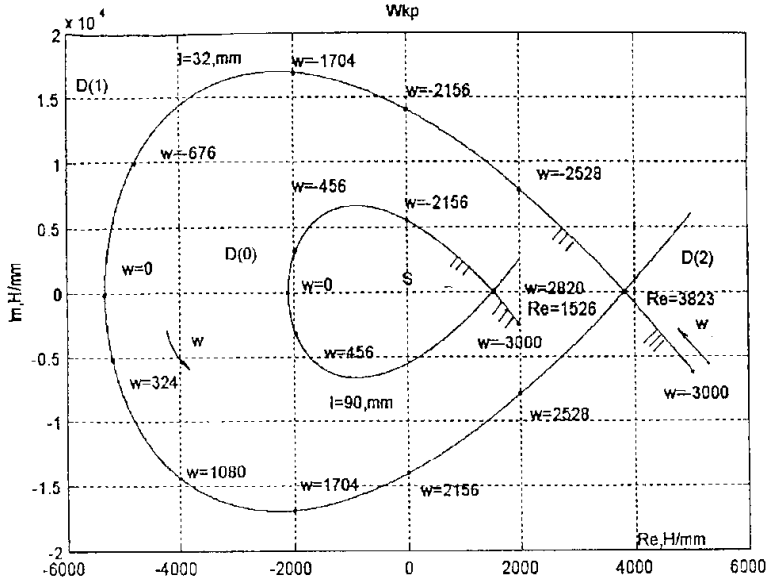


Figure 1.19. One-parameter *D*–partition

For $K_p$ = 0; m. (0,0) the polynomial of the 5th degree turns into the equation:

$$1.36 \cdot 10^{-6} p^5 + 6.5 \cdot 10^{-4} p^4 + 1.79 p^3 + 715.8 p^2 + 591205 p + 1.9 \cdot 10^8 = 0,$$

all five roots of which ($p_{1,2}$ = -0.9±8.1j; $p_{3,4}$ = -0.59± 7.9j; $p_5$ = -3.45) lie in the left half-plane of the roots. The resulting curves in the complex plane divide the space into three regions *D*(0), *D*(1) and *D*(2) and the transition through the boundary D-partition corresponds to the transition of the roots of the equation through the imaginary axis.

Analysis of the stability region in the $K_p$ parameter plane during boring with a cutter ($L_k$ = 32 mm) shows that the region is limited by the maximum value $K_p$ = 3823 N/mm at $f$ = 449 Hz. The corresponding limiting value of the chip width $b_{\text{lim}}$ = 1.8 mm (for structural steel $\varsigma$ = 2.2;

$\sigma_B$ = 750 MPa). With an increase in the length of the cantilever, the $K_p$ value sharply decreases – at $L_k$ = 90 mm, the stability region is limited to $K_p$ = 1526 N/mm, the frequency value $\omega$ = 2820 $s^{-1}$ and the limiting width $b_{\text{lim}}$ = 0.7 mm.

Analysis of the stability of the SAT dynamic system allows designers to determine the ultimate length without vibration processing $L_k$ when designing adjustments and assessing the technological capabilities of machine tools. For this purpose, we express the dynamic parameters: $m_1$, $h_1$, $c_1 = f(L_k)$, using the static form (1.8). Let us substitute the obtained expressions into the characteristic polynomial of the transfer function denominator (1.45) and obtain a dependence connecting $L_k^{'}$ with the dynamic parameters of the system:

$$L_k^{'} = 2.35\cdot10^{-7}L_k + 3.9\cdot10^{-9}L_k^2 + 2.54\cdot10^{-11}L_k^3 \quad (L_k^{'} \in \Delta);$$

$$L_k^{'} = -\frac{L_1(2734\text{-}0.004\omega^2) + 0.4L_2\omega}{(2734\text{-}0.004\omega^2)^2 + 0.16\omega^2} - \text{j}\cdot\frac{L_2(2734\text{-}0.004\omega^2) - 0.4L_1\omega}{(2734\text{-}0.004\omega^2)^2 + 0.16\omega^2},$$

where $L_1 = 3.6\cdot10^{-12}\ \omega^4 - 4.3\cdot10^{-6}\ \omega^2 + 1.04;\ L_2 = 9\cdot10^{-13}\ \omega^5 + 9.2\cdot10^{-9}\ \omega^3 + 0.003\ \omega).$

In Figure 1.20 is a graph showing the dependence of the magnitude $L_k$ on the frequency.

For the critical frequency $\omega$ = 2820, $s^{-1}$, an equation can be written to determine the limiting value $L_k^{\text{lim}}$:

$$2.35\cdot10^{-7}L_k + 3.9\cdot10^{-9}L_k^2 + 2.54\cdot10^{-11}L_k^3 = 1.09\cdot10^{-4},$$

having one real root $L_k^{\text{lim}}$ = 111 mm. Specific cutting force $K_p$ = 1194, N/mm characterizes the limiting possibilities for rigidity of the considered SAT node.

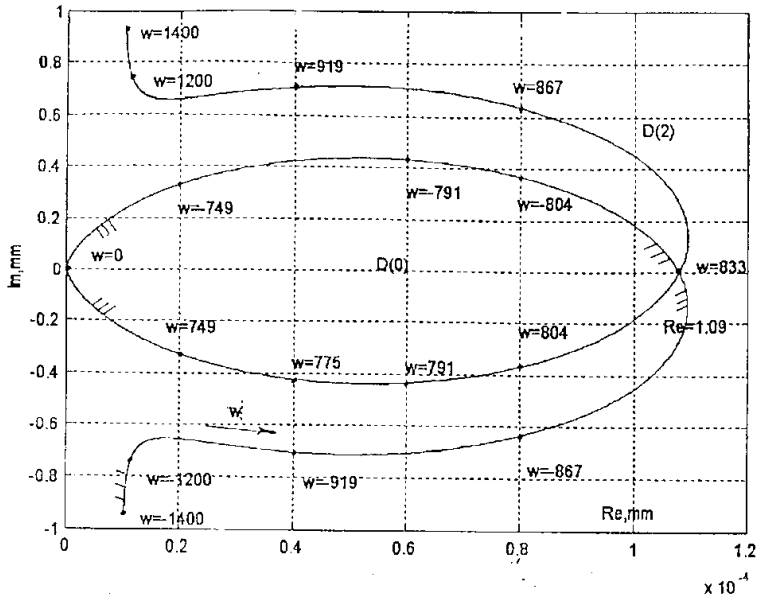


Figure 1.20. D - partition of parameter $l_k'$

Based on the research carried out, an assessment of the dynamic quality of the SAT system of the milling machine is given. For this, using the method of initial parameters, an elastic-deformation model of the system was developed, and also the diagrams of the amplitudes of the initial parameters were constructed. Formed static and dynamic forms of the system under consideration. The influence of the arbor link – the tool is modeled by the matrix of the elastic-friction joint, taking into account the oscillation damping at the joint boundary.

Using the apparatus D-partitions, the influence of the cantilever part of the node ($L_k$) on the stability of the system was estimated, the stability domains $D(0)$ in the complex plane were constructed, and quantitative estimates of the limiting rigidity of the cutting process $K_p$ and the length of the cantilever $L_k^{\lim}$ of the SAT dynamic system for milling machine were given.

# 2. RESEARCH OF THE CARRYING SYSTEMS DYNAMIC FOR MILLING-DRILLING-BORING MACHINES TYPE

Considering the design of the machine tool as a closed-loop dynamic system [1, 2, 3], most often they resort to schematizations obtained in the works of V.A. Kudinov [1].

In the general case, the equivalent elastic system of a machine tool (EESMT) of a Technological Complex (TC) of a milling-drilling-boring machine can be represented as a linear system with many degrees of freedom. The system includes several concentrated and distributed elements with corresponding inertial, elastic and dissipative characteristics.

## *2.1. Experimental research of the machine technological complex*

During preliminary experiments on the basic model TC of SF68VF4 [9, 29, 43], designed and manufactured at the Lugansk machine-tool plant, the following were obtained: displacement of the tool and the workpiece mounted on the rotary table under the action of the weight of the nodes and the forces $P_{x,y,z}$. At the same time, the most unfavorable carrier system layout of the nodes for the machine was considered (Figure 2.1) – the spindle is in the most extreme position; table with the workpiece in the lowest position.

To assess the influence of TC parameters on the level of dynamic compliance, it is necessary to construct vibration modes at those natural frequencies that are characterized by a relatively high level of vibrations of the tool and workpiece [44–47]. Analysis of the experimental amplitude-

frequency characteristics showed that low-frequency oscillations $f_i$ (Hz) are of greatest interest:

$$fi = \{16.5; 20.2; 24.6; 28.6; 44.2\}.$$

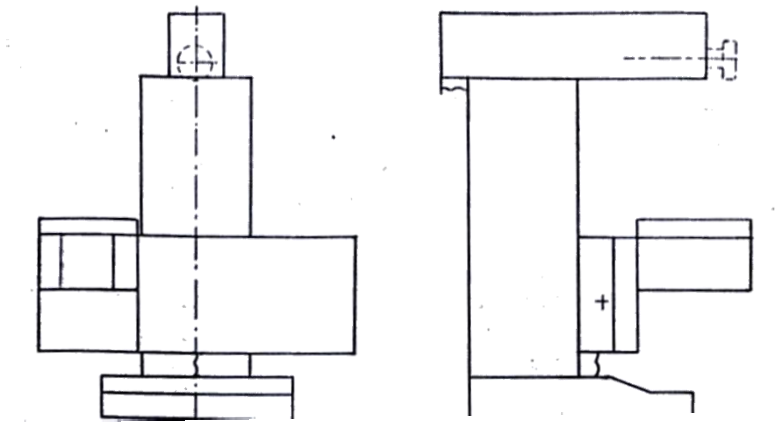

Scheme I

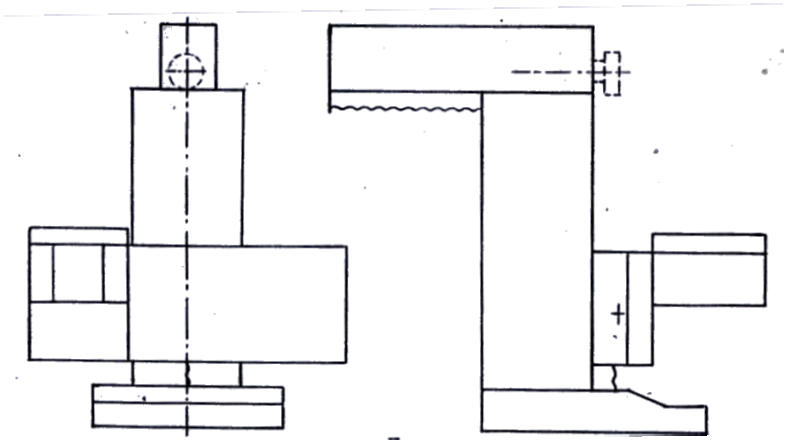

Scheme II

Figure 2.1. Layout of machine units

At the above frequencies, the vibration modes of the carrier system were calculated, the numerical values of which for the tool and workpiece are given in Table 2.1.

Table 2.1

**Nodal displacements**

| Node | direction | Natural frequency, Гц | | | | | |
|---|---|---|---|---|---|---|---|
| | | 16.5 | 20.2 | 24.6 | 28.6 | 40.9 | 44.2 |
| Cutting tool | X | -0,02 | -0,021 | 0,032 | 0,0063 | -0,0015 | 0,04 |
| | Z | -0,013 | -0,018 | -0,016 | 0,028 | 0,0034 | 0,02 |
| | Y | -0,012 | -0,027 | -0,03 | -0,0036 | -0,001 | 0,012 |
| | $F_x$ | $-0{,}26\cdot10^{-5}$ | $0{,}48\cdot10^{-5}$ | $0{,}11\cdot10^{-4}$ | $-0{,}34\cdot10^{-4}$ | $-0{,}2\cdot10^{-6}$ | $-0{,}22\cdot10^{-4}$ |
| | $F_z$ | $-0{,}14\cdot10^{-4}$ | $-0{,}35\cdot10^{-4}$ | $0{,}54\cdot10^{-4}$ | $-0{,}53\cdot10^{-5}$ | $-0{,}32\cdot10^{-6}$ | $0{,}27\cdot10^{-4}$ |
| | $F_y$ | $0{,}21\cdot10^{-4}$ | $0{,}13\cdot10^{-4}$ | $0{,}79\cdot10^{-6}$ | $0{,}19\cdot10^{-4}$ | $-0{,}61\cdot10^{-7}$ | $-0{,}72\cdot10^{-4}$ |
| Workpiece | X | 0,17 | -0,031 | -0,035 | $0{,}57\cdot10^{-3}$ | $-0{,}14\cdot10^{-4}$ | 0,047 |
| | Z | 0,065 | -0,1 | -0,04 | -0,021 | $-0{,}63\cdot10^{-4}$ | 0,046 |
| | Y | 0,037 | -0,11 | -0,034 | 0,036 | $-0{,}1\cdot10^{-3}$ | 0,053 |
| | $F_x$ | $-0{,}64\cdot10^{-5}$ | $0{,}78\cdot10^{-4}$ | $0{,}23\cdot10^{-4}$ | $0{,}15\cdot10^{-4}$ | $-0{,}23\cdot10^{-6}$ | $-0{,}96\cdot10^{-4}$ |
| | $F_z$ | $-0{,}1\cdot10^{-3}$ | $-0{,}12\cdot10^{-3}$ | $0{,}42\cdot10^{-4}$ | $-0{,}56\cdot10^{-4}$ | $-0{,}2\cdot10^{-6}$ | $-0{,}18\cdot10^{-4}$ |
| | $F_y$ | $0{,}14\cdot10^{-3}$ | $-0{,}89\cdot10^{-4}$ | $0{,}41\cdot10^{-4}$ | $-0{,}51\cdot10^{-4}$ | $-0{,}65\cdot10^{-6}$ | $-0{,}29\cdot10^{-4}$ |

This table shows the numerical values of linear displacements along the X, Y, Z axes (mm) and angular displacements relative to the $F_x$, $F_y$, $F_z$ axes (μm/mm).

Figure 2.2 graphically shows vibration modes at frequencies of 24.6 and 28.6 Hz, characterized by intense displacements of the spindle head in the YOZ plane and the table with the workpiece in the XOZ plane. In this case, elastic deformations were recorded with the most unfavorable arrangement of machine nodes (Figure 2.1, Scheme 1) and the following loading option: $P_{z1}$ = -1000 N; $P_{y1} = P_{x1}$ = 1000 N (attached at the end of the spindle).

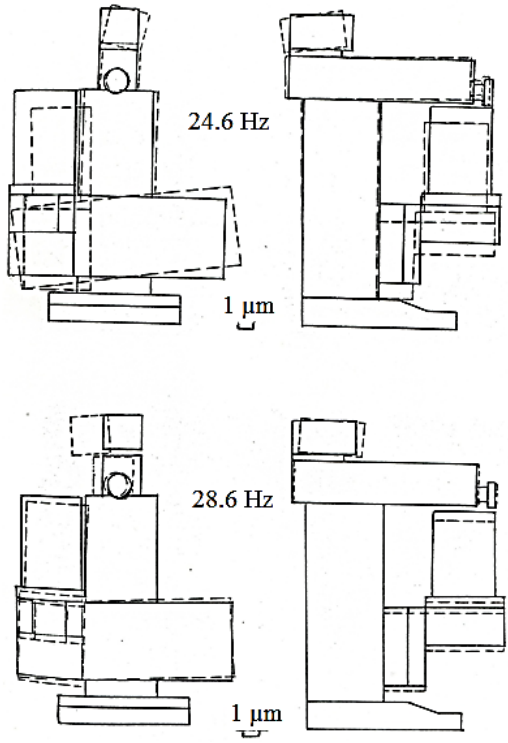


Figure 2.2. Machine vibration modes

The graphic representation of the deformations of the elastic links of the TC allows you to more clearly navigate the first stage of calculations and, therefore, improve the quality of the final calculations.

As shown by the results of the experimental research, the modules (amplitude-frequency characteristics) of the mutual characteristics ($W_{yx}$, $W_{yz}$, $W_{zx}$, $W_{xx}$) turned out to be significantly smaller in comparison with the modules of the main characteristics $W_{xx}$ and $W_{yy}$ in the entire frequency range (10 ... 400 Hz). This allows us to consider the vibrations of the machine tool along different coordinate axes to be weakly coupled and to

consider its spatial elastic system, consisting of two independent subsystems in the plane Y0Z and X0Z.

### *2.2. Classification of the main machine nodes*

Based on the displacements picture of the TC elastic system points, the classification of its main nodes with division into arrays and rods (elastic beams) is carried out [48–50]. The arrays include a tool, a rotary table, a workpiece and drives of feed and main movement (Table 2.2). As you know, arrays are understood as those elements of the machine, the proper deformations of which can be neglected in comparison with the contact deformations at their joints with other elements, which gives reason to represent them in the form of concentrated masses (Figure 2.3).

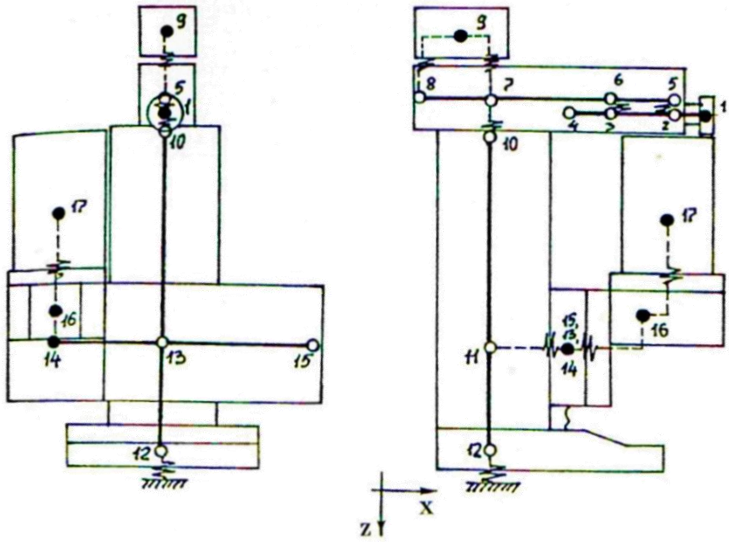


Figure 2.3. Design diagram of the machine

Table 2.2

**Classification of main nodes**

| Designation (machine part number) | Machine node |
|---|---|
| Lumped masses (arrays) | |
| 1 | Tool |
| 9 | Main drive |
| 14 | Feed drive (Y-axis) |
| 16 | Rotary table |
| 17 | Workpiece |
| Rods | |
| 2-3-4 | Spindle assembly |
| 5-6-7-8 | Spindle head |
| 10-11-12 | Column |
| 14-13-15 | Carriage |
| Joints | |
| 2-5, 3-6 | Spindle assembly supports |
| 7-9, 8-9 | Engine mounts |
| 7-10 | Spindle head – column |
| 11-13 | Column – carriage |
| 14-16 | Carriage – vertical table |
| 16-17 | Rotary table – workpiece |
| Support | |
| 12-0 | Foundation – base |

At the junction "rotary table-part", only the angular compliance in the YOZ and YOX planes will be taken into account.

The analysis of vibration modes made it possible to neglect the compliance of some joints, which significantly reduced the complexity of the preparatory stage of the calculation. For example, the compliance of the "column-carriage" and " carriage-table vertical" joints (Figure 2.3) should be considered only in the direction of feed movement (X-axis) and only during milling when the clamping mechanisms of these machines are turned off [51–53]. In other cases, these joints can be considered absolutely rigid. Links between points 7-9; 8-9 can be thought of as between points belonging to the same array and considered as a rigid constraint. The same applies to the pair 7-10. At the junction "rotary table - part", only the angular compliance in the YOZ and YOX planes will be taken into account.

The spindle of the machine is shown on the design diagram in the form of a weightless elastic beam with three concentrated masses on two elastic damping supports. The tool itself, if its deformations can be neglected (rigid boring bar, cutter), is represented as an array.

Thus, the real elastic system of the machine tool is replaced by a design diagram, i.e. a system with a finite number of freedom degrees in the form of 5 concentrated masses, connected by elastic and dissipative (dissipating vibration energy) elements, usually with linear characteristics. Each mass in the general case can have six degrees of freedom and its motion must be described by six second-order differential equations.

Reducing the labor intensity of the exact calculation of the above system is associated with the allocation of the main nodes that have the greatest impact on the level of dynamic quality indicators. The specific version of the selection depends, in turn, on the assigned task [54, 55]. So in the tasks of analyzing and assessing the accuracy of TC in the process of functioning (shaping the surfaces of parts), the spindle assembly is of decisive importance [44]. This is confirmed by the above researches using spectral analysis, which showed that in the circular patterns of the surface of the workpiece, only frequencies are present that are characteristic of the

vibration of the spindle assembly, i.e. the frequency spectrum of the spindle axis trajectory is copied entirely onto the part.

At the same time, another forming unit of the TC based on SF68F4 in the general picture of the deformation state significantly affects the quality of the products:

- at a vibration frequency $f$ = 16.5 Hz, there are intense vibrations of the rotary table and the carriage in the direction of the X and Y axes, which leads to torsion of the carriage housing and deformation at the column-carriage and carriage-table joints;

- at a frequency of $f$ = 20.2 Hz, rocking oscillations of the carriage with the table relative to the column in the YOZ plane occur, which are determined by the angular stiffness of the joint of the column slideways with the carriage in the YOZ plane with the total mass of the table workpiece and the carriage;

- at a frequency of $f$ = 28.6 Hz, there are also intense vibrations of the spindle head and the rotary table in the YOZ plane (Figure 2.7).

Although the elastic systems of the SF68F4 CNC machines type are a multi-mass connected system, the violation of the shape and quality of the machined surface depends, first of all, on such main and shaping units as the "Spindle-Tool" (S-T) and "Table-Workpiece" (T-W). Hence, we can conclude that the considered elastic system with a satisfactory approximation can be considered as two-mass. This is also confirmed by the constancy of the elastic moment amplitude at the lowest vibration mode.

The relative smallness of the vibration amplitudes (Figure 2.6), the presence of the elastic system preload, created by the cutting forces and the weight of its element, and the applicability of the superposition principle (in the range of acting disturbances) allow us to consider this system to be linear, described by a system of ordinary second-order differential equations.

### *2.3. Design schemes and models of a two-mass machine system*

For the machine of the drilling-milling-boring group of type SF68F4, the design diagram of the equivalent elastic system (Figure 2.4) includes two concentrated masses $m_1$ (subsystem "S-T") and $m_2$ (subsystem "T-W"), having linear characteristics of stiffness $K_1$ and $K_2$ and damping $h_1$ and $h_2$. Mutual influence of masses $m_1$ and $m_2$ occurs during cutting with a cutting rigidity coefficient $K_p$ [65]. With this formulation of the problem, the tool and the workpiece are connected by the cutting process.

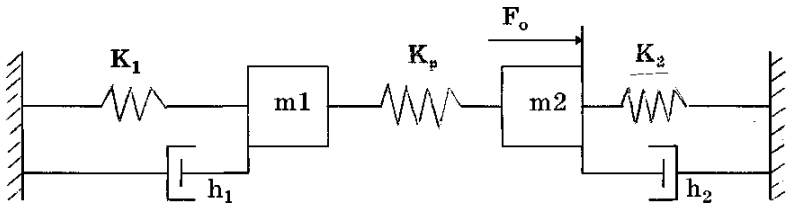


Figure 2.4. Design diagram of an equivalent elastic system: $m_1$ – the concentrated mass of the S-T subsystem; $m_2$ – the concentrated mass of the T-W subsystem; $h_1$ and $h_2$ – damping factors

The mutual influence of masses $m_1$ and $m_2$ occurs during cutting with a cutting stiffness coefficient $k$. Such a two-mass system can be described by a system of second-order differential equations with practically constant coefficients, i.e. vibrating links:

$$\begin{aligned} m_1\ddot{y}_1 + h_1\dot{y}_1 + k_1y_1 - k(y_2 - y_1) &= 0; \\ m_2\ddot{y}_2 + h_2\dot{y}_2 + k_2y_2 - k(y_2 - y_1) &= F_0, \end{aligned} \tag{2.1}$$

where $y_1$ – displacement of the S-T subsystem;
$y_2$ – displacement of T-W subsystem;
$F_0$ – the disturbing force arising from the imbalance of the spindle and the arbor, as well as the unevenness of the allowance.

To consider the dynamic properties, it is necessary to take into account the dynamic characteristics of the cutting process [1, 56, 57]; as an inertial link of the first order:

$$T_p\dot{F}_p + F_p = K_p y, \tag{2.2}$$

where $K_p = K_s \cdot b = (1.3 \ldots 1.5)\, \sigma_B \cdot b$ – cutting stiffness;
$K_s$ – specific cutting force, N/mm;
$b$ – chip width, mm;
$\xi$ – shrinkage factor;
$\sigma_B$ – ultimate tensile strength of the processed material, MPa;

The time constant of chip formation $T_p$ is determined by the dependence:

$$T_p = \alpha \cdot a \cdot \xi / V,$$

where $\alpha$ – proportionality coefficient;
$a$ – chip thickness, mm;
$V$ – speed, m/s;
$F_p$ – cutting force (reduced to the normal coordinate), N.

Taking into account the expression for the averaged stiffness S-T and equation (2.1) due to expression (2.2), it is possible to construct a system of integral-differential equations

$$\begin{gathered} m_1\ddot{y}_1 + h_1\dot{y}_1 + k_1 y_1 - F_p = 0; \\ m_2\ddot{y}_2 + h_2\dot{y}_2 + k_2 y_2 + F_p = F_0; \\ T_p\dot{F}_p + F_p = K_s(y_2 - y_1). \end{gathered} \tag{2.3}$$

Representation (2.3) is correct for the case when the velocities of the longitudinal feeds are relatively small in comparison with the values of the S-T transverse vibrations.

In operator form (using the Laplace transform: $p$ = d/dt), system (2.3) can be represented as:

$$\begin{aligned}(m_1p^2 + h_1p + k_1)y_1 - \frac{K_s}{T_pp+1}(y_2 - y_1) = 0;\\ (m_2p^2 + h_2p + k_2)y_2 - \frac{K_s}{T_pp+1}(y_2 - y_1) = F_0(p).\end{aligned} \quad (2.4)$$

After transformations, we obtain the transfer function W(p) for the disturbing action $F_0$(p):

$$W(p) = \frac{Z(p)}{F_0(p)} = \frac{A(p)(T_pp+1)}{K_s[A(p)+B(p)]+(T_pp+1)A(p)B(p)}, \quad (2.5)$$

where $Z(p)$ – output parameter of the system:

$$Z(p) = y_2(p) - y_1(p)$$

$$A(p) = m_1p^2 + h_1p + k_1;$$
$$B(p) = m_2p^2 + h_2p + k_2.$$

The relative displacement of the masses "S-T" and "T-W" is an algebraic sum: $Z = y_2$-$y_1$ and the movement of the part $y_2$ includes two components:

$y_2$' – caused by the action of the disturbing force $F_0$;

$y_2$" – caused by the action of the elastic link "S-T".

Based on the above interpretation, the structural diagram of the TC can be presented in the form:

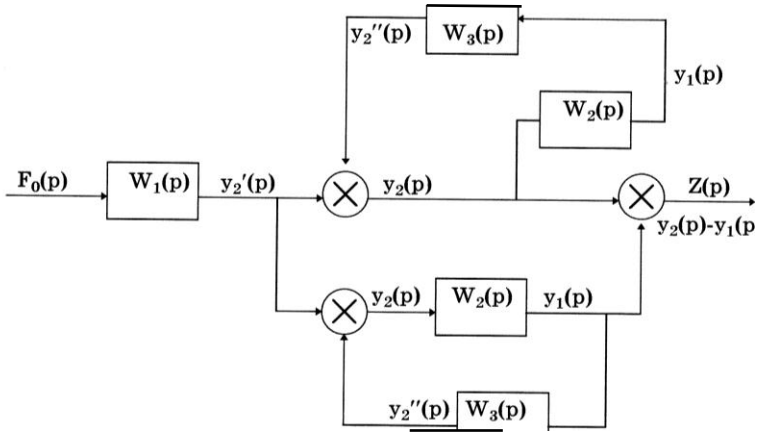


Figure 2.5. Block diagram of the machine technological complex

In Figure 2.5 shows the transfer functions $W_1(p)$, $W_2(p)$ and $W_3(p)$, reflecting the transformations: of the disturbing force $F_0$ into some components:

- component of the spindle displacement $W_1(p)$;

- the resulting displacement of the workpiece in the displacement of the link "S-T" $W_2(p)$;

- the influence of the cutting process and the resulting displacement of the elastic link "S-T" into the second component of the workpiece displacement $W_3(p)$, which reflects the dynamics of the link "T-W".

The transfer function in operator form for the TC as a whole can be represented as:

$$W(p) = \frac{W_1(p)[1-W_3(p)]}{1-W_2(p)W_3(p)} \quad (2.6)$$

# 3. SPINDLE DYNAMICS UNDER RANDOM IMPACT

## *3.1. Frequency response of the Spindle-Cantilever system*

The elastic link "Spindle-Cantilever", S-C (Figure 1.7) can be considered as a system with inertial, elastic and damping parameters. The force $F_0(t)$ (input signal) and displacement $y(t)$ (output signal) are represented as stationary random processes (functions of time) with a Gaussian distribution law and zero mathematical expectation. Based on the motion equation of the S-C system:

$$m\ddot{y} + h\dot{y} + ky = F_0(t) \tag{3.1}$$

a frequency response $H(f)$ can be defined, which identifies the relationship between the amplitudes $|H(f)|$ and the phases $\varphi(f)$ of the output and input signals.

As is known [58], the frequency response of the system is defined as the Fourier transform $Y(f)$ of the system's response (in this case, it is the displacement $y(t)$) to the impulse action:

$$Y(f) = \int_0^\infty y(t) e^{-j2\pi ft} dt = H(f),$$

where $f$ – cyclic frequency in Hz.

The transformation of both sides of equation (3.1), because the Fourier transform of the impulse action of the force $F(t) = \delta(t)$ is equal to unity, is

the following expression in terms of the amplitude and phase characteristics:

$$H(f) = |H(f)| e^{-j\theta(f)}, \tag{3.2}$$

where

$$|H(f)| = \frac{1/k}{\sqrt{(1-(f/f_n))^2 + (2lf/f_n)^2}}; \tag{3.3}$$

$$\phi(f) = arctg \frac{2lf/f_n}{1-(f/f_n)}. \tag{3.4}$$

In expression (3.4), we introduced the notation:

$$l = \frac{h}{2\sqrt{km}}; \; f_n = \frac{1}{2\pi}\sqrt{\frac{k}{m}},$$

where $l$ – dimensionless quantity characterizing the damping of oscillations;

$f_n$ – natural frequency of continuous oscillations (in Hz).

Note that the dimension $|H(f)|$ coincides with the dimension of compliance, mm/N.

When considering a specific spindle assembly [31, 40] (Figure1.7, Table 1.2), which has the following parameters: {$m$ = 25 N; $h$ = 13.96 N·s/mm; $K$ = 38900 N/mm} – coefficient $l$, natural frequency $f_n$ and resonant frequency $f_r$ take the following values: {$l$ = 0.02; $f_n$ = 19.86 Hz; $f_r$ = 19.84 Hz}. The resonant frequency is obtained by minimizing the denominator of the expression $|H(f)|$ (3.3).

The graphs $|H(f)|$ and $\varphi(f)$ given by expressions (3.3, 3.4) are shown in Figure 3.1 (a, b).

Analysis of expressions (3.3, 3.4) and the resulting graphs allows you to calculate and evaluate:

1. The shift of the amplitude characteristic maximum downward relative to the natural frequency $f_n$ at $l \le 1/\sqrt{2}$. This maximum corresponds to the resonant frequency $f_r$ and the numerical value: $|H(f_r)| = \frac{1/k}{2l\sqrt{1-l^2}} = 6{,}43 \cdot 10^{-4}$, mm/N.

2. The bandwidth at the half-energy level of the amplitude characteristic as $B_r = f_2 - f_1$, and in the case of small damping $l \le 0{,}1$ is expressed in terms of $f_r$:

$$B_r = 2l \cdot f_r = 0.79 \text{ Hz}.$$

3. A change in the phase response from $0^0$ at frequencies much less than $f_n$ to $180^0$ at frequencies much higher than $f_n$. The shape of the curve in Figure 3.1, b depends on the coefficient $l$, but at $f = f_n$ the phase $\varphi(f)$ is equal to $90^0$ regardless of the damping value $l$.

When solving problems of the dynamics of technological systems, the most common law of change in the force $F(t)$ as an input characteristic is the harmonic law: $F(t) = F_0 \cdot \sin 2\pi ft$.

The output signal is the displacement of the spindle node $y(t)$, obtained by multiplying the amplitude of the input signal $F_0$ by the amplitude characteristic of the system, determined by the formula (4.3) and the phase shift $\varphi(f)$ by an amount equal to the phase characteristic (3.4):

$$y(t) = \frac{F_0 \sin\left(2\pi ft - \varphi(t)\right)}{k\sqrt{\left(1 - \frac{f}{f_n}\right)^2 + \left(2lf / f_n\right)^2}}.$$

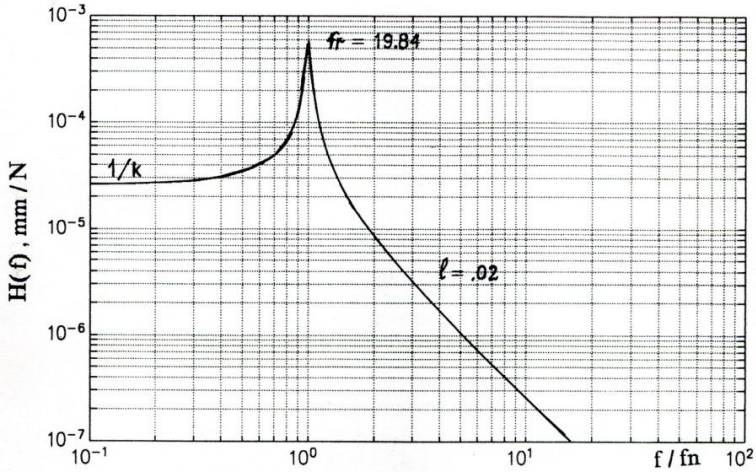


a

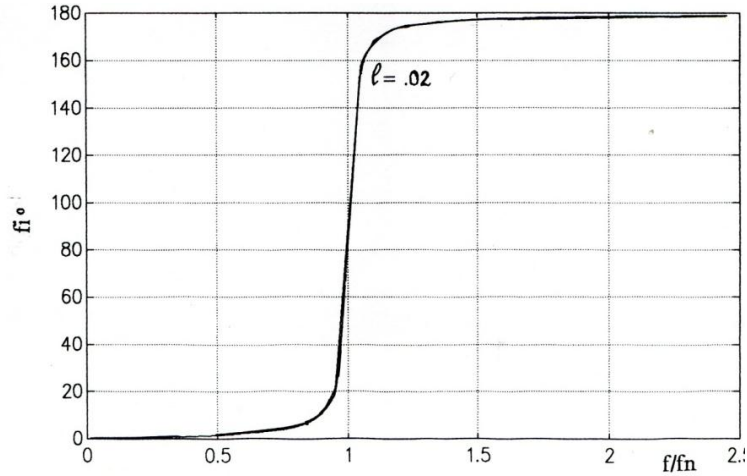


b

Figure 3.1. Amplitude (a) and frequency (b) parameters of the spindle

For a linear system with constant parameters, the frequency response $H(f)$ depends only on frequency and does not depend on either time or the type of the input signal.

The harmonic function $F(t)$ at the input produces an output that is also a harmonic function with the same frequency; the deviation of the amplitudes of the output and input signals is equal to the amplitude characteristic of the system $|H(f)|$ (3.3), and the phase shift between the output and input signals is set by the phase characteristic of the system $\varphi(f)$ (3.4).

The best approximation to the real picture of the TS oscillations is a polyharmonic process, which is the sum of the constant component and a certain number of harmonics. The experiment showed that the periodic oscillatory process of the spindle assembly is formed by the sum of two harmonic processes with frequencies of 20 and 28 Hz, i.e. the period of this process is 0.2 s.

As is known, the presence of periodic components in a random process appears itself in the form of delta functions in its spectral density (sharp peaks). These peaks, especially at low amplitudes, can be mistakenly attributed to narrow-band random noise. But in the estimate of the spectral density calculated at high-frequency resolution, periodic components of even small amplitudes appear in the form of sharp maxima, which will grow in proportion to the decrease in the bandwidth.

Let us consider the dependence $F(t)$ as a polyharmonic signal with amplitudes $F_1$ and $F_2$:

$$F_i(t)=F_1 sin 2\pi f_1 t + F_2 sin 2\pi f_2 t, \qquad (3.5)$$

which is mixed with the process at the output of the random noise generator (white noise signal).

The change in forces in time at the input of the spindle assembly has a complex character, simulated by a noise signal. With the help of the "Signal Processing" software environment [35], the procedure for reproducing a complex signal and identifying the periodicity is carried out as follows:

1) set the interval and discreteness of the time axis:

$$t = 0: 0.001: 0.6;$$

2) introduce an expression for the signal $F_i(t)$ (4.5);

3) simulate a random component of the "white noise" type using the "rand (normal)" command [59] with zero mean and unit variance;

4) combine the signal by superimposing a random component on a harmonic one:

$$Z_i(t) = F_i(t) + 2\text{rand}(t);$$

5) calculate the spectral density $S_F(iw)$:

$$S_F(i\omega) = \lim_{T\to\infty} \frac{\bar{Z}_i(i\omega) \cdot \bar{Z}_i^*(i\omega)}{2T},$$

where $\bar{Z}_i(i\omega) = \bar{Z}_i^*(-i\omega)$ – complex conjugate functions representing the Fourier transform for the function $Z_i(t)$.

To implement the last stage of the calculation and subsequent graphical interpretation of the random function, we will use the discrete Fourier transform.

With the number of samples N = 256 (256-point fast Fourier transform (FFT)), the FFT of the signal $y_i(t)$ can be realized using Matlab – the "fft" command:

$$\bar{Z}_i(i\omega) = fft(y_i(t), 256).$$

For the first 128 points (the other 128 points are symmetric) of the $S_F(iw)$ spectrum, graphical representation is carried out using the commands:

$f$ = 1000·(0:127)/256;
plot ($f$, $S_F(i\omega)$(1:128)).

Figure 3.2 shows a graph of the synthesized signal $Z_i(t)$ (Figure 3.2, a) and a graph of the spectral density (Figure 3.2, b). A clear separation of the two harmonics was achieved by reducing the sampling step "filtering high-frequency noise components".

The obtained frequency characteristics of the input parameters allow us to proceed to solve the problem of elastic-deformation description in a random setting.

Let us establish the dependences connecting the spectral and mutual spectral densities of the spindle (rod) oscillation parameters in the *i*-th section with the corresponding characteristics of the disturbing forces. Denoting the Fourier transform of the rod deflection in the $i_{th}$ section through $\overline{y}_i(j\omega)$, we have:

$$\overline{y}_i(j\omega) = \int_{-\infty}^{\infty} \xi_i(t) e^{-j\omega t} dt \text{ , (3.6)}$$

where $\xi_i(t)$ – transverse displacement of the rod in the *i*-th section at time *t*; $\omega=2\pi f$.

As is known [60], if the domain of integration is not bounded, then the transformation $\overline{y}_i(j\omega)$ does not exist for a stationary random process expressed by the ensemble of realizations $\xi(t)$.

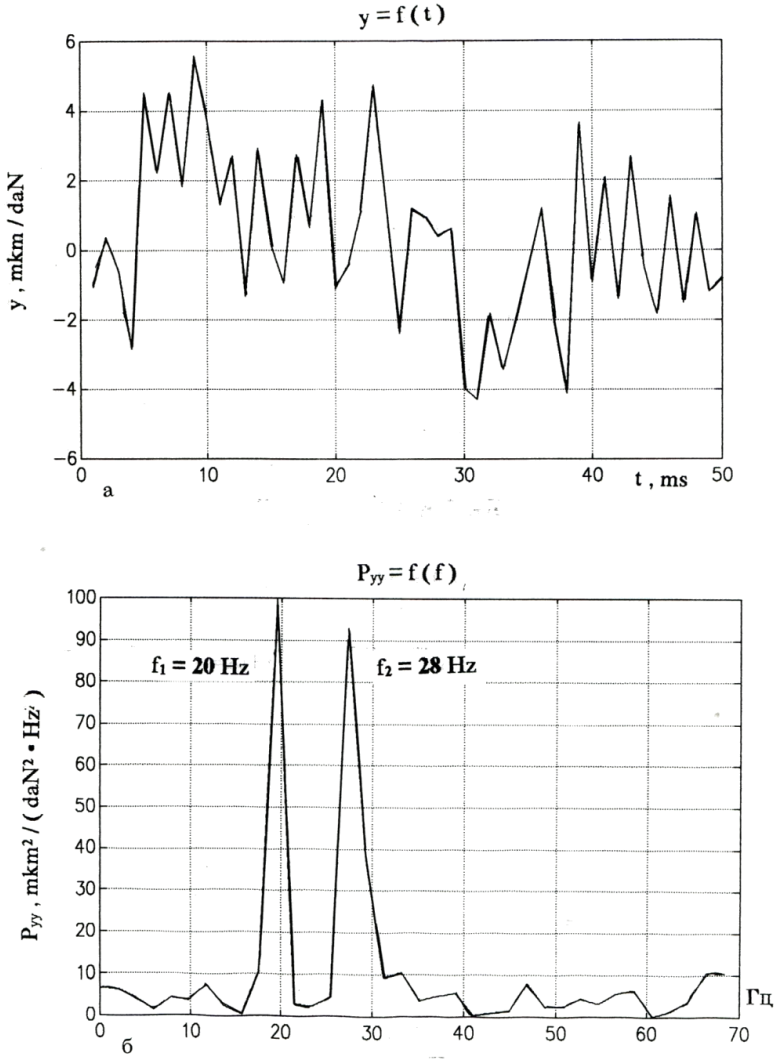


Figure 3.2. The output signal (a) and its spectrum (b)

### *3.2. Finite Fourier Transform and Spectral Windows*

If the elastic link "S-T" is considered as a linear system (additive and single-row) with constant parameters, then to ensure physical feasibility, the lower limit of integration in the Fourier transform is equal to 0, and not - ∞.

In practice, the parameter ξ(*t*) is specified on an interval of finite length *T*, so that $\bar{y}(j\omega)$ it is estimated by the finite (discrete) Fourier transform:

$$\bar{y}_T(j\omega) = A(j\omega, T) = \int_0^T \xi(t) e^{-j\omega t} dt$$

As a result of the final Fourier transform, the current spectrum $A(j\omega, T)$ of the signal $y_i(j\omega)$ is obtained.

The limitation of the observation interval is accompanied by spectrum distortion, which is modeled by a rectangular weight function *w* (*t*):

$$w(t) = \begin{cases} 1, \ 0 \le t \le T ; \\ 0, \text{ in other cases.} \end{cases}$$

The weight sequence {*w*(*t*)} is called a rectangular window [58, 61].

Let the signal ξ(*t*) be defined on the interval $t \in (-\infty, \infty)$ and is characterized by the Fourier transform $A(j\omega)$. If the observation time is limited by the interval $t \in [-T/2, T/2]$, then the signal $\xi_1(t) = \xi(t) \cdot w(t)$ with frequency частотой $\omega_1$ is actually observed. Integral Fourier transform $F\left|\xi_1(t)\right|$ – the spectrum of this signal is represented as:

$$F\left|\xi_1(t)\right| = A_1(j\omega) = \int_{-\infty}^{\infty} \xi(t)\, w(t) e^{-j\omega t} dt = T \int_{-\infty}^{\infty} A\,[j(\omega - \omega_1)] \frac{\sin(\omega_1 T/2)}{\omega_1 T/2} d\omega_1.$$

The transition to a finite interval $T$ leads to the convolution of the Fourier transform of the original signal $\xi(t)$ of infinite length with a function of the form $\text{sinc}(x) = (\sin x)/x$, where $x = \omega T/2$, as a result of which the calculated signal spectrum $\xi(t)$ turns out to be distorted (spectrum spreading).

For the harmonic signal $\xi(t)$ characterizing the rod displacement, the following expression is used for the autocorrelation (covariance) function:

$$R_{\xi\xi}(\tau) = \frac{\xi_0^2}{2}\cos\omega_0\tau \ ,$$

where $\tau$ – time shift, s;
$\omega$ – circular frequency, $s^{-1}$.

The harmonic signal can be represented as:

$$\xi(t) = \frac{\xi_0(e^{j\omega_0 t} - e^{-j\omega_0 t})}{2j} \ ,$$

whose two-sided spectrum consists of two components

$$A(j\omega) = \frac{\xi_0^2}{4}[\delta(\omega+\omega_0) + \delta(\omega-\omega_0)],$$

represented in the form of two delta functions localized at the points $\omega = -\omega_0$ and $\omega = \omega_0$.

Analysis of this signal on a limited interval gives the current spectrum $A_1(j\omega)$:

$$A_1(j\omega) = \frac{\xi_0^2}{4}\left[\frac{\sin[T(\omega+\omega_0)/2}{T(\omega+\omega_0)/2} + \frac{\sin[T(\omega-\omega_0)/2}{T(\omega-\omega_0)/2}\right].$$

This spectrum is continuous and dispersed along the frequency axis. Its shape is determined by the sum of two functions sinc($\omega T/2$), which are oscillatory with damped side lobes. The main lobes of the sinc($\omega T/2$) functions have equal levels $\xi_0^2 T/2$, and their centers coincide with the frequencies $\omega = \pm\omega_0$. With an increase in the interval $T$, the spectrum is compressed, which is concentrated near the initial frequencies $\omega = \pm \omega_0$.

Analysis of the spectral rectangular window (the spectrum of the window's sample sequence) shows that it has a lobe shape – the main and side lobes (Figure 3.3, a) [61].

The presence of side lobes leads to leakage of components whose frequencies are far from the main maximum of the spectral window, and to a strong distortion of the spectral estimate.

The level of the side lobes of the window is characterized by the value of $K$ (dB):

$$K = 20 \log A(0)/A_1,$$

where $A_1$ – maximum value of the modulus of the largest of the side lobes of the spectral window (Figure 3.3, b). For the considered case of a rectangular window, the maximum side-lobe level is 0.217 (or -13.27 dB on a logarithmic scale), and the decay rate of the side peaks is 18 dB per octave ($\omega_2/\omega_1=2$). The side-lobe maxima are slowly reduced to 0.004 (or -48 dB) at half the sample rate.

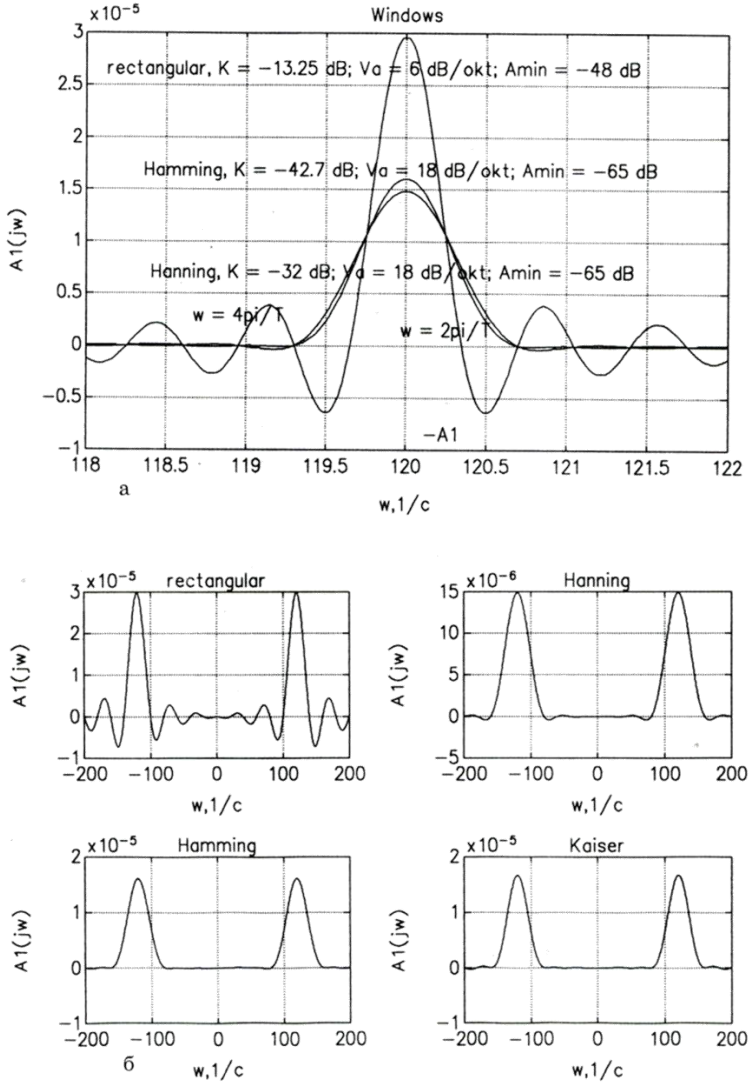


Figure 3.3. Spectral estimation of the output signal:
a – comparison of spectra; b – spectral windows

The use of a rectangular weighting function in the time domain leads to energy leakage from the main to the side lobes (Figure 4.3, a) of the function of the corresponding spectral window [40, 58, 60]. Since half of the side lobes of the spectral window have negative values, it becomes possible to obtain erroneous (negative in sign) statistical estimates of spectral characteristics (sample spectrum). This circumstance is due to the magnitude of the extreme values of the first two lobes, which add up to about 20% of the maximum of the main lobe. To get rid of energy leakage into the side lobes, more complex weighting functions must be used.

The latter include the Hanning, Hamming and Kaiser windows shown in Figure 3.3.

The width of the main lobe of the frequency response of the Hamming window is twice that for a rectangular window. At the same time, the maximum side-lobe level is significantly lower than that of the rectangular window characteristic and amounts to 0.0074 (or -42.7 dB), and the envelope of the side-lobe maxima falls to about 0.000059 (or -65 dB) at a frequency equal to half the sampling rate. Thus, for the Hamming window, 99.96% of the total spectrum energy is contained in the main lobe.

The Kaiser window (Figure 3.3, a) is characterized by an even more intense fall-off of the side maxima, but the width of the main lobe (corresponding to the expansion of the filter's transition band) is 1.5 times greater than the corresponding parameter of the Hamming window.

For the Kaiser window, the level of the largest side lobe is 0.00133 (or -57 dB), and the envelope of the maxima of the side lobes drops to about 0.00002 (or -94 dB).

The use of the Hamming and Hanning spectral windows makes it possible to reduce the variance of the spectral estimate. For the case of dividing the total observation length, the signal $T$ into 10 segments ($T_p$ = 0.1$T$), $3/4 \cdot T/T_p$, i.e. decreases to 7.5% of the variance of the estimate corresponding to the sample (unsmoothed) spectrum. At the same time, the error in estimating the spectral characteristics consists of two components – the variance ($D$) and the bias of the estimator $b(\xi)$ of the random variable

ξ. The bias $b(\xi)$ is the systematic component of the error (variance – fluctuation component):

$$b(\xi) = M\{\xi - \xi\},$$

where $M\{\cdot\}$ is averaging over the set of realizations.

As you know, the choice of the frequency band (filter band) $\Delta f$ and the observation interval $T$ should be based on a compromise: $T\Delta f \to \infty$ ($T \to \infty$; $\Delta f \to 0$; $\Delta f\ T \to \infty$), because to obtain high statistical accuracy it is necessary to reduce the variance of the estimate, which for a given $T$ corresponds to an increase in $\Delta f$. However, in this case, the estimate bias increases, which is proportional to the square of the bandwidth $\Delta f$ [60].

For the case of smooth spectra, when the bias of the estimate can be neglected, statistical uncertainty is characteristic:

$$\Delta f = \left(\bar{\varepsilon}^2 T\right)^{-1},$$

when the band $\Delta f$ and the time $T$ cannot be known simultaneously without the value of the normalization error $\varepsilon^2$. One of the options for a compromise is to use the ratio [60]:

$$\Delta f = \alpha T^{\beta - 1},\ \alpha > 0,\ 0 < \beta < 1.$$

### *3.3. Experimental determination of the statistical characteristics of the spindle*

At the first natural frequency, the unit compliance obtained by the Fourier transform from the displacement (deflection) of the rod in the $0_{th}$ section takes on the value:

$$\bar{y}_0(j\omega) = H(j\omega) = \frac{1/k}{1-\left(\frac{\omega}{\omega_n}\right)^2 + jl\frac{\omega}{\omega_n}} = \tag{3.7}$$

$$= \frac{2.57\cdot 10^{-5}}{(1-6.96\cdot 10^{-5}\omega^2) + j\ 3.34\cdot 10^{-4}\omega}.$$

Fourier transforms of other initial parameters are determined similarly. When studying the displacements of the rod, we use the Fourier transform matrix $\mathbf{Z_0}$ of the following form:

$$\mathbf{Z_0} = \begin{vmatrix} \bar{y}_0(j\omega) \\ 0 \\ 0 \\ 0 \end{vmatrix}.$$

To simplify the problem, in the case when the damping forces are proportional to the speed of transverse movement, and the sections of the rod between the concentrated masses are considered weightless, then the dependence between the Fourier transforms on the parameters at the boundaries of the cross-section "0-1" (Section 2.1) will be:

$$\bar{y}_1(j\omega) = U_1 G_0 \bar{y}_0 - \bar{S}_0,$$

where $\bar{\mathbf{S}}_\mathbf{0}$ – matrix taking into account the effect of the concentrated force $F_0(t)$:

$$\mathbf{S_0} = \begin{vmatrix} 0 \\ 0 \\ 0 \\ \dfrac{\bar{F}_0(j\omega)l^3}{EI} \end{vmatrix}$$

where $\bar{F}_0(j\omega)$ – Fourier transform of the force $F_0(t)$.

The transfer matrix $\mathbf{U_1G_0}$ takes into account the stiffness of the massless section of the rod $\mathbf{U_1}$ and the concentrated mass of the cantilever (boring bar) $\mathbf{G_0}$:

$$\mathbf{U_1} = \begin{vmatrix} 1 & 0.15 & 0.003 - 0.009\,j & 1.49 \cdot 10^{-4} - 4.46 \cdot 10^{-5}\,j \\ 0 & 1 & 0.04 - 0.01\,j & 0.003 - 00009\,j \\ 0 & 0 & 1 & 0.15 \\ 0 & 0 & 0 & 1 \end{vmatrix};$$

$$\mathbf{G_0} = \begin{vmatrix} 1 & 0 & 0 & 0 \\ 0 & 1 & 0 & 0 \\ 0 & -1.1 \cdot 10^{-8}\omega^2 & 1 & 0 \\ 4.94 \cdot 10^{-6}\omega^2 & 0 & 0 & 1 \end{vmatrix};$$

$$\mathbf{U_1G_0} = \begin{vmatrix} \begin{pmatrix} 1 + 7.36 \cdot 10^{-10}\omega^2 - \\ -2.2 \cdot 10^{-10}\,j\omega^2 \end{pmatrix} & \begin{pmatrix} 0.15 - 7.7 \cdot 10^{-11}\omega^2 + \\ +9.9 \cdot 10^{-12}\,j\omega^2 \end{pmatrix} & \begin{pmatrix} 0.003 - \\ -0.0009\,j \end{pmatrix} & \begin{pmatrix} 1.49 \cdot 10^{-4} - \\ -4.46 \cdot 10^{-5}\,j \end{pmatrix} \\ \begin{pmatrix} 1.48 \cdot 10^{-9}\omega^2 - \\ 4.45 \cdot 10^{-9}\,j\omega^2 \end{pmatrix} & \begin{pmatrix} 1 - 4.4 \cdot 1 - {}^{-10}\omega^2 + \\ +1.1 \cdot 10^{-10}\,j\omega^2 \end{pmatrix} & \begin{pmatrix} 0.04 - \\ -0.01i \end{pmatrix} & \begin{pmatrix} 0.003 - \\ 0.0009\,i \end{pmatrix} \\ 7.4 \cdot 10^{-7}\omega^2 & -1.1 \cdot 10^{-8}\omega^2 & 1 & 0.15 \\ 4.94 \cdot 10^{-6}\omega^2 & 0 & 0 & 1 \end{vmatrix}.$$

The value $\bar{y}_1(j\omega)$ takes on a complex value:

$$\bar{y}_1 = \frac{2.57 \cdot 10^{-5} - 1.8 \cdot 10^{-9}\omega^2 - 9.46 \cdot 10^{-19}\omega^3 - 1.32 \cdot 10^{-18}\omega^4}{(1 - 7 \cdot 10^{-5}\omega^2)^2 + 2.79 \cdot 10^{-8}\omega^2} -$$

$$- j\frac{4.3 \cdot 10^{-9}\omega + 5.65 \cdot 10^{-15}\omega^2 + 3.16 \cdot 10^{-18}\omega^3 + 3.96 \cdot 10^{-19}\omega^4}{(1 - 7 \cdot 10^{-5}\omega^2)^2 + 2.79 \cdot 10^{-8}\omega^2}.$$

The calculation of displacements in other conditional cross-sections of the elastic link "spindle-cantilever" was performed similarly. Dependences of displacement on frequency $y_i = f(\omega)$ for "0" and "1" cross-sections are shown in Figure3.4, a; b. The maximum displacement value corresponds to the resonant frequency $\omega_r = 119.56$ s$^{-1}$.

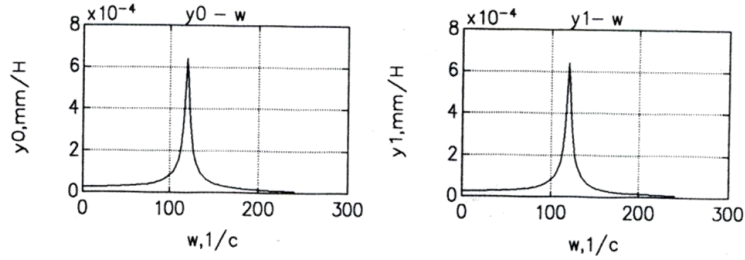


Figure 3.4. Spindle displacement graphs in "0" and "1" sections

Consider a sample that includes N = 241 independent values $\bar{y}_0(j\omega)$ of the normal value (2.7); ω = 0, 1, ..., 240 s$^{-1}$.

Let us find 90% confidence intervals for the mean $\mu_{y_0}$ and variance $\sigma^2_{y_0}$ of a random variable $\bar{y}_0(j\omega)$ from the known dependencies:

$$\left(\bar{y}_0 - \frac{st_{240;\alpha/2}}{\sqrt{241}}\right) \le \mu_{y_0} < \left(\bar{y}_0 + \frac{st_{240;\alpha/2}}{\sqrt{241}}\right);$$

$$\frac{240s^2}{\chi^2_{240;\alpha/2}} \le \sigma^2_{y_0} < \frac{240s^2}{\chi^2_{240;1-\alpha/2}},$$

where $s$ – sample standard deviation;

$\alpha$ – the level of significance;

$t_{(N-1),\alpha}$ – Student's test with ($N$-1) degrees of freedom and confidence level 1-$\alpha$ (confidence level);

$\chi_{(N-1),\alpha}$ – square distribution with ($N$-1) degrees of freedom and the same level of confidence (Helmert's criterion).

Using the tabular data, we determine the values of the Student and Helmert criteria: for $\alpha = 0.1$ criterion $t_{240;\,005} = 1.6514$.

Helmert's criterion $\chi_{N;\alpha}$ for large $N$ ($N$> 120) is calculated by the formula [58]:

$$\chi_{N-1;\alpha} \approx (N-1)\left(1-\frac{2}{9(N-1)}+Z_\alpha\sqrt{\frac{2}{9(N-1)}}\right)^3,$$

where $Z_\alpha$ – corresponding percentage point of the standard normal distribution.

For the confidence level (1-$\alpha$)=0.9 and $Z_\alpha$=1.64 we find:

$$\chi^2_{240;0.05} = 277.02;\ \chi^2_{240;0.95} = 205.23.$$

The main statistical characteristics – sample mean $\bar{y}$, variance $s^2$, and standard deviation $s$ are determined by the known dependencies:

$$\bar{y} = \frac{1}{N}\sum_{i=1}^{N} y_i = 7.05\cdot 10^{-6} - 1.97\cdot 10^{-5} i;\ |\bar{y}| = 2.09\cdot 10^{-5}\ \frac{mm}{N};$$

$$s^2 = \frac{1}{N-1}\left(\sum x_i^2 - N(\bar{x})^2\right) = 1.24\cdot 10^{-8}\,\frac{mm^2}{N^2};$$

$$s = \sqrt{s^2} = 1.19\cdot 10^{-4}\ \frac{mm}{N}.$$

The confidence intervals for characteristics $\mu_{y_0}$ and $\sigma^2_{y_0}$ with a 90% confidence level are:

$$2.03 \cdot 10^{-5} \le \mu_{y_0} < 2.74 \cdot 10^{-5};$$
$$1.08 \cdot 10^{-8} \le \sigma^2_{y_0} < 1.46 \cdot 10^{-8}.$$

Figure 3.5 shows the confidence interval for the characteristic of displacement $y_0$ in the zero section.

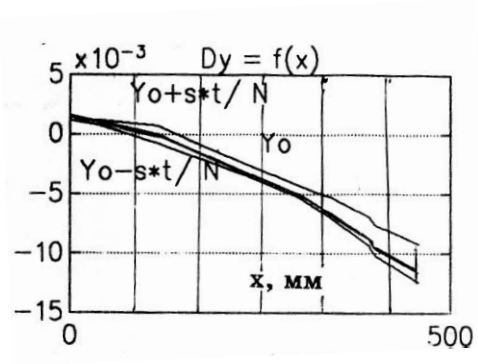


Figure 3.5. The confidence interval for $y_0$

For the case of harmonic input $x^*(t)$ expressed in displacement units $x^*(t) = F(t)/k$, the one-sided spectral density $G_{xx}$ is represented as:

$$G_{xx} = \frac{F_0^2}{k^2 \cdot 2} \delta(f - f_0),$$

where $\delta(f - f_0)$ – delta function localized at $f = f_0$.

The one-sided spectral density of the output signal $G_{yy}$, as a real even function of $f$, is determined from the following dependence:

$$G_{yy} = |H(f)|^2 \cdot G_{xx} = \frac{F_0^2 \delta(f - f_0)}{2[1-(f / f_n)^2]^2 + \left(2l\frac{f}{f_n}\right)^2} = \tag{3.8}$$

$$= \frac{F_0^2}{2\left[1-(f / f_n)^2\right]^2 + \left(2l\frac{f}{f_n}\right)^2}\Bigg|_{f=f_0} \cdot \delta(f - f_0) = 8.12 \cdot 10^4 \cdot \delta(f - f_0),$$

where $|H(f)|$ – amplitude characteristic of the elastic link of the spindle (2.3, b), mm/N;

$f_0$ – cyclic frequency, Hz;

$f_n$ – natural frequency of continuous oscillations, Hz;

$l$ – oscillation damping coefficient.

The corresponding covariance functions $R_{xx}(\tau)$ and $R_{yy}(\tau)$ are even functions of $\tau$ (time shift) are:

$$R_{xx}(\tau) = \frac{F_0^2}{k^2 \cdot 2}\delta(f\text{-}f_0);$$

$$R_{yy}(\tau) = \frac{F_0^2 \pi f_n e^{-2\pi f_n l|\tau|}}{2 \cdot 4l} \cdot \cos\left(2\pi f_n \sqrt{1-l^2}\,|\tau|\right) +$$

$$+ \frac{l}{\sqrt{1-l^2}} \cdot \sin\left(2\pi f_n \sqrt{1-l^2}\,|\tau|\right)\Bigg|_{f_n = f_0}.$$

Graphs of functions $x^*(t)$ and $R_{yy}(\tau)$ are presented in Fig. 3.6, a; b.

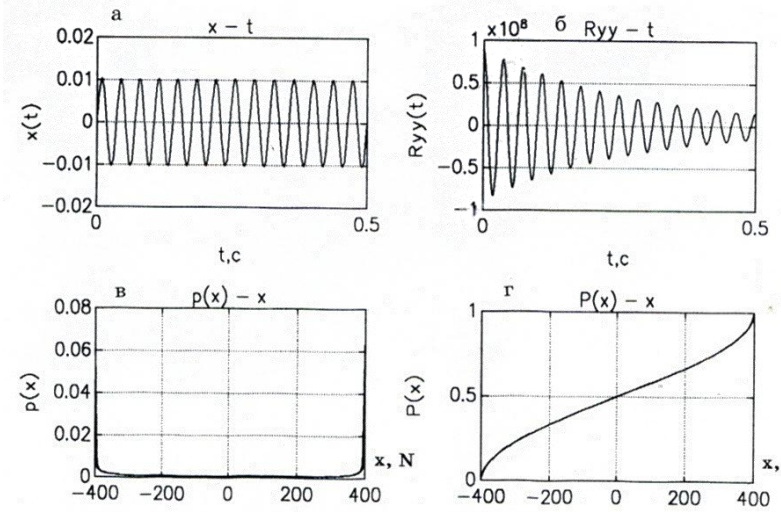


Figure 3.6. Spindle static characteristics

It should be noted that the input signal $x(t) = F(t)$, described by a harmonic function, has the following values of the probability density $p(x)$ and the distribution function $P(x)$:

$$p(x) = \begin{cases} \left(\pi\sqrt{F_0^2 - x^2}\right)^{-1}, & |x| < F_0; \\ 0, & |x| \geq F_0, \end{cases}$$

$$P(x) = \begin{cases} 0, & x < -F_0; \\ \dfrac{1}{\pi}\left(\dfrac{\pi}{2} + \arcsin\dfrac{x}{F_0}\right), & -F_0 \leq x \leq F_0; \\ 1, & x > F_0. \end{cases}$$

The graphs of the functions $P(x)$ and $p(x)$ are shown in Figure 4.6, c; d.

In the general case of estimating the covariance function, the error $\varepsilon$ is equal to:

$$\varepsilon(R_{yy}(\tau)) \approx \frac{1}{\sqrt{2BT}}\left(1+\rho_{yy}^{-2}(\tau)\right)^{1/2},$$

where $\rho_{yy}(\tau) = \frac{R_{yy}(\tau)}{R_{yy}(0)}$.

For various variants of the ratios of the covariance functions ρ = (0.2; 0.34; 0.56; 1), the graph $\varepsilon$ is shown in Figure 3.7.

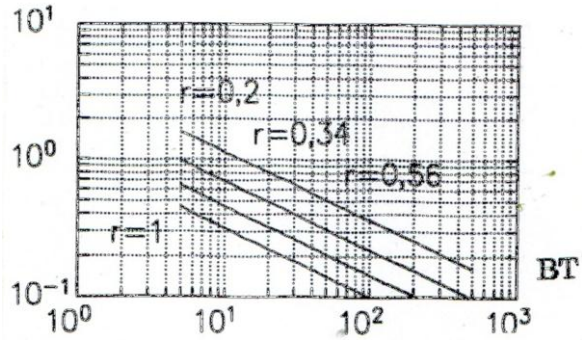


Figure 3.7. Normalized random error

The relationships between the input $x(t)$ and the output process $y(t)$ are described by the mutual covariance $R_{xy}(\tau)$ and the mutual spectral density $G_{xy}(f)$.

The one-sided, physically measurable mutual spectral density as a ratio for the mutual spectrum of input and output processes is a complex expression:

$$G_{xy}(f) = H(f) \cdot G_{xx}(f).$$

The last expression can be split into two formulas containing, respectively, the amplitude $|H(f)|$ and phase $\varphi(f)$ characteristics of the system:

$$G_{xy}(f) = \left|G_{xy}(f)\right| \cdot e^{-j\theta_{xy}(f)};$$

$$\left|G_{xy}(f)\right| = \left|H(f)\right| G_{xx}(f);\ \theta_{xy}(f) = \varphi(f).$$

The delta function $\delta(f-f_0)$ is included in the amplitude characteristic of the cross-spectrum.

To estimate the spectral density of oscillations of the "spindle-cantilever" (S-C) system (a system with one degree of freedom), let us assume about the form of the input action in the form of white noise. This assumption implies a narrowing of the bandwidth of the $B_e$ spectrum. Within this narrow band, the spectral density $G_{xx}(f)$ changes little and can be expressed: $G_{xx}(f) = G$, where $G$ – constant, measured in units of the S-C mass displacement, the spectral density of the disturbance entering the system. In this case, the spectral density of the output signal (displacement) $G_{yy}(f)$ (3.8) is represented as:

$$G_{yy} = \frac{F_0^2 / k^2}{\left[1-(f / f_n)^2\right]^2 + (2lf / f_n)^2}.$$

As noted above, the error in estimating the spectral characteristic includes two components – the bias $b_y$ and the variance $\sigma_y$.

To determine the maximum bias $\varepsilon_b(G_{yy})$, we use the relationship [58]:

$$\varepsilon_b(G_{yy}) = -(B_e/B_r)/3,$$

where $B_r$ – half-energy passband in the region of the resonance maximum of the $B_r$ spectrum ($B_r$ = 0.79 Hz). Usually, $B_e = B_r/4$ = 0.198 Hz is taken,

which gives an insignificant systematic error $\varepsilon_b \approx$ -2%. A minus sign means that the spectral density estimate is below the true value.

When determining the variance of the spectral density, assuming the form of the input signal of the white noise type, it was noted that the spectrum of the output process is essentially independent of frequency [58]. Consequently, for a small width $B_e$, the normalized random estimation error is:

$$\varepsilon_r(G_{xx}(f)) = \frac{1}{\sqrt{B_e T}}.$$

In contrast to the systematic error $\varepsilon_b$, the error $\varepsilon_r$ decreases with an increase in the realization length $T$ and for $B_e$ = 0.198 Hz should exceed 500 s ($\varepsilon_r \approx 10\% = 0.1$).

If we consider the estimate of the quantity $\overset{\circ}{G}_{xx}(f)$ obtained by the finite Fourier transform in the form:

$$G_{xx}(f) = \frac{2}{T}\left|X(f,t)\right|^2, \qquad (3.9)$$

where $|X(f,t)|^2 = X_k^2(f,T) + X_i^2(f,T)$ – amplitude characteristic, the real and imaginary components of which are normative uncorrelated random variables with zero means and equal variances (the Fourier transform is a linear operation).

A decrease in the error of the spectral value calculated by the above equation is achieved by calculating estimates for nd different (non-overlapping) sections of realizations of length $T$ each and their subsequent averaging. In this case, the minimum total implementation length required to obtain a spectrum estimate is $T_r = n_d T$; resolution $B_e = 1/T$ and the smoothed estimate has an error:

$$\varepsilon_r = \frac{1}{\sqrt{B_e T_r}}.$$

The expression for the minimum realization length $T_r$ and the number of averaging $n_d = B_e T_r$ required to obtain spectral estimates with a given error $\varepsilon$ is:

$$T_r = \frac{1}{B_e \varepsilon^2};\ n_d = \frac{1}{\varepsilon^2}.$$

For a given resolution, $B_e = 0.198$ Hz and an error $\varepsilon = 0.1$, the number of averaging is $n_d = 100$, and the implementation length, as already mentioned, is $T_r \geq 500$ s.

The confidence interval with a confidence level of 1-α for the spectral density $G_{xx}(f)$ based on the estimate $\tilde{G}_{xx}(f)$ is written as

$$\frac{(N-1)G_{xx}(f)}{\chi^2_{N-1;\alpha/2}} \leq G_{xx}(f) \leq \frac{(N-1)G_{xx}(f)}{\chi^2_{N-1;1-\alpha/2}}, \qquad (3.10)$$

where $N$ is the number of independent observations of a random variable (input signal $x(t) = F(t)$);

$\chi^2_{N-1;\alpha/2}$ – Halmert criterion with (N-1) degrees of freedom and confidence level (1-α).

The estimate $G_{xx}(\omega)$ calculated by the formula (3.9) represents the current spectrum (3.6), which must be multiplied by a scale factor $\sqrt{\frac{8}{3}}$ that considers the loss caused by using the Hanning spectral window.

Thus, $G_{xx}(\omega)$ it can be represented as:

$$G_{xx}(\omega)=\sqrt{\frac{8}{3}}\frac{2}{T}\left[\frac{\xi_0^2 T}{4}\left(\frac{\sin(T(\omega+\omega_0)/2}{T(\omega+\omega_0)/2}+\frac{\sin(T(\omega-\omega_0)/2)}{T(\omega-\omega_0)/2}\right)\right]^2.$$

Figure 3.9 shows a graph of the current spectrum smoothed by the Hanning window.

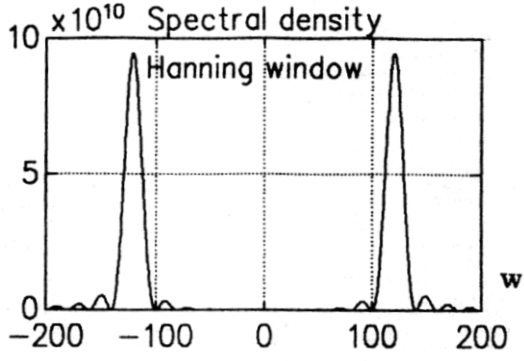


Figure 3.9. Evaluation of the sample spectrum $\hat{G}_{xx}(\omega)$

The confidence interval for the spectral density $G_{xx}(\omega)$**,** at $\omega = 90\ s^{-1}$ in accordance with (3.10) will be equal to

$$\frac{(N-1)G_{xx}(\omega)}{\chi^2_{N-1;\alpha/2}} \le G_{xx}(\omega) \le \frac{(N-1)G_{xx}(\omega)}{\chi^2_{N-1;1-\alpha/2}}.$$

At a frequency of $\omega = 90$, $s^{-1}$, the estimate of the spectral density of the input signal is $G_{yy}(f) = 3.1\cdot10^9\ N^2/Hz$, and the confidence interval is within the following limits (at a confidence level of 0.9):

$$2{,}69\cdot10^9 \le G_{xx}(\omega) \le 3{,}69\cdot10^9.$$

# 4. MODELING OF SPINDLE NODES OF METAL CUTTING MACHINES IN THE "APM WINMACHINE" ENVIRONMENT

## *4.1. Modeling the spindle node of a multipurpose lathe*

An analysis of the balance of compliance and vibration modes of the main nodes of lathes showed that the main shaping nodes: Spindle-Workpiece (S-W) and carriage group-tool (Ca-T) predetermine the quality of the machine as a whole. The characteristics of rigidity and vibrostability of the spindle on elastic supports depend on the size of the cantilever part of both the spindle itself and the length of the workpiece. The fixation of the processing scheme with a certain overhang and the construction on this basis of the calculation schemes [15, 62, 63] do not make it possible to effectively control the rigidity and vibrostability within the working space of the machine.

The approach to the construction of static formulas (*sf*) of the spindle presented in [3] is promising. This approach is effective when using unified spindle nodes equipped with a wide range of modular equipment. At the same time, the authors considered one variant of loading with a single cantilever force, without taking into account the forces in the gearing "gearbox output shaft - spindle".

Consider a variant of the combined loading of a two-bearing spindle node (Figure 4.1) of a multi-purpose machine model MC-03, mounted on angular contact ball bearings 4-46209 and 4-46112, mounted according to the "tandem-O" scheme with a spring-type preload (rear support) and by interference with two intermediate bushings for the double front support.

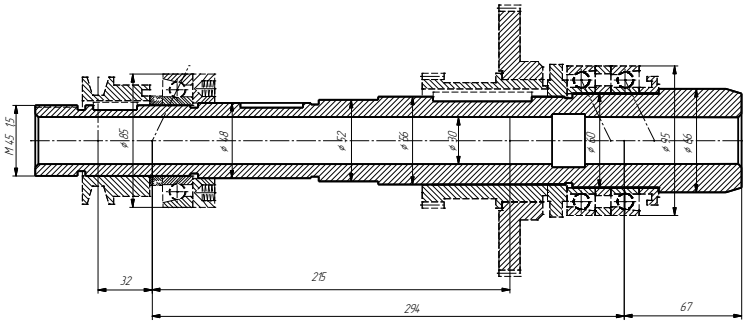


a

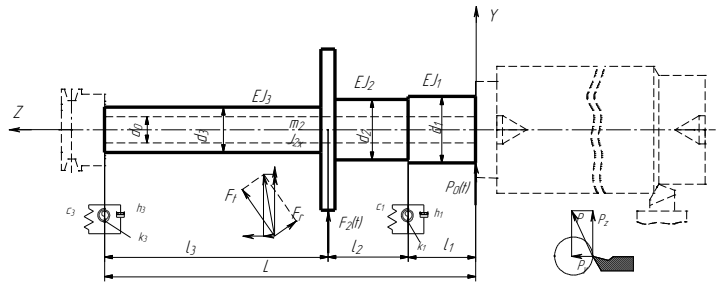


b

Figure 4.1. Structural (a) and design (b) schemes

The considered machine is equipped with a set of modular equipment:

- a three-jaw chuck fixed to the spindle with an intermediate flange;
- a rotating center mounted in the tapered hole of the spindle quill and designed for processing long parts;
- grinding arbor mounted in the tapered bore of the spindle;
- drill chuck with a set of bushings with an angular table pre-mounted on the support table (and, if necessary, a vice);
- boring bar, mounted on the threaded part of the spindle, providing boring operations for the manufacture of parts mounted on an additional corner table with a carriage;
- a milling arbor with an end mill with the necessary set of taper bushings, installed in the taper hole of the spindle (the machine is equipped with an angle table and a vice).

To assess the characteristics of the compliance of the spindle node, considering the size of the working area of the machine, a program was developed in the mathematical environment "Maple" [64–66] and using the kernel of symbolic mathematics, a static form was obtained $sf = f(l_k)$ for various cantilever lengths $l_k$ of the spindle node of a multi-purpose machine MC03:

$$sf = 0{,}29 \cdot 10^{-4} + 0{,}332 \cdot 10^{-6} \cdot l_k + 0{,}507 \cdot 10^{-8} \cdot l_k^2$$

A resulting analytical form is an effective tool for determining and modeling the stiffness characteristics within the working space of the machine. There is a possibility of a quick statistical calculation of this or that adjustment, using the nomograms "$sf - l_k$", which consists of two parts: the statistical form $sf$ and the graph of the cantilever compliance $\Delta_k$.

Analysis of the results obtained shows the presence of a significant reserve of stiffness (the maximum deflection on the spindle cantilever (Figure 4.1) is $y_{\max} = f = 0.027$ mm, and the angle of rotation of the cantilever section is 0.0289 rad). In this case, the deflection arrow on the inter-support part at $[f] = 0.0003 \cdot l$ should not exceed $y_{\max}^{\lim} = 0.0873$ mm. The permissible angle of rotation of the spindle end must not exceed $[\theta] = 0.0572$ degrees. Close numerical values of compliance are obtained as a result of calculations using the APM Shaft module [26, 67].

At the same time, the APM Shaft module cannot consider the angular compliance of the spindle node, which affects the deformation parameters of the designed structure [67–70].

For effective modeling, calculation of the stress-strain state taking into account the angular compliance of the supports, we use the module for complex analysis of three-dimensional structures APM Structure3D [26, 71, 72].

In the process of modeling in the APM Structure 3D environment, a "skeleton" model of the spindle structure is created (Figure 4.2), in which the boundaries of the rod elements are determined by the nodes at those

points where the load is applied or the bending stiffness of the section changes. Each rod has specific dimensions and is connected with nodes to the rest of the structure rods.

To calculate this structure, you must additionally set:

- cross-sections for each of the rods;
- supports for the created structure, which determines its position in space;
- external loads acting on the structure;
- material parameters of structural elements.

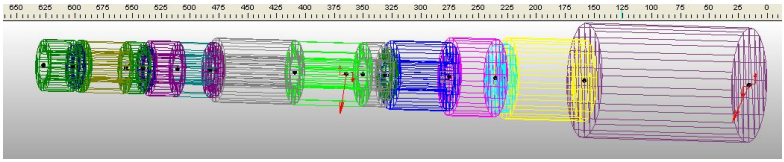

Figure 4.2. Skeleton model of the spindle structure

A feature of specifying supports is the ability to combine in one support the rigid and elastic fastening, each of which is a completely different object. They will work together when they act in different directions of the coordinate system at the node. For the designed structure, displacements in the direction of action of forces $P_y$ (Z-axis) and $F_r$ (elastic fastening) and rotation around the Z-axis are allowed. In the rigid restraint mode, by turning on the checkboxes in the fields for displacement in the direction of the axis, restrictions on displacement in the direction of the X and Y axes, as well as rotations around the same axes, should be set.

Calculation in the APM Structure3D environment allows you to evaluate the complete picture of the stress-strain state of the spindle in any of its sections, including the assessment of loads, force factors, etc., presented in the "Results" menu item. In Figure 4.3. presents the stress field characteristic of a typical turning operation performed on a multi-purpose machine MC-03 and the stress distribution in the *i*-th section of the spindle.

Per the colour scale (Figure 4.3), the maximum values of the equivalent stress SVM (according to the energy theory of strength) do not exceed the permissible yield stresses ([τ] = 635 MPa for the Steel 20X spindle material) even with a yield safety factor $k_\tau = 2$.

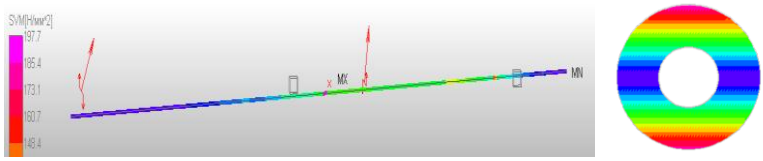


Figure 4.3. Spindle stress field of the machine MC-03

Evaluation of the dynamic quality of functioning is associated with the determination of natural frequencies and the corresponding natural vibration modes. The calculation of these dynamic characteristics was carried out in the APM Structure 3D module [26]. By default, the system calculated 16 natural frequencies and shapes with an accuracy of 0.01%. In Figure 4.4 is a table of natural frequencies and the 3rd and 4th natural forms, describing the configuration of the spindle model, vibrating with the corresponding frequencies.

When the elastic system of the spindle unit vibrates, the main bending form prevails, therefore, the system can be considered as a second-order linear vibrational link, the transfer function $W(iw)$ of which is shown in Figure 4.5. Programs for constructing the transfer function, amplitude-phase frequency (APFC), amplitude-frequency $A = f(w)$ and phase-frequency characteristics $\varphi = f(w)$ were developed in the mathematical environment "Matlab".

The APFC of elastic systems makes it possible to compare various adjustments with the modular equipment listed above in the cutoff length segment of the characteristic on the imaginary axis *Im*. The ratio of the segment length to the static compliance determines the dynamic factor at resonance for the i-th natural vibration frequency. In contrast to static compliance, the dynamic coefficient takes into account inertial and

damping properties and, therefore, more fully characterizes the elastic system of the spindle node of a multi-purpose lathe model MS-03.

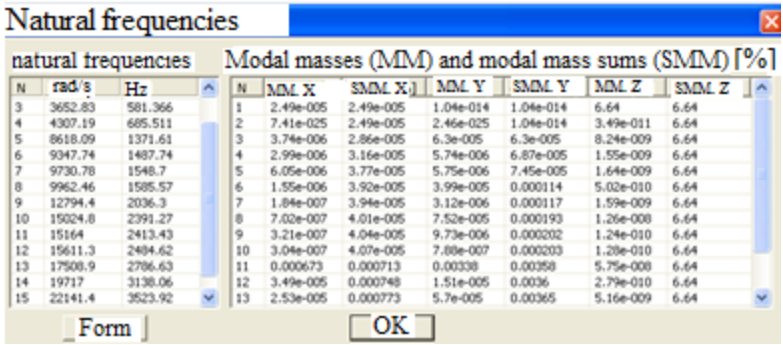


а

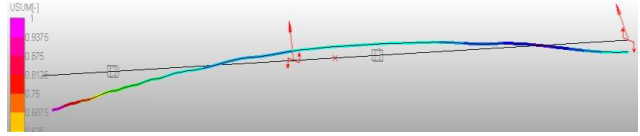

б

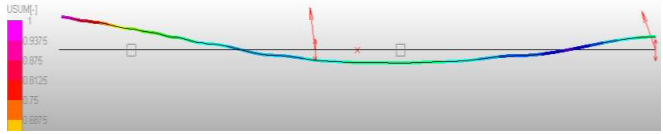

в

Figure 4.4. Spindle dynamic characteristics:

a – table of natural frequencies; b – the natural form of oscillations at the 3rd natural frequency; c – the natural form of oscillations at the 4th natural frequency

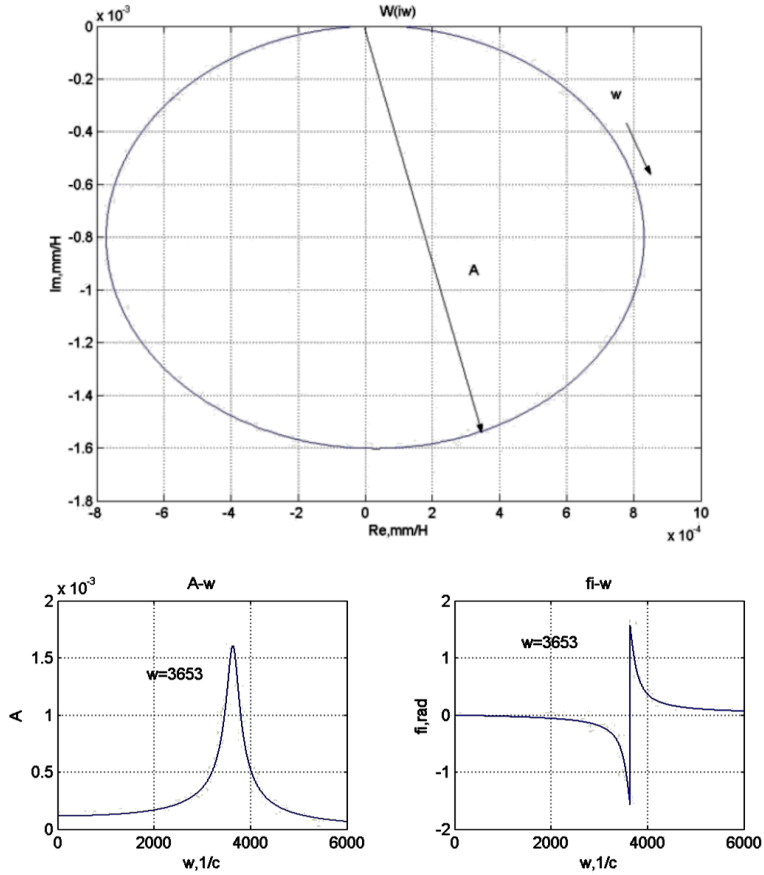


Figure4.5. Frequency characteristics of the spindle node

### *4.2. Modeling the spindle node of a multipurpose milling machine using the APM Structure 3D module*

The spindle units of milling machines as the end links of the drive for the machine main movement are evaluated according to a set of criteria: load capacity, accuracy, rigidity and reliability. Several works are known

[18, 35, 73] that use approximate and refined calculation methods, based mainly on the use of matrix calculus algorithms and numerical methods of initial parameters. At the same time, the most common representation of the spindle node considers it as a linearly deformable system, in which the displacement of the spindle nodes is expressed as a linear function of the applied forces does not allow solving this problem in a complex manner.

Let us consider the problem of calculating the horizontal spindle of the main motion drive for a multi-operation machine model SF68VF4. The design and calculation diagram of this machine spindle node is shown in Figure 4.6.

For modern milling machines, double-bearing spindles are often used, which differ in size and design of the cantilever part. In the SF68VF4 machine, the spindle is mounted on two supports on double angular contact ball bearings with a preload according to the "tandem - O" scheme. In the front support, bearings of an extra-light series 2-446113 GOST 832-78 with a contact angle $\alpha = 26^0$ are used. The outer rings of these bearings are facing each other with opposite ends. The tandem connection type is characterized by its ability to withstand large axial unidirectional loads. The radial load capacity and the radial stiffness depend on the amount of preload performed. When mounting such a connection, it is necessary to strictly check the coincidence of the contact angles of the bearings $\alpha$. The rear support is mounted with two extra-light series angular contact ball bearings 2-446112 GOST 832-78.

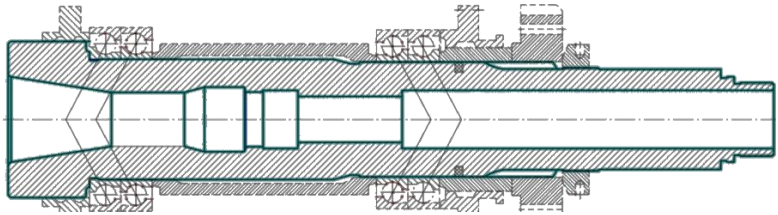

Structural scheme

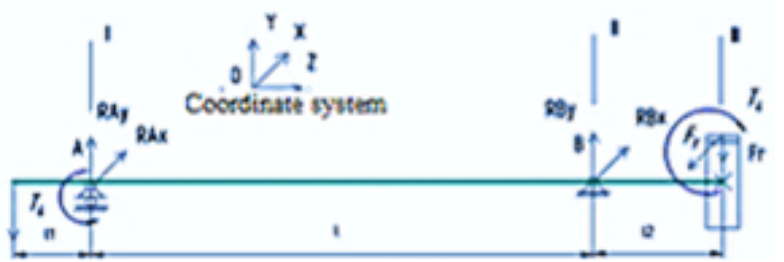


Figure 4.6. Structural and design diagram of the spindle node

In the general case, this design scheme should be considered as a statically indeterminate beam on four supports (bearing-support), which in the general case have linear *A* and angular compliance α (Figure 4.6). To reduce the labor intensity, it is sufficient to correctly replace the double bearings with one support, passing to a two-support design scheme [73, 74].

According to the proposed design scheme, SN is represented as an elastic system "spindle-cantilever" (S-C), the compliance of which Δ is determined as the sum of the individual components: $\Delta = \Delta_1 + \Delta_2 + \Delta_3$. To determine these components, we will form a mathematical model of the elastic system in the form of a set of static equations:

$$R_r + R_f - R' = 0; \tag{4.1}$$

$$R_r \cdot (l + l_1) + R_f \cdot l_1 + R' \cdot l_k - m_r - m_f = 0. \tag{4.2}$$

We add two equations to this statically indeterminate second-order system:

- deflection equation (for a beam of constant cross-section):

$$y(x) = y_0 + \theta_0 \cdot x + \frac{m_r \cdot x^2}{2 \cdot E \cdot I} - \frac{R_r \cdot x^3}{6 \cdot E \cdot I} - \frac{R_f \cdot (x-l)^3}{6 \cdot E \cdot I} + \frac{m_f \cdot (x-l)^2}{2 \cdot E \cdot I} \quad (4.3)$$

- the equation of the angle of rotation

$$y'(x) = \theta_0' + \frac{m_r \cdot x}{E \cdot I} - \frac{R_r \cdot x^2}{2 \cdot E \cdot I} - \frac{R_f \cdot (x-l)^2}{2 \cdot E \cdot I} + \frac{m_f \cdot (x-l)}{E \cdot I}. \quad (4.4)$$

where $E$ – modulus of elasticity of the spindle material; $I$ - an average axial moment of inertia of the spindle cross-section.

Equation (4.3) was obtained from the elastic line equation using the method of initial parameters [3, 18], and equation (4.4) was obtained by calculating the derivative concerning the coordinate.

For a given design scheme (Figure 4.2), the boundary conditions are satisfied:

$$\begin{aligned} y(0) &= A_r \cdot R_r; \qquad & y'(0) &= a_r \cdot m_r; \\ y(l) &= A_f \cdot R_f; \qquad & y'(l) &= a_f \cdot m_f. \end{aligned} \quad (4.5)$$

after substitution into equations (4.3) and (4.4), it allows one to compose a system of four linear algebraic equations with unknowns $R_f$, $R_r$, $m_n$, $m_r$. Let's write this system in matrix form:

$$\begin{Vmatrix} 1 & 1 & 0 & 0 \\ l+l_1 & l_1 & -1 & -1 \\ A_r - \frac{l^3}{6 \cdot E \cdot I} & -A_f & \left(a_r \cdot l + \frac{l^2}{E \cdot I}\right) & 0 \\ -\frac{l^2}{2 \cdot E \cdot I} & 0 & \left(a_r + \frac{l}{E \cdot I}\right) & -a_f \end{Vmatrix} \cdot \begin{Vmatrix} R_r \\ R_f \\ m_r \\ m_f \end{Vmatrix} = \begin{Vmatrix} R' \\ -R' \cdot l_k \\ 0 \\ 0 \end{Vmatrix} \quad (4.6)$$

*Defining a static spindle form*

Calculation $y(x)$ and $y'(x)$ is carried out for the coordinate X coinciding with the right end of the spindle $x=(l+l_1)$. Several options are possible here. The first is numerical, typical for the situation of designing special and specialized machine tools. For universal and broadly universal machine tools, when the basic designs of the control cabinet are unified and only the designs of the cantilevers are changed, a general solution with the selection of the component $\delta_{st}=(\Delta_2+\Delta_3)$ is advisable. The latter is assigned the name of the static form SN [3, 73] and is defined as follows:

$$\Delta_2 = y(x)\big|_{x=l+l_1}; \quad \Delta_3 = l_k \cdot y'(x)\big|_{x=l+l_1}.$$

Spindle node compliance Δ, reduced to the cutting place, is calculated according to the dependence

$$\Delta = y(l+l_1)+l_k \cdot y'(l+l_1)+\Delta_1 = \Delta_1+\delta_{st},$$

where $\Delta_1$ depends only on the design and dimensions of the cantilever, and for a beam of the constant cross-section can be expressed in the form:

$$\Delta_1 = \frac{l^3}{3 \cdot E \cdot I_k}.$$

Experiments to assess the rigidity of the spindle node were carried out. In the planning process, experiments are broken down into a series of experiments (according to the number of factors). The minimum number of experiments $N_{\min}=5$ in each series. After conducting experiments according to the drawn-up plan, the displacements of the spindle node at

the end of the spindle *y* are measured at least three times to determine the average values. The compliance values are calculated at the same point. Experimental and calculated data are presented in Table. 4.1.

Table. 4.1.

**Experienced and calculated data**

| Loading $F_r$, N | $(y)_{calc}$ | $(y)_{opt}$ | Error $y$,% |
|---|---|---|---|
| 2000 | 0.0103 | 0.0095 | 7.8 |
| 3000 | 0.0155 | 0.014 | 9.7 |
| 4000 | 0.0207 | 0.022 | 6 |
| 5000 | 0.0258 | 0.0282 | 8.5 |

Based on the data obtained, a graph of experimental dependences is built (Figure 4.7): $F_r = f(y)$.

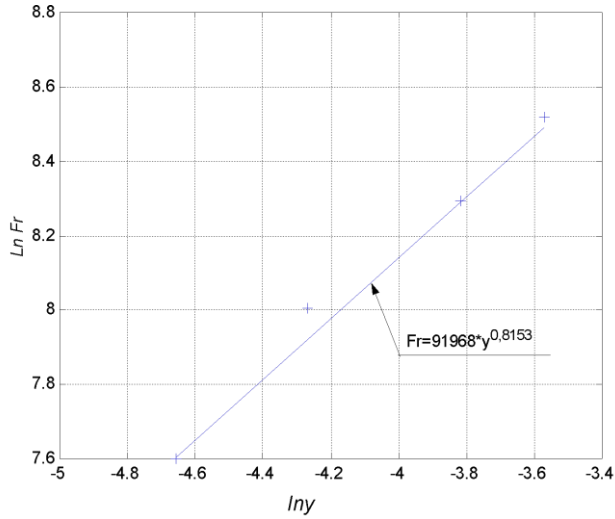


Figure 4.7. Empirical dependence $F_r = f(y)$ graph

*Investigation of the compliance of Drilling-Milling-Boring machine tools using static forms*

During the formation of static forms according to the above method, machine tools representing the drilling-milling-boring group were identified:

1. Drilling-milling-boring machine MC51 with spindle taper 30 AT5 following GOST 15945-82.

2. Universal specialized machine model SF68PF4 with a 40 cone following GOST 936-82 for horizontal and vertical spindles.

3. Multi-purpose specialized horizontal machine model MTs200PF4V with a 40AT5 cone following GOST 15945-82.

Received static formulars:

$$\delta = \left(\Delta_2 + \Delta_3\right) = y(x) + l_k \cdot y'(x)$$

for the above machines MC51, SF68PF4 (SF68), MTs200PF4V (MTs200) are given in Table. 4.2.

Table. 4.2

**Static formulars of spindle units**

| Initial data | | | | | | | Static formular δ, mm/N |
|---|---|---|---|---|---|---|---|
| Pattern | Dimensions, mm | | Compliance ($\times 10^{-8}$), mm/N | | | | |
| | $l$ | $l_1$ | $A_r$ | $A_f$ | $a_r$ | $a_f$ | |
| MC51 | 114 | 35 | 631 | 589 | 0.15 | 0.15 | $(-85.25-2.00\ l_k+0.11\ l_k^2)\ 10^{-8}$ |
| SF68 | 148 | 68 | 399 | 393 | 0.06 | 0.06 | $(30.37+0.61\ l_k+0.042\ l_k^2)\ 10^{-8}$ |
| MTs200 | 193 | 95 | 439 | 432 | 0.06 | 0.06 | $(66.75+4.85 l_k+0.069\ l_k^2)\ 10^{-8}$ |

The designer often needs to quickly make a static calculation of a particular adjustment. This can be done using a nomogram, which consists of two parts: a static formular $\delta$ (Figure 4.8, a), built according to the formulas of Table 4.2, and a compliance graph of the cantilever $\Delta_1$ (Figure 4.8, b), built for cantilevers of constant cross-section and various values diameters $d_k$. The cantilever is considered as a beam clamped in the support section and loaded at the cutting point with a unified force.

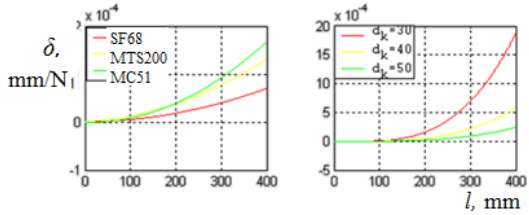


Figure 4.8. Compliance of spindle assemblies (nomogram):
a) – static forms; b) – compliance of cantilevers

To determine the compliance of the spindle node reduced to the cutting place on the nomogram, it is enough to know the overhang to the cutter $l_k$ and the diameter $d_k$ of the cantilever. The compliance δ at the cutter is determined by the sum $\Delta_2 + \Delta_3$ of the values and $\Delta_1$ found on the nomogram.

In some cases, the inaccuracy in determining the general compliance of the spindle node is associated with the absence of data on the elastic properties of bearing supports in the design model. Let us consider how the inaccuracy in determining the linear compliance $A_0$ of one bearing affects the results of a static calculation [3]. For the spindle node of the machine tool model SF68PF4, the calculated value of compliance $A_r = 3.99 \cdot 10^{-6}$ and $A_f = 3.93\ 10^{-6}$, mm/N. Let's take two more values of linear compliance with deviations:

1. $A_{r1} = 2.59 \cdot 10^{-6}$ and $A_{r2} = 5.39 \cdot 10^{-6}$, mm/N; 2. $A_{f1} = 2.55 \cdot 10^{-6}$ and $A_{f2} = 5.305 \cdot 10^{-6}$, mm/N,

and angular compliance of one bearing:

1. $a_{r1} = 0.039 \cdot 10^{-8}$ and $a_{r2} = 0.081 \cdot 10^{-8}$, 1/(N·mm); 2. $a_{f1} = 0.039 \cdot 10^{-8}$ and $a_{f2} = 0.081 \cdot 10^{-8}$, 1/(N·mm)

In this case, the formulars will look like:

1. $\delta = (-71.05 + 0.62\, l_k + 0.044 \cdot l_k^2) \cdot 10^{-8}$;

2. $\delta = (161.67 + 1.148\, l_k + 0.043 \cdot l_k^2) \cdot 10^{-8}$.

In Figure 4.9, the dependences δ on $l_k$ are plotted, from which it follows that even a significant (up to 35%) deviation of the linear compliance $A_0$ of one bearing in both directions (over or understatement) from the nominal value has little effect on the compliance of the spindle-cantilever system as a whole:

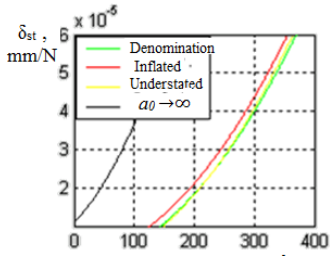


Figure 4.9. Investigation of the Spindle Node static formular machine SF68PF4

On the other hand, if you do not take into account the angular stiffness of a single bearing ($a_0 \to \infty$), then we get the following static form (Figure 4.8 – curve marked with a solid line):

$$\delta = (1093 + 16.09\, L_k + 0.097\, l_k^2)\ 10^{-8}.$$

It is necessary to consider the angular compliance of a single bearing since the calculated value δ of the spindle node increases by 3.2 times. Besides, as can be seen from the calculations, a change in the linear compliance $A_r$ and $A_f$ of the spindle supports within a fairly wide range without a corresponding change in its diameter does not significantly change the compliance of the spindle node (does not exceed 35%).

The complication of calculations of spindle nodes for rigidity and vibrostability, taking into account the distribution and modes of change in stresses, sizes and sections, requires the use of advanced computer-aided design systems. One of the effective means of solving time-consuming design tasks for creating optimal machine-building structures is the APM Structure 3D module [28, 39].

The APM Structure 3D module is designed to analyze the stress-strain state of arbitrary three-dimensional machine-building structures consisting of a rod, plate, shell and volume elements in their arbitrary combination. The calculation is performed by a numerical method - the finite element method (FEM) and allows you to calculate the values of stresses and strains at any point in the structure, taking into account the own weight of each of the elements and taking into account stress concentrators. Determination of unknown force factors at each of the mesh nodes and internal force factors within each finite element provide information for spline, threaded and other connections.

The use of the APM Structure 3D module involves the construction of a 3D model of the spindle assembly. In the environment of the integrated CAD KOMPAS [11, 64], three-dimensional models of the main motion drive for the SF68PF4 machine have been built. It gives an idea of the device and kinematic chains of transmission of motion from the electric motor to the spindle of the machine equipped with a high-speed head (Figure 4.9 and Figure 4.10).

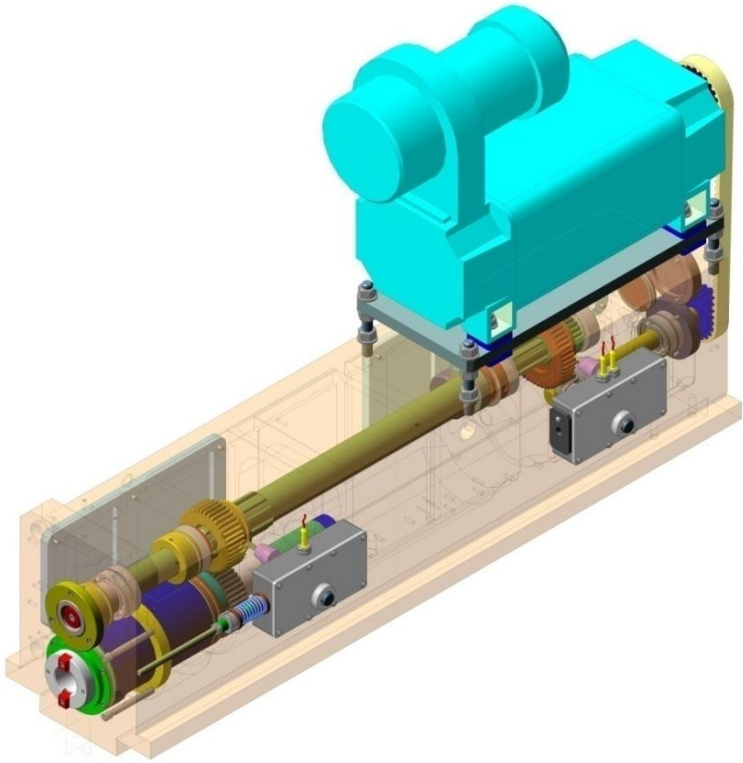

Figure 4.9. 3D model of the main drive

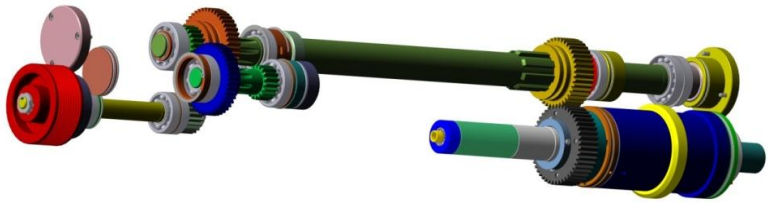

Figure 4.10. Kinematics of the main movement of the milling machine

Using a set of KOMPAS applied libraries, a solid model of the assembly of the spindle node of the SF68PF4 machine tool (Figure 4.11) and the spindle itself (Figure 4.12)

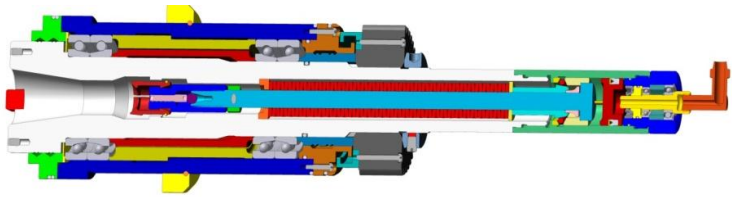

Figure 4.11. Three-dimensional model of the spindle node assembly (section)

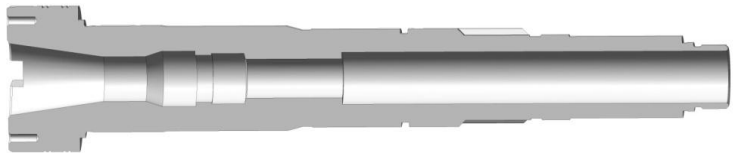

Figure 4.12. Three-dimensional model of the spindle (section)

To perform comprehensive engineering analysis, both individual parts and assemblies, we will use the APM FEM module [26, 67, 75], equipped with the CAE-library that implements the solution of engineering problems by the finite element method.

The APM FEM system is a module integrated into KOMPAS-3D and represents a toolkit for the preparation and subsequent finite element analysis of a three-dimensional solid model.

The development of a 3D model and the assignment of material is carried out using the KOMPAS-3D system. Within APM FEM, you can apply loads of various types, specify boundary conditions, create a finite element mesh, and perform a calculation. In this case, the procedure for generating finite elements is carried out automatically.

APM FEM allows you the following types of calculations to carry out:

- static calculation;
- calculation of stability;
- calculation of natural frequencies and vibration modes;
- thermal calculation.

As a result of calculations performed by the APM FEM system, the following information can be obtained:

- a map of the distribution of loads, stresses, deformations in the structure;

- safety factor of the structure;

- frequencies and forms of natural vibrations of the structure;

- a map of temperature distribution in the structure;

- mass and inertia moment of the model, coordinates of the gravity center.

The APM FEM system was developed at STC APM for express finite element strength analysis in KOMPAS-3D. The more advanced functionality of finite element analysis of imported models is available in the APM WinMachine system in the APM Studio and APM Structure3D modules.

At the same time, APM Structure3D provides the ability to edit finite element meshes (FE-mesh), create combined (rod-plate-volumetric) models, as well as solve high-dimensional problems.

In the process of solving the problems of rigidity and vibrostability of structures, fixings and applied loads are assign; coincident faces are assign (for FE-analysis of an assembly); FE-mesh is generated; calculation and viewing of results in the form of maps of stresses and displacements are performed.

For the above spindle design (Figure 4.12), an FE mesh is built (Figure 4.13).

The FE-mesh is generated using the *FE-mesh* command. The parameters of this operation are the *Maximum length of the side of the element*, the *Maximum coefficient of thickening at the surface* and the *Coefficient of expansion in the volume*. So the parameter *Maximum thickening factor on the surface* determines how much the next element can be made (where necessary) smaller. Thus, when moving to smaller parts of the structure, the FE-mesh generator gets the right to create a finite element *k* times smaller than the previous FE.

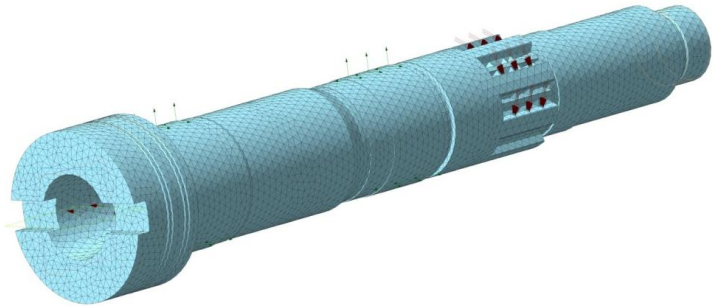

Figure 4.13 Generation of finite element mesh by calculation method MT FRONTAL (using multi-core processor)

To assess the stress-strain state in various sections of the spindle, we will carry out a static calculation by the finite element method. The module can use the Frontal calculation method, which is intended for structures consisting of a large number of finite elements. The method differs in that the ensemble stiffness matrix is not compiled directly in the computer's RAM, and the system of equations is solved by the “front” in all degrees of freedom. The global matrix is saved to disk. A distinctive feature of MT_Frontal is the use of a multi-core processor. The fields of stresses and displacements in different sections of the spindle are shown in Figure 4.14 and Figure 4.15.

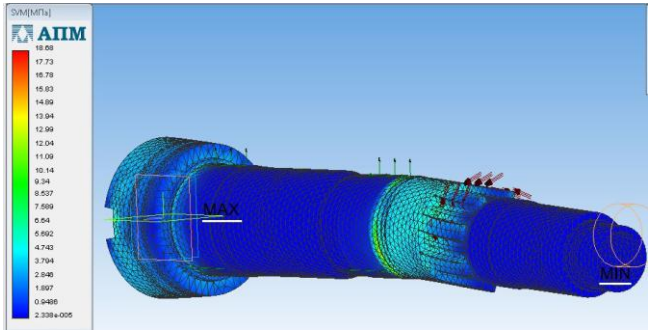


Figure 4.14. Fields of equivalent von Mises stresses (4th energy theory of strength)

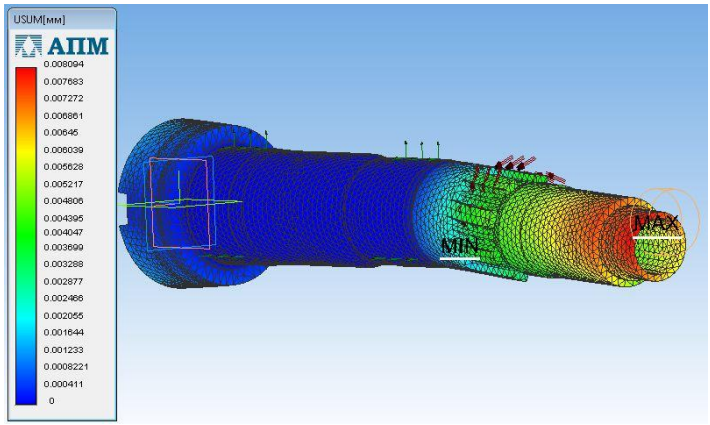


Figure 4.15. Accumulated Linear Displacement Fields

To control the quality of finite element splitting and assess the stress state, a part of the mesh can be hidden by setting the *Viewing depth* (Figure 4.16). By default, the section plane is the same as the view plane.

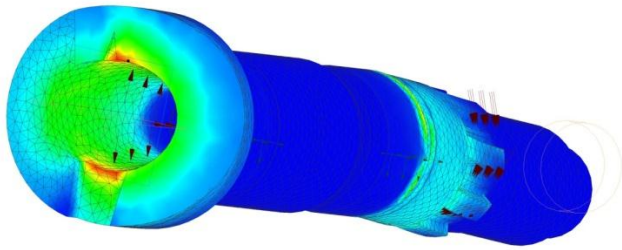

Figure 4.16. Fields of equivalent von Mises stresses
(using depth tools)

Figure 4.17 allows you to estimate the level of spindle deformations:

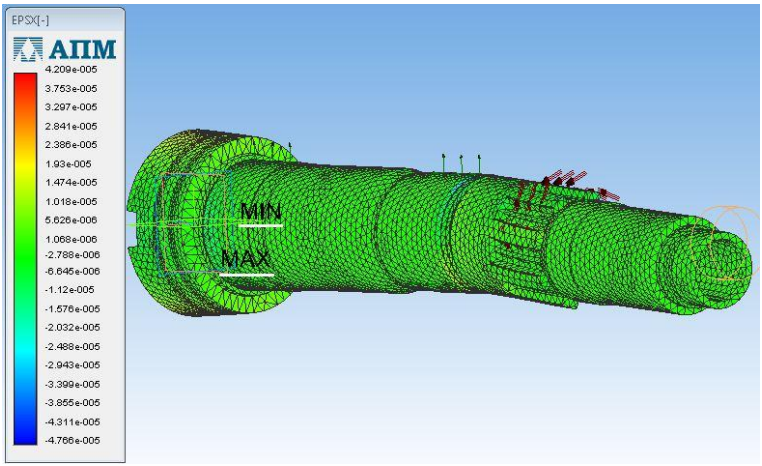


Figure 4.17. Displacement fields

To calculate stability in the APM FEM module there is a choice of a solution method. The less time-consuming *Arnoldi iteration* method is used as a worker - a method for solving a generalized eigenvalue problem that allows you to obtain a safety factor with relatively little processor time. However, the method does not allow obtaining a solution for systems with a large number of degrees of freedom. The parameters of the relative computational accuracy and the maximum number of iterations are set for both methods.

To assess the level of natural vibrations (Figure 4.18), the "Subspace" and "MKL Subspace" methods are used. MKL Subspace is used by default, as it is the fastest when working with sparse matrices.

For this, the *Eigenfrequencies* command is updated, with the help of which a window is formed with the natural frequencies and modal masses of the structure. Click the shape button to view the vibration form. For the selected frequency, the corresponding vibration forms are displayed on the screen (Figure4.19 and Figure4.20).

Natural frequencies

Natural frequencies — Modal masses (m.m.) and modal mass sums (m.m.s.)

| N | Rad/s | Hz | S | m.m. X, % | m.m.s. X, % | m.m. Y, % | m.m.s. Y, % | m.m. Z, % | m.m.s. Z, % |
|---|---|---|---|---|---|---|---|---|---|
| 1 | 8971.2 | 1427.81 | 0.00070... | 0.0302 | 0.0302 | 15.9 | 15.9 | 8.91e-005 | 8.91e-005 |
| 2 | 9018.28 | 1435.3 | 0.00069... | 15.8 | 15.8 | 0.0302 | 15.9 | 6.56e-006 | 9.57e-005 |
| 3 | 32078.5 | 5105.45 | 0.00019... | 0.00192 | 15.8 | 0.000346 | 15.9 | 2.15e-005 | 0.000117 |
| 4 | 34839.7 | 5544.91 | 0.00018... | 0.0119 | 15.9 | 7.16 | 23.1 | 0.00271 | 0.00283 |
| 5 | 34950.7 | 5562.57 | 0.00017... | 7.19 | 23 | 0.00989 | 23.1 | 0.000292 | 0.00312 |

Form OK

Figure 4.18. Frequencies of natural vibrations of the spindle

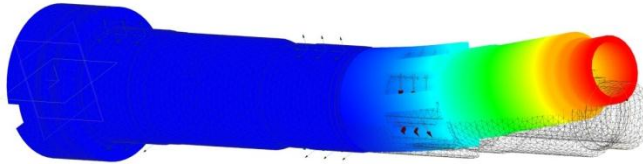

Figure 4.19. Form of vibration of the spindle at the 1st natural frequency

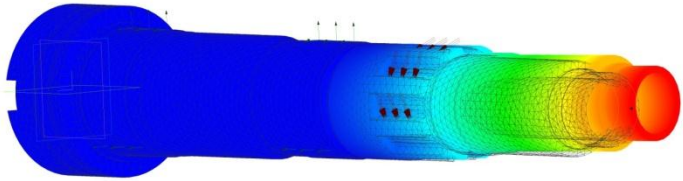

Figure 4. 20. Form of the spindle vibration at the 2nd natural frequency

The module also allows you to determine other inertial characteristics of the designed spindle structure (Figure 4.21)

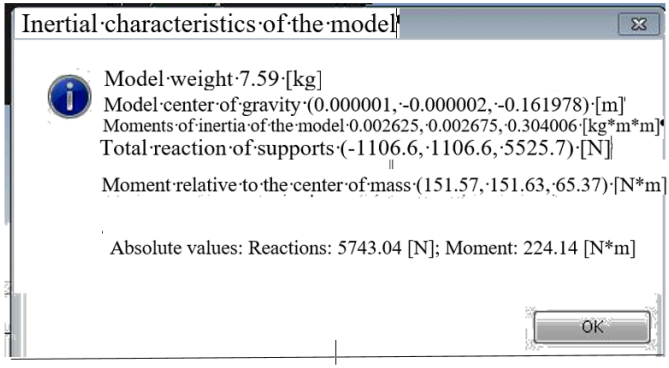


Figure 4.21. Inertial characteristics of the spindle model: weight; the center of gravity of the model; moments of inertia of the model

To obtain a complete picture of the spindle stress-strain state in any of its sections, including the assessment of loads, force factors, etc., it is necessary to use another APM Structure 3D module, which is part of the APM WinMachine CAD. Table 4.2 shows the calculation results

Table 4.2

**Loads on nodes. Load: Load 0**

| N | Type | Node number | Projection | | | Module |
|---|---|---|---|---|---|---|
| | | | on X | on Y | on Z | |
| 0 | Force, H | 0 | -6442.00 | 0.00 | -5187.00 | 8270.69 |
| 1 | Force, H | 3 | -2355.00 | 0.00 | -2616.00 | 3519.87 |

**Nodes displacement (Load 0)**

| N | Linear displacement [mm] | | | Angular displacement [Grad] | | |
|---|---|---|---|---|---|---|
| | X | Y | Z | X | Y | Z |
| 0 | -0.0707 | 6.56e-038 | -0.0576 | 0.0251 | -0.0454 | -0.0297 |
| 1 | -0.0504 | 6.56e-038 | -0.0412 | 0.0135 | -0.00234 | -0.0182 |
| 2 | -0.0226 | 2.54e-037 | -0.0219 | -0.000167 | 0.00946 | -0.00135 |
| 3 | -0.0254 | 3.1e-021 | -0.0293 | -0.00428 | 0.0191 | 0.00236 |

Efforts at member nodes (Load 0)

**Rod, index 0 (Rod 0)**

| Node number | Force [N] | | | Moment [N*m] | | |
|---|---|---|---|---|---|---|
| | $F_x$ (axial) | $F_y$ | $F_z$ | $M_x$ (torsion) | $M_y$ | $M_z$ |
| 0 | -0.00 | 5187.00 | 6442.00 | 347.00 | 0.00 | -29.00 |
| 1 | -0.00 | 5187.00 | 6442.00 | 347.00 | -289.89 | -262.41 |

**Rod, index 1 (Rod 1)**

| Node number | Force [N] | | | Moment [N*m] | | |
|---|---|---|---|---|---|---|
| | $F_x$ (axial) | $F_y$ | $F_z$ | $M_x$ (torsion) | $M_y$ | $M_z$ |
| 1 | 0.00 | 1485.91 | 1894.83 | 138.92 | -121.73 | -102.34 |
| 2 | 0.00 | 1485.91 | 1894.83 | 138.92 | -390.79 | -313.34 |

**Rod, index 2 (Rod 2)**

| Node number | Force [N] | | | Moment [N*m] | | |
|---|---|---|---|---|---|---|
| | $F_x$ (axial) | $F_y$ | $F_z$ | $M_x$ (torsion) | $M_y$ | $M_z$ |
| 2 | -0.00 | -2616.00 | -2355.00 | 347.00 | -346.18 | -384.55 |
| 3 | -0.00 | -2616.00 | -2355.00 | 347.00 | 0.00 | -0.00 |

Total structure weight – 7.89 kg
Maximum displacement – 0.09 mm (Rod 0) (Load 0)

**Nod stress (max.), [MPa] (Load 0)**

| N | Name | Nodes | Equivalent stress |
|---|---|---|---|
| 0 | Rod 0 | 0,1 | 124 |
| 1 | Rod 1 | 1,2 | 24.7 |
| 2 | Rod 2 | 2,3 | 12.2 |

Maximum stress 123.6 MPa (Rod 0) (Load 0)

Analysis of the results obtained allows you to choose the best design solutions, working with various loads and their combinations. At the same

time, it becomes possible to design structures close to equal strength in terms of strength, rigidity and vibrostability criteria.

### *4.3. Modeling the spindle node of the machining center model MTs200PF4*

Spindle node (SN) of machining centers are complex mechanical systems consisting of elastic elements of various types, combined into a single structure of the shaping generating units of the machine and are the object of modeling and research.

There are several significant factors [1, 2, 50] that affect the process of creating a rational version of the spindle node. These include some design and technological characteristics: unit layout; the geometry of the parts included in it; material properties of parts (modulus of elasticity, density, damping coefficient, etc.); axial interference of bearings and methods of their creation and others. In addition, the designer's decision-making is influenced by technological characteristics: errors of parts (different dimensions, roughness, deviation from roundness, etc.) and assembly errors. Finally, the influence of operating conditions (external loads, lubrication parameters, thermal conductivity, etc.) is important.

There are quantitative relationships between the input and output data, which determine the spindle node complex mathematical model, the research of which can be carried out in the environment of various computer-aided design systems.

It is advisable to research the influence of input factors on the spindle design using integrated CAD systems. The construction of a complex mathematical model of the SN is preceded by the choice of a CAD system, in which 3D modeling and research of the properties of the designed object will be carried out. There are many requirements for design systems, including adaptability, customizability of systems for the tasks of a particular industry, the use of libraries, reference books and applications

that significantly expand the capabilities of the basic CAD package, the use of photorealistic tools, and others.

To create 3D models of complex mechanical engineering structures, it is promising to use the well-known integrated CAD KOMPAS-3D, developed by ASCON. The fundamental difference between KOMPAS-3D is the use of its mathematical kernel and parametric technologies, and the cost of its implementation at the enterprise is an order of magnitude lower than the well-known foreign CAD systems. In the new version of the KOMPAS-3D system [76, 77], the user interface has been improved, the functionality of three-dimensional modeling has been significantly expanded, tools for working with graphic documents, variables, and application libraries have been replenished. CAD KOMPAS-3D V18 is one of the advanced updates to this popular package, which will be based on the technology of integrated end-to-end 3D product design.

At the same time, the creation of a complex spindle node is not limited to its geometric modeling. It is impossible to produce competitive products without a comprehensive engineering analysis of the designed facility. The adopted design solutions should provide static strength and rigidity, stability and suitable dynamic characteristics leading to the optimal option.

As a result of integration with CAD APM WinMachine [27], a CAE-library appeared in the KOMPAS-3D system, which implements solutions of engineering problems by the finite element method as applied to the problems of engineering analysis. At the same time, it should be borne in mind that at the same time the internal structure of the production organization and the lack of the necessary funds do not allow implementing a single end-to-end ideology of information exchange.

An alternative to the implementation of a single integrated system within the design and technological departments of an enterprise is the problem of data transfer between systems with different presentation formats. In favour of this approach and the factor of continuity of old and new projects, the use of existing databases [78]. The problem of data transfer is effectively solved in the SolidWorks system, which in the basic

version supports a large set of formats for importing three-dimensional objects and 2D drawings. In addition to the standard tools for importing files through the dxf, step, iges, sat formats, the SolidWorks system is equipped with translators for models of parts and assemblies from other systems.

Thus, the problem arises of improving the process of 3D modeling and research of the spindle node of the machining center using the integrated CAD KOMPAS and SolidWorks.

To research this problem, interrelated tasks are solved, which are formulated as follows:

1. Develop a 3D model of the spindle node using CAD KOMPAS.

2. To carry out a research of the stress-deformation characteristics of the spindle node using the finite element method in the CAD environment SolidWorks.

3. Assess the dynamic characteristics of the projected spindle node.

Consider the spindle assembly of the MTs200PF4V machining center, which is a two-bearing structure (Figure 4.22), mounted on two rolling bearings:

- front support in the form of triplex – a set of three angular contact ball bearings 2-46113, mounted according to the "Tandem-X" scheme with a preload in the form of two bushings of different heights;

- the rear support is a set of two angular contact ball bearings 2-46111, mounted according to the "X-shaped" scheme with a preload in the form of two bushings of different heights.

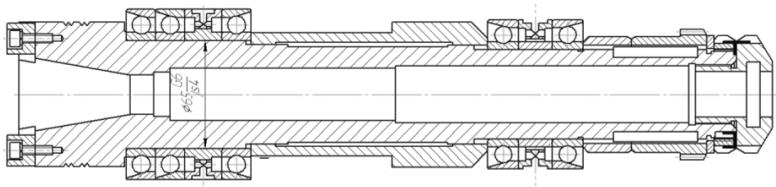

Figure 4.22. Structural diagram of the spindle assembly

Based on the developed solid models of individual parts in the KOMPAS-3D environment (Figure 4.23), a 3D model of the spindle device structure was created [79, 80], the realism of which was achieved thanks to the Photo360 module included in SolidWorks (Figure 4.24).

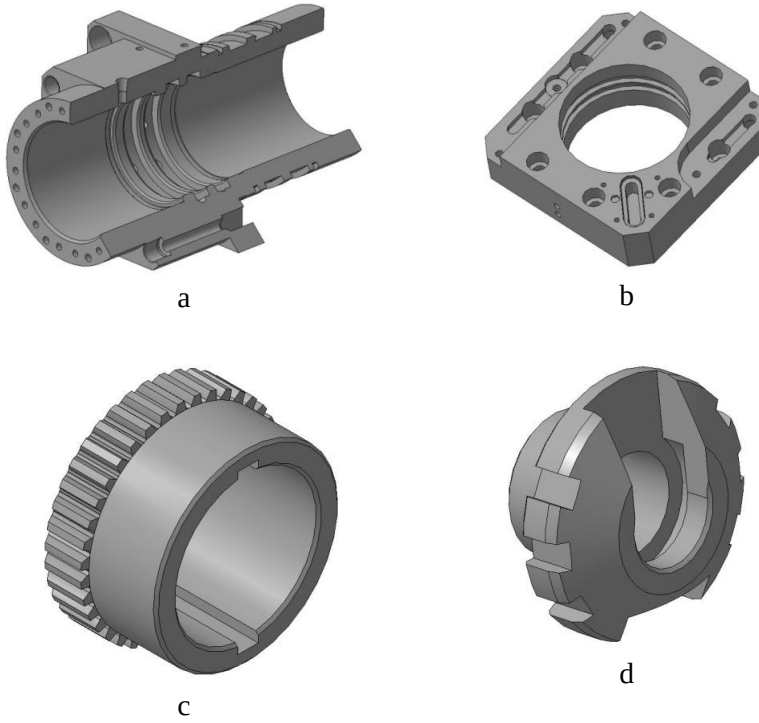


Figure 4.23. Solid model parts:
a - sleeve; b - flange; c - half-coupling; d – nut

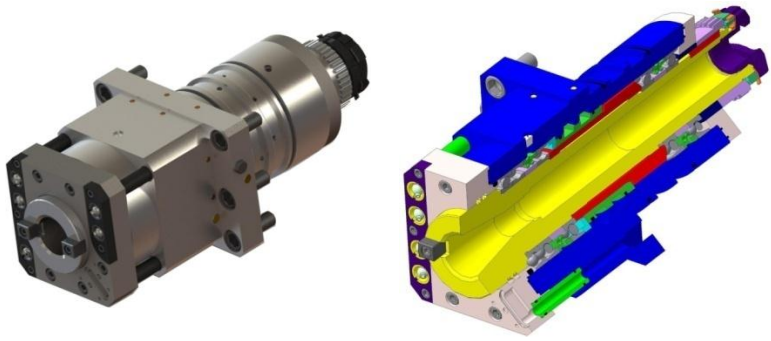

a b

Figure 4.24. Solid model of the spindle assembly:
a – 3D model with rendering; b – SN section

The research of the spindle assembly according to the stiffness criterion is carried out using SolidWorks Simulation (SW Simulation). This module, which is part of SolidWorks, fully integrates with the 3D model of the product created in CAD KOMPAS, which makes it possible to optimize the design. The 3D design changes are carried over to the product drawings. Solidworks Simulation provides stress, loss of stability, and frequency and thermal analysis.

Static research of the spindle is carried out in SolidWorks in a certain sequence, starting with the specification of the material, the choice of the attachment points and the type of supports, followed by loading by forces and moments [81–83]. A feature of the SW Simulation engineering analysis package is that both the imposition of constraints and the application of forces are carried out to the surface as a whole. In this regard, an additional procedure is introduced for splitting surfaces by constructing auxiliary planes and parting lines projected onto the spindle surface. At this stage, it is effective to define the supports that are modeled by the bearings in SW Simulation and enter their axial and radial stiffness.

To assess the manufacturability of the structure assembly, it is effective to use animation tools (Figure 4.25), performed in SolidWorks Simulation [19].

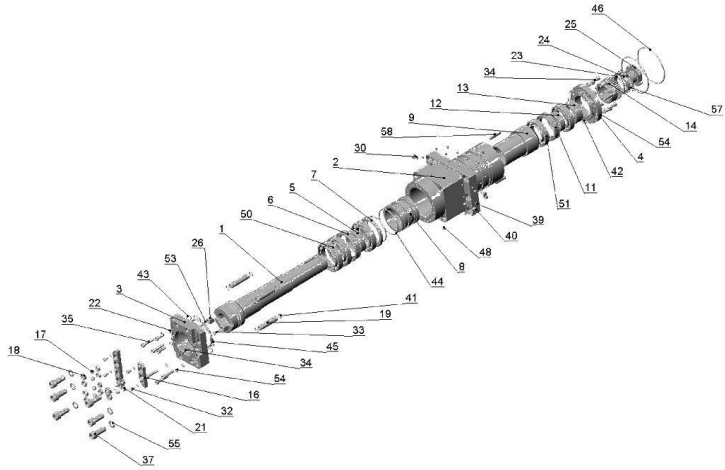


Figure 4.25. OTs200 spindle assembly animation

The procedure for creating a finite element mesh in SW allows both to use the system recommendations and to control the size of the finite element to increase the accuracy of calculations [84]. When calculating the stress-strain state, the units of measurement and the type of the diagram are selected in the Properties Window. As a result of such a calculation of the spindle, displacement diagrams were obtained on an enlarged scale (Figure 4.26).

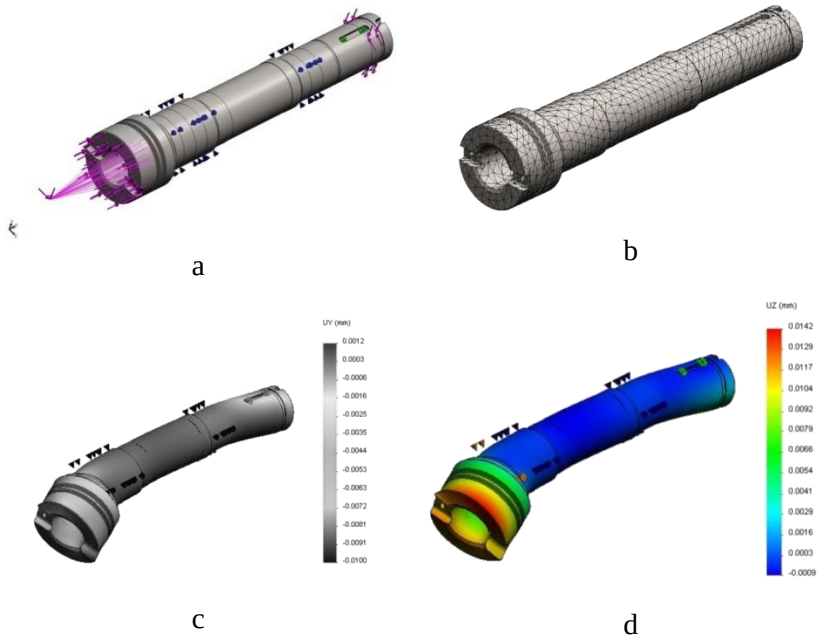


Figure 4.26. Spindle calculation results: a – fixing and loading scheme; b – finite element mesh; c – displacement in the horizontal plane; d – displacement in the vertical plane (on a larger scale)

As a result of calculations of the stress-strain state by Mohr's method, the displacements of the spindle node under the action of cutting forces and the force that can arise in the gear clutch in the event of shaft misalignment were estimated [85–87]. The most difficult case was calculated when the cutting force and the force acting in the cam clutch are oriented in the same direction.

The total deflection is found by the formula:

$$y_{\Sigma} = \sqrt{y_h^2 + y_v^2} = \sqrt{0.017^2 + 0.027^2} = 0.031 \text{ mm}.$$

With a permissible deflection of 0.04 mm, it can be argued that the required rigidity is provided.

The resulting elastic line of the spindle corresponds to the design model with rigid supports. Considering the compliance of the supports [26] somewhat changes the picture of the stress-strain state, the characteristics of which are presented in Table 4.3

Table 4.3

**Summary table of spindle stiffness characteristics**

| Section Coordinates, mm | Displacement, mm | | | | | | | Bending angle, grad | | |
|---|---|---|---|---|---|---|---|---|---|---|
| | Fixed support | | | Elastic support | | | Allowable value | Fixed support | Elastic support | Allowable value. |
| | Vert. | Hor. | Total | Vert. | Hor. | Total | | Total | Total | |
| 0 | 0.027 | 0.017 | 0.031 | 0.075 | 0.084 | 0.113 | 0.04 | 0.022 | 0.045 | 0.06 |
| 98 | - | - | - | 0.017 | 0.041 | 0.044 | | 0.012 | 0.036 | |

According to calculations, displacements in the front support on three angular-contact thrust bearings (with a fixed stiffness j = 98000 N/mm) slightly exceed the permissible values. At the same time, the presence of parts that provide axial fixation (spacers, rings) increases the rigidity of the spindle device, which makes it possible to consider the considered design option as satisfying the rigidity criterion.

To assess the dynamic quality of the spindle functioning, the MatLab mathematical environment was used, in which programs for researching frequency characteristics were developed [59]. In the complex-frequency domain, the amplitude and phase-frequency characteristics of the elastic system of the spindle, the cutting process, the open and closed-loop system "Spindle-Cutting process" is built (Figure 4.27 - Figure 4.31)

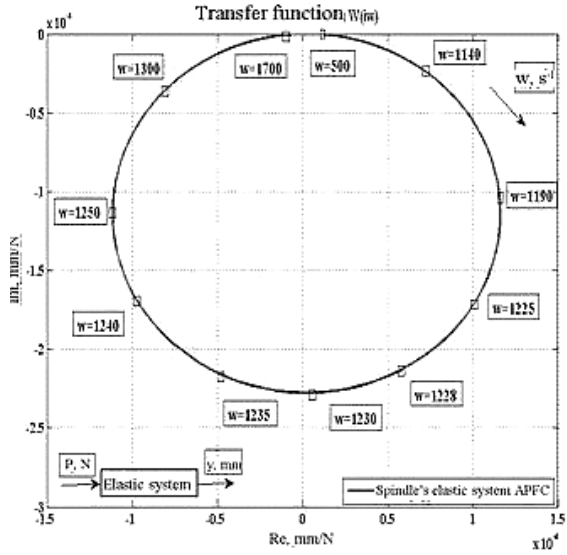


Figure 4.27. APFC of the elastic system of the spindle machine model MTs200PF4V

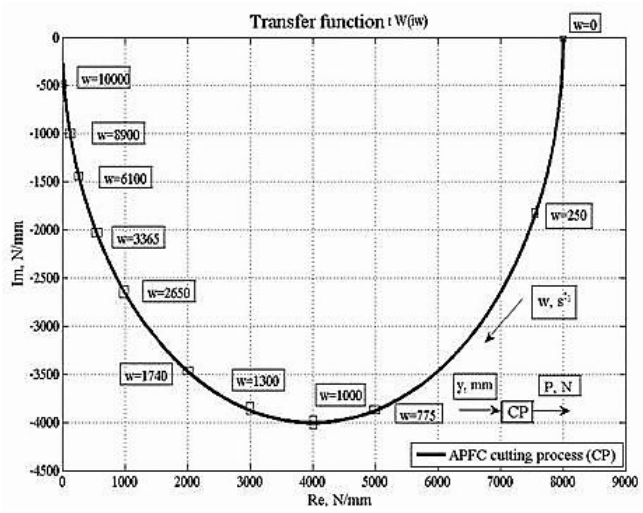


Figure 4.28. APFC of the cutting process on the machine model MTs200PF4V

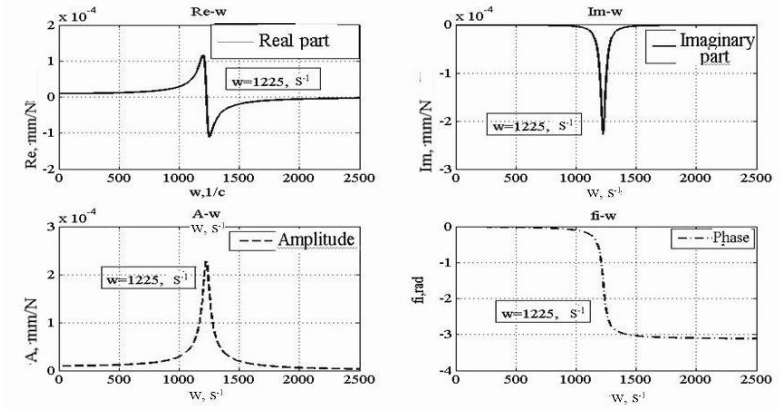


Figure 4.29. Frequency characteristics of the elastic spindle system

APFC of the elastic spindle systems makes it possible to compare various adjustments with modular equipment in terms of the length of the segment cut off by the characteristic on the imaginary *Im*-axis. The ratio of the length of this segment to the static compliance determines the dynamic factor at resonance for the i-th natural vibration frequency. Unlike static compliance, the dynamic coefficient takes into account the inertial and damping properties and, therefore, more fully characterizes the elastic system of the spindle assembly of the MTs200PF4V model machining center.

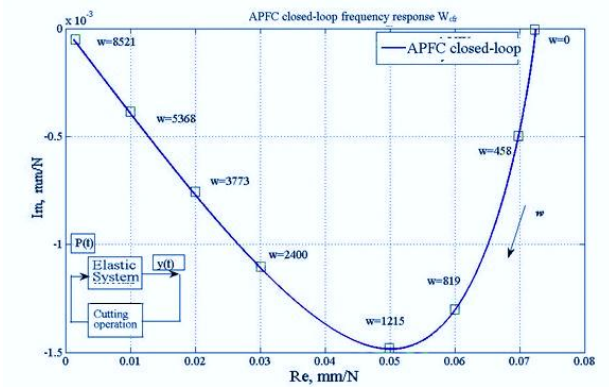


Figure 4.30. APFC of the closed system "spindle-cutting operation"

The analysis of the results obtained indicates the effectiveness of the complex procedure of 3D-modeling in CAD KOMPAS-3D and the calculation of the stress-strain state by the method of finite elements in SolidWorks Simulation. This approach is to implement the procedure of multivariate design and search for the optimal design of the spindle assembly in terms of rigidity and vibrostability.

## CONCLUSIONS

1. Methods and procedures for the dynamics of spindle units of metal-cutting machines, as closed-loop dynamic systems, including a set of elastic links and work processes have been developed.

2. The dynamics of the elastic link "Spindle-Arbor-Tool" (SAT) of multifunctional CNC machines of the drilling-milling-boring group has been researched. Static and dynamic forms of the spindle assembly have been obtained, linking the SAT compliance and the length of the Arbor-Tool cantilever overhang, which allow modeling structures with a variable cantilever part.

3. Considered the presentation of the conical connection of the spindle and the arbor shank, in the form of a matrix of an elastic-friction joint, elastic concerning transverse and angular displacements. The APFC of the spindle assembly with and without regard to the compliance of the Spindle-Arbor joint is constructed. Taking into account the compliance of the Spindle-Arbor joint with the help of the hinge matrix leads to an increase in the vibration amplitude three times up to 0.083 μm/H) at increased frequencies. The modulus min*Re* also decreases to - 0.0439 μm/N.

4. The calculation of the dynamic characteristics of rapidly rotating spindles, taking into account the centrifugal forces and gyroscopic moments in the bearings at a steady state of motion. It is noted that at speeds of rotation of the bearing inner ring (duplexed supports on angular contact thrust bearings are considered) more than 1100 rpm, it is necessary to take into account the inertial factors $F_c$ and $M_g$ and consider this calculation problem as quasi-static.

5. Software has been developed and frequency characteristics of open and closed-loop systems "Spindle-Arbor-Tool" – "Cutting Process" –

"Table-Workpiece" in the MATLAB mathematical environment have been built.

6. A research of the stability of elastic links "Spindle-Arbor-Tool" and "Table-Workpiece" was carried out using the toolkit of one- and two-parameter D-partitions based on the analysis of the number of the characteristic equation roots. Experimentally researched two options of adjustments at different lengths of the cantilever and determined the optimal value of the depth of cut, the cutting coefficient and the time constant of chip formation, ensuring stable operation of the cutting process. The analysis of the SAT dynamic system stability allows designers when designing adjustments and assessing the technological capabilities of machine tools, to determine the maximum length of the cantilever (overhang of the tool block) for vibration-free processing.

7. The values of the natural frequencies of the carrier system of the drilling-milling-boring machine are determined and the vibration modes are constructed at those natural frequencies that are characterized by a relatively high level of vibration of the tool and the workpiece. The analysis of the experimental amplitude-frequency characteristics showed that low-frequency oscillations of the carrier system are of the greatest interest. Based on the pattern of points displacements of the machine elastic system, classification of its main nodes with division into arrays and rods (elastic beams) is carried out. The analysis of vibration modes made it possible to neglect the of some joints compliance, which significantly reduced the complexity of the preparatory stage of the calculation. Such joints include the "column-carriage" and "carriage-vertical table" joints. The graphic representation of the TC elastic links deformations allows you to more clearly orient yourself at the first stage of the dynamic's calculations and, therefore, improve the quality of the final calculations.

8. The procedure to the real picture approximation of the spindle assembly oscillations using the polyharmonic process is considered. With the help of the "Signal Processing" software environment, the process of

reproducing a complex signal and the allocation of its periodicity is realized. To improve the estimates of the signal spectral density at the input of the spindle elastic system, the spectral windows of Hamming and Hanning are used, which makes it possible to reduce the variance of the spectral estimate. The analysis of the efficiency of using various spectral windows in the "Signal Processing" environment is presented.

9. Experimental researches of the spindle node dynamics of a multifunctional lathe have been carried out, and in the mathematical environment "Maple" (using the kernel of symbolic mathematics) a static form has been obtained to assess the compliance of the spindle with varying the length of the tool block. The calculation of the spindle stress-strain state in any of its cross-sections in the APM Structure3D environment has been carried out. It makes it possible to evaluate the complete picture, including the assessment of loads, force factors, etc. It is shown that during the vibrations of the spindle node elastic system, the basic bending shape prevails. It gives a basis for considering the designed object as a second-order linear vibrational link. With the help of the constructed APFC, it is possible to compare various adjustments in terms of the dynamism coefficient, which takes into account the inertial and damping properties and, therefore, more fully characterizes the elastic system of the spindle assembly of a multi-purpose lathe.

10. Static forms of multifunctional milling machines are calculated and nomograms, consisting of constant and variable parts are constructed. To perform a comprehensive engineering analysis of both the spindle and the spindle assembly, the APM FEM module was used. This module integrated into KOMPAS-3D and equipped with a CAE-library that implements solutions of engineering problems by the finite element method.

11. A comprehensive procedure for modeling and analyzing the design of the spindle assembly for a multifunctional machining center using CAD KOMPAS and CAD SolidWorks has been implemented.

12. Solid models of the main parts of the spindle device consisting of 149 units in the CAD KOMPAC 3D environment were built. Based on 3D models of components, the assembly of the spindle node is implemented using the procedures for imposing realistic textures in the Photo360 module. The modeling of the assembly process of the structure using the animation tools SolidWorks Simulation has been performed.

## REFERENCES

1. Kudinov V.A. Dynamics of machine tools. – Moscow: Mechanical Engineering, 1967. – 360 p.

2. Orlikov M.L. Dynamics of machine tools. – Kyiv: High school, 1989. – 272 p.

3. Popov V.A., Loktev V.A. Dynamics of machine tools. – Kyiv: Technics, 1975. – 136 p.

4. Kaminskaya V.V., Kushnir E.F. Dynamic characteristics of the cutting process during drain chip formation / Machine tools and instruments, 1979, № 5. – P. 27–30.

5. Kaminskaya V.V., Eremin A.V. Calculation analysis of dynamic characteristics of lathes of various layouts / Machine tools and instruments, 1985, №7. – P. 3–6.

6. Greenglaz A.V., Gurychev S.E., Kaminskaya V.V. Comparison of multi-purpose machines by dynamic characteristics / Machine tools and instruments, 1989, №6. – P. 11–13.

7. Kaminskaya V.V., Greenglaz A.V. Computational analysis of the dynamic characteristics of the bearing system of the machine / Machine tools and instruments, 1989, №2. – P. 10–13.

8. Khomyakov V.S., Dosko S.I., Terentyev S.A. Increasing the efficiency of calculation and analysis of the dynamic characteristics of machines at the design stage / Machines and instruments, 1991, №6. – P. 7–12.

9. Eremin A.V. Chekanin A.V. Calculation of the rigidity of the bearing system of the machine based on the super element approach / Machine tools and instruments, 1991, №6. – P. 12–16.

10. Khomyakov V.S., Dosko S.I., Zoi Liu Identification of elastic machine systems based on modal analysis / Machine tools and instruments, 1988, №7. – P. 11–14.

11. Krol O.S., Osipov V.I. Modeling of construction spindle's node machining centre SVM1F4/Comission of Motorization and Power Industry of Agriculture. – OL PAN, 2013, Vol.13, is.3, Lublin, Poland. – P. 108–113.

12. Krol, O., & Sokolov, V. (2018). Modelling of spindle nodes for machining centers. In *Journal of Physics: Conference Series* 1084. Institute of Physics Publishing. https://doi.org/10.1088/1742-6596/1084/1/012007

13. O Krol and V Sokolov. 3D modelling of angular spindle's head for machining centre / *Journal of Physics: Conf. Series* **1278** (2019) 012002. – VSPID-2018. https://doi.org/10.1088/1742-6596/1278/1/012002

14. Krol O. Modeling of vertical spindle head for machining center / O. Krol, V. Sokolov, P. Tsankov // Journal of Physics: Conference Series 1553 (2020) 012012. – VSPID-2019. http://doi.org/10.1088/1742-6596/1553/1/012012

15. Khanov A.M., Kobityansky A.E., Shafranov A.V. Research of the dynamics of spindle nodes of machine tools based on mathematical modeling / Bulletin of PSTU. Mechanical engineering, 2012, Vol.14, No. 2. – P. 27–33.

16. Khanov, A.M., Kobityansky A.E., Shafranov A.V., Pepelyshev A.V. Program for calculating the dynamics of spindle nodes on rolling bearings / Bulletin of PSTU. Mechanical engineering, materials science, 2010, Vol. 12, No. 2. – P. 15–21.

17. Khomyakov V.S., Kochinev N. A., Sabirov F. S. Modeling and experimental study of the dynamics of the characteristics of the spindle assembly / Bulletin of the Tula State University. Technical sciences, 2011, No 3. – P. 251–258.

18. Design of metal-cutting machine tools and machine-tool systems: Handbook-textbook. In 3 volumes. Vol. 2. Part 1. Calculation and design of units and elements of machine tools / A. S. Pronikov, E. I. Borisov, V. V. Bushuev et al. – Moscow: Mechanical Engineering, 1995. – 371 p.

19. Alyamovsky A.A. Engineering calculations in SolidWorks Simulation. – Moscow: DMK Press, 2010. – 464 p.

20. Kuznetsov Yu. N. Analysis of the dynamic system spindle-chuck-part of a lathe / Bulletin of mechanical engineering, 1990, No. 8. – p. 42–47.

21. Kuznetsov Yu. N., Sidorko V.I., Vachev A.A. Improvement of the dynamic quality of the cartridge-part system of a bar machine / Machine tools and instruments, 1987, No. 12. – P. 13–15.

22. Gurzhiy A.N., Strutinsky V.B. Improvement of a multi-spindle lathe based on the analysis of stochastic oscillatory processes of its dynamic system / Reports of the International Conference "Mechanics and New Technologies", Sevastopol, 1995. – P. 62–67.

23. Kushnir E.F. Determination of the amplitude-phase frequency characteristic of the elastic system of the machine during cutting / Machine tools and instruments, 1983, №3. – P. 11–13.

24. Kaminskaya V.V. Investigation of oscillations during machine operation and ways to improve their dynamic quality / Dynamics of machine tools, Kuibyshev: Regional House of Technology, 1980. – P. 112–115.

25. Kaminskaya V.V., Kushnir E.F., Feldman M.S. Determination with the help of a computer the frequency characteristics of elastic systems of machine tools according to information obtained during intermittent cutting / Methods for solving problems of mechanical engineering on computing machines, Moscow: Nauka, 1979. – P.57–62.

26. Zamriy A.A. Practical training course CAD/CAE APM WinMachine. Teaching aid. – Moscow: APM Publishing House, 2007. – 144 p.

27. Magomedov A., Alekhin A. Integrated finite element analysis in KOMPAS-3D / CAD/CAM/CAE observer. – 2010, No. 8 (60). – P. 1–5.

28. Ivovich V.A. Transitional matrices in the dynamics of elastic systems. – Moscow: Mechanical Engineering, 1969. – 200 p.

29. O Krol and V Sokolov Modeling of carrier system dynamics for metal-cutting machines/IEEE Proceedings 2018 International Russian Automation Conference (RusAutoCon) P. 1 – 5.
https://doi.org/10.1109/rusautocon.2018.8501799

30. Krol O.S., Porkuian O.V., Sokolov V.I. and Tsankov P.G. Vibration Stability of Spindle Nodes in the Zone of Tool Equipment Optimal Parameters/Comptes rendus de l'Acade'mie bulgare des Sciences. – Sofia: "Prof. Marin Drinov" Publishing House of Bulgarian Academy of Sciences, 2019. – Vol. 72. – No. 11. – P. 1546–1556. https://doi.org/10.7546/CRABS.2019.11.12

31. Krol O.S., Krol A.A., 2011: Calculation of compliance SF68VF4 machine dynamics shaping and modeling // Vestnik SevNTU. Ser. Engineering and Transportation. – is. 117, 81–84. (in Russian)

32. Krol, O.S., Suhorutchenko, I.A. (2014). Trehmernoe modelirovanie obrabatyivayuschiy tsentra SVM1F4 v KOMPAS 3D [Solid modeling of machining centre SVM1F4 in KOMPAS 3D]. Eastern-European Journal of Enterprise Technologies], 4/7(70), 13–18.

33. Linchevsky P.A. Influence of AIDS System Compliance on Accuracy of Diamond Boring Machines in Double Cutting Machinery / Metal-cutting machines. – Kyiv: Technics, 1982, No. 10. – P. 56–58.

34. Krol O. S. Metody i procedury dinamiki shpindel'nyh uzlov [Methods and procedures for the dynamics of spindle nodes]: monografiya. Lugansk: Izd-vo VNU im. V. Dalya, 2014. – 154 p.

35. Balmont V.B. Gorelik I. G., Figatner A. M. Calculations of high-speed spindle nodes / NIITEMR, Ser. 1, 1987, No. 1. – 52 p.

36. Krol O., Shevchenko S., Sukhorutchenko I and Lysenko A. (2014). 3D-modeling of the rotary table for tool SVM1F4 with non-clearance worm gearing. TEKA Commission of Motorization and Energetic in Agriculture, 14, 1, 126-133.

37. Krol O., Sukhorutchenko I. 3D-modeling and optimization spindle's node machining centre / Teka Komisji Motoryzacji I Energetyki in Rolnictwa. – OL PAN, 2013, Vol.13, is.3, Lublin, Poland. – P. 114–119.

38. Metal-cutting machines / Ed. V.E. Push. – Moscow.: Mechanical engineering, 1985. – 256 p.

39. Zhuravlev V.F. Mechanics of ball bearings of gyroscopes – Moscow: Mechanical Engineering, 1985. – 272 p.

40. Krol, O. & Sokolov, V. (2020). Modeling of Spindle Node Dynamics Using the Spectral Analysis Method. In *Lecture Notes in Mechanical Engineering* (pp. 35–44). Springer. https://doi.org/10.1007/978-3-030-50794-7_4

41. Theory of automatic regulation. Part 1 / Ed. A.V. Netushil: Textbook. – Moscow: High school, 1967. – 424 p.

42. Krol O.S., Golovanov D. V. One- and two-parameter D-partitions in the problems of optimization of technological systems / Reliability of cutting tools and optimization of technological systems. Vol. 2. – Kramatorsk: DSMA, 1997. – P. 29–40.

43. Krol O.S., Krol A.A. Calculation of the compliance of the machine SF68VF4 and modeling of the dynamics of shaping /

Bulletin of SevNTU, No. 117 "Machinery and transport". – Sevastopol: View of SevNTU, 2011. – p. 81–84.

44. Krol O.S., Shevchenko S.V., Sokolov V.I. Design of metal-cutting tools in the middle of APM WinMachine. Textbook. – Lugansk: SNU, 2011. – 388 p.

45. Krol O, Shumakova T, Sokolov V. Design metal cutting instruments by dint of system of KOMPAS. – Lugansk: V. Dahl EUNU, 2013. – 144 p.

46. Krol O.S., Sokolov V.I. 3D Modeling Of Machine Tools For Designers. – Sofia: Prof. Marin Drinov Academy Publishing House of Bulgarian Academy of Sciences, 2018. – 140 p. https://doi.org/10.7546/3D_momtfd.2018

47. Krol O., Belkov M. Study dynamics machining centre SF68VF4 / Teka Komisji Motoryzacji i Energetyki Rolnictwa, OL PAN, 2014, Vol.14, is.2, Lublin, Poland. – P. 59–67.

48. Krol O.S., Krol A.A., Sindeeva E.V. Modeling of the design of the four-shaft in the CAD APM "WinMachine" / Resource-saving technologies of production and processing of materials in mechanical engineering/ Collection of scientific papers. – Lugansk: Publishing House of Volodymyr Dahl East Ukrainian National University, 2008. – P. 139–143.

49. Krol O.S., Juravlev V.V. Modeling of spindle for turret of the specialized tool type SF16MF3 / TEKA Commission of Motorization and Energetics in Agriculture. – OL PAN, 2013, Vol.13, is.4, Lublin, Poland. – P. 141–147.

50. Krol O., Sokolov V. Rational choice of machine tools for designers. – Sofia: Prof. Marin Drinov Academic Publishing House of Bulgarian Academy of Sciences, 2019. – 113 p.
https://doi.org/10.7546/RCMTD.2019

51. V Sokolov, O Krol and O. Stepanova. Nonlinear simulation of electrohydraulic technological equipment/ J. Physics: Conf. Series **1278** (2019) 012003. – VSPID-2018. Doi: https://doi.org/10.1088/1742-6596/1278/1/012003

52 Sokolov V., Krol O. Determination of Transfer Functions for Electrohydraulic Servo Drive of Technological Equipment. In: Ivanov V. et al. (eds) Advances in Design, Simulation and Manufacturing. DSMIE 2018. Lecture Notes in Mechanical Engineering. Springer, Cham, 2019. – P. 364–373. https://doi.org/10.1007/978-3-319-93587-4_38

53. Sokolov V., Krol O., Stepanova O. Automatic control system for Electrohydraulic drive of production equipment/IEEE Proceedings 2018 International Russian Automation Conference (RusAutoCon) P.1 – 6. https://doi.org/10.1109/rusautocon.2018.8501609

54. Krstić, B., Krstić, M. (2016). Rational choice theory and Social Research. Sociologija, 58 (4), 598-611.

55. Krstić, M. (2012). The role of rules in the evolution of the market system: Hayek's concept of evolutionary epistemology. Economic annals, 57 (194): 123-140.

56. Krol O. Selection of machine tools optimal cutting modes for designers. – Sofia: Prof. Marin Drinov Academic Publishing House of Bulgarian Academy of Sciences, 2020. – 240 p. https://doi.org/10.7546/SMTOCMD.2020

57. Krol O. S., Hmelovskij G. L. Optimizacija i upravlenie processom rezanija: uchebnoe posobie. Kiev: UMK VO, 1991. – 140 p.

58. Bendat J., Pirsol A. Applied analysis of random data. – Moscow: Mir, 1989. – 540 p.

59. MATLAB. User's Guided for MS-DOS personal computers. - The Math Works, Jnk., 1989. – 204 p.

60. Solodovnikov A.I., A.M. Spivakovsky Fundamentals of theory and methods of spectral information processing. – Leningrad: Leningrad State University, 1986. – 272 p.

61. Krol O.S. Methods and procedures for optimizing cutting conditions. Monograph. – Lugansk: Publishing house VDEUNU, 2013 – 260 p.

62. Krol O., Sokolov V. (2019) Parametric Modeling of Gear Cutting Tools. In: Gapiński B., Szostak M., Ivanov V. (eds) Advances in Manufacturing II. Lecture Notes in Mechanical Engineering. Springer, Cham. https://doi.org/10.1007/978-3-030-16943-5_1

63. Krol O., Sokolov V. (2019) Parametric Modeling of Transverse Layout for Machine Tool Gearboxes. In: Gapiński B., Szostak M., Ivanov V. (eds) Advances in Manufacturing II. MANUFACTURING 2019. Lecture Notes in Mechanical Engineering. Springer, Cham. https://doi.org/10.1007/978-3-030-16943-5_11

64. Krol O.S., Osipov E.I., Krol A.A. Simulation of IT-1 machine tool drive in APM WinMachine environment / Bulletin of Volodymyr Dahl East Ukrainian National University. – Lugansk: SNU, is. 2 (191). Part 1, 2013. – P. 112–115.

65. Krol O., Tsankov P., Sokolov V. Rational choice of two-support spindles for machining centers with lubrication system/EUREKA: Physics and Engineering, is. 3, 2018. – P. 52–58. https://doi.org/10.21303/2461-4262.2018.00648

66. Krol O., Sokolov V. Rational choice of machining tools using prediction procedures/EUREKA: Physics and engineering, is. 4, 2018. – P. 14–20. https://doi.org/10.21303/2461-4262.2018.00667

67. Shelofast V.V., Chugunov T.B. Fundamentals of machine design. Examples of problem solving. – M.: Publishing house of APM, 2004. – 240 p.

68. Yakovenko I., Permyakov A., Prihodko O., Basova Y., Ivanova, M.. Structural optimization of technological layout of modular machine tools. In Tonkonogyi V. et al. (eds). Advanced Manufacturing Processes. InterPartner-2019. Lecture Notes in Mechanical Engineering. Springer 2020; 352–363. https://doi.org/10.1007/978-3-030-40724-7_36

69. Ivanov V. Process-oriented approach to fixture design. In Ivanov V. et al. (eds) Advances in Design, Simulation and Manufacturing. DSMIE-2018. Lecture Notes in Mechanical Engineering. Springer, Cham 2019; 42–50. https://doi.org/10.1007/978-3-319-93587-4_5

70. Ivanov V, Dehtiarov I, Pavlenko I, Liaposhchenko O, Zaloga V. Parametric optimization of fixtures for multiaxis machining of parts. In: Hamrol A., Kujawińska A., Barraza M. (eds) Advances in Manufacturing II. MANUFACTURING 2019. Lecture Notes in Mechanical Engineering. Springer, Cham 2019; 2: 335-347. https://doi.org/10.1007/978-3-030-18789-7_28

71. Krol O.S., Krol A.A. Simulation of the multi-purpose lathe spindle node in the APM WinMachine environment/Machine tool reliability and optimizing technological systems. Collection of scientific papers. – Kramatorsk: vol. 26, 2010. – P. 112–117.

72. Krol O.S., Krol A.A. Building spindle models of a multi-purpose lathe in the APM WinMachine environment/Bulletin of Volodymyr Dahl East Ukrainian National University. – Lugansk: SNU, is. 3 (145). Part 2, 2010. – P.143–148.

73. Push A.V. Spindle units. Quality and reliability. – Moscow: Mechanical Engineering, 1992. – 288 p.

74. Krol O., Sokolov V. Parametric modeling of machine tools for designers. – Sofia: Prof. Marin Drinov Academic Publishing House of Bulgarian Academy of Sciences, 2018. – 112 p. https://doi.org/10.7546/PMMTD.2018

75. Krol O. Engineering forecasting of machine tools for designers. – Sofia: Prof. Marin Drinov Academic Publishing House of Bulgarian Academy of Sciences, 2019. – 114 p. https://doi.org/10.7546/EFMTD.2019

76. Malyukh V. N. New KOMPAS-3 D V14 / Isicad.ru, No. 102, 2013. – p. 76–81.

77. Malyukh V.N. Introduction to modern CAD systems. The course of lectures. – Moscow: DMK Press, 2012. – 192 p.

78. Mukhovannaya E.Yu., Mikhailov M.A., Kholin M.I., Novoselov V.I. Open SolidWorks: unity and struggle of opposites / CAD and Graphics, No. 3, 2000. – P. 59–63.

79. Krol O.S., Burlakov E.I. Modeling of the spindle unit of the machining center / Bulletin of the National Technical University "KhPI". – Kharkiv: NTU "KhPI", is. 11(985), 2013. – P. 33–39.

80. Krol O.C., Krol A.A., Burlakov E.I. Solid modeling and investigation of the spindle node of the machining center / Bulletin of the National Technical University "KhPI". – Kharkiv: NTU "KhPI", is.16(989), 2013. – P. 14–18.

81. Schevchenko S., Mukhovaty A., Krol O.: Gear transmission with conic axoid on parallel axes. In: Proceedings of the 5th International Conference on Industrial Engineering (ICIE 2019). ICIE 2019. LNME, vol. 1, pp. 1–10. Springer, Cham (2020).
https://doi.org/10.1007/978-3-030-22041-9_1

82. Shevchenko S., Muhovaty A., Krol O. Geometric Aspects of Modifications of Tapered Roller/ Procedia Engineering 150 (2016) 1107 – 1112. https://doi.org/10.1016/j.proeng.2016.07.221

83. Shevchenko S., Muhovaty A., Krol O. Gear Clutch with Modified Tooth Profiles / Procedia Engineering 206 (2017) 979–984. http://doi.org/10.1016/j.proeng.2017.10.581

84. Krol O.S. Methods and procedures of 3D-modeling of metal-cutting machine tools and instruments. Monograph: Severodonetsk, EUNU, 2015. – 120 p.

85. Krol O. Engineering forecasting of machine tools for designers. – Sofia: Prof. Marin Drinov Academic Publishing House of Bulgarian Academy of Sciences, 2019. – 114 p. https://doi.org/10.7546/EFMTD.2019

86. Krol O.S., Shevchenko S.V., Sindeeva E.V., Pokintelytsa N.I. Design of mechanical gears of metal-cutting machines with the help of a system APM WinMachine. Handbook. – Lugansk: Publishing House of Volodymyr Dahl East Ukrainian National University, 2007. – 200 p.

87. Krol, O. S. (2012) Construction of parametrical models of belt transmissions with the use of the system APM WINMACHINE. East.-Eur. J. Enterp. Technol., 2/7(62), 37–51.

## CONTENT